

学位論文

Electrochemical Syntheses of Redox Complex Networks  
and Ultra-long Wires Covalently Bound to Carbon

(炭素電極に共有結合したレドックス錯体  
ネットワーク・極長ワイヤの電気化学合成)

平成 26 年 12 月博士（理学）申請

東京大学大学院理学系研究科

化学専攻

吳 國暉

Kuo-Hui Wu



## Abstract

This thesis is focused on electrochemical syntheses of bis(terpyridine)metal complex polymers with network and wire structures on carbon electrode and their applications. This thesis involves five chapters. Chapter 1 is an introduction of research background and research direction. In Chapter 2, the electrochemical synthesis of bis(terpyridine)iron network complex on glassy carbon and its application in electric energy storage are described. In Chapter 3, the preparation of bis(terpyridine)iron network-carbon nanotube hybridized material and its energy storage application are included. In Chapter 4, the electrochemical synthesis of ultra-long bis(terpyridine)metal molecular wire and their characterizations are explained. Chapter 5 is the conclusion of this thesis.

In chapter 1, the research background is introduced. First, the chemical properties, synthetic methods and various applications of bis(terpyridine)metal complexes, such as molecular electronics, light harvesting units and sensors, are explained. Second, several surface modification methods and their characteristics are introduced. Third, the distinguishing feature of supercapacitors and their preparations are described. Forth, molecular electronics and their operation theory are introduced. Finally, the aim of this thesis, using electrochemical polymerization methods to prepare functional complex polymers on carbon, is explained.

In Chapter 2, a bis(terpyridine)iron network complex was synthesized via electrochemical polymerization on a glassy carbon electrode. This network complex shows high capacity retention at high scan rates. When scan rate increases to  $10 \text{ Vs}^{-1}$ , the capacity only decreases by 24% compared with scan rate of  $0.025 \text{ Vs}^{-1}$ . Moreover, it can be charged to 80% in 0.08 s, 90% in 0.16 s and 95% in 0.35 s. On the other hand, the charged material can be discharged to 80% in 0.08 s, 90% in 0.16 s and 95% in 0.62 s. Finally the network complex is highly stable for continuous charging and discharging process. After 3000 cycles, the capacity of this network only decreases 5%.

In Chapter 3, the bis(terpyridine)iron network complex was successfully immobilized on a carbon nanotube porous electrode. This complex network-carbon nanotube hybridized material also can be charged and discharged at high scan rates and shows good stability under continuous operation. Moreover, as the carbon nanotube electrode provides much higher effective surface area, the areal capacitance of this

hybridized material increases dramatically comparing with only the network complex on glassy carbon.

In Chapter 4, ultra-long bis(terpyridine)metal complex wires arrays on carbon electrodes were synthesized by electrochemical polymerization. Their chemical structures were characterized to be a linear rigid wire with azobenzene bridging by Raman spectroscopy. From AFM measurements, the molecular wire arrays show uniform length structure on electrode surface. On the other hand, this electrochemical method also can produce very long molecular wire. The longest one is found to be 7410 layers and corresponds to 14.82  $\mu\text{m}$ , which is the longest bis(terpyridin)metal complex wire known. Moreover, according to electrochemical measurements, electrons in this wire can move freely, although it is longer than 14  $\mu\text{m}$ . Finally, this electrochemical method also can synthesize hetero metal wires on carbon electrodes, which show unique diode properties. In short, this electrochemical method can not only efficiently generate long molecular wires, but can also be used to link different molecule components to form a molecular device.

In Chapter 5, the researches of this thesis are concluded.

## Table of content

<b>Chapter 1 General introduction</b> .....	<b>1</b>
1.1 Bis(terpyridine)metal complexes .....	2
1.1.1 Chemical properties of terpyridines and bis(terpyridine) metal complexes ....	3
1.1.2 Terpyridine syntheses.....	7
1.1.3 Bis(terpyridine)metal complex syntheses .....	9
1.1.4 Applications of bis(terpyridine)metal complexes .....	11
1.2 Molecular engineering and surface modification .....	14
1.2.1 Molecular self-assembly .....	16
1.2.2 Stepwise surface modifications .....	19
1.2.3 Electrochemical polymerizations .....	22
1.3 Supercapacitors .....	24
1.3.1 Carbon nanotube based supercapacitors .....	26
1.3.2 Graphene based supercapacitors .....	28
1.4 Molecular scale electronics.....	30
1.6 The aim of this thesis .....	32
1.7 References.....	33
<b>Chapter 2 Electrochemical syntheses of bis(terpyridine)iron network complex     covalently bound to glassy carbon</b> .....	<b>41</b>
2.1 Introduction.....	42
2.2 Experimental section.....	45
2.2.1 Materials.....	45
2.2.2 Instruments .....	45
2.3 Results and discussion .....	47
2.3.1 Synthesis of the monomer complex for electrochemical polymerization .....	47
2.3.2 Electrochemical synthesis of the network complex on a glassy carbon electrode .....	48
2.3.3 The investigation of the role of oxygen in the electrochemical polymerization .....	51
2.3.4 The mechanism of the electrochemical polymerization reaction.....	53

2.3.5 Surface structure characterization of the network complex .....	56
2.3.6 Energy storage performance of the network complex .....	58
2.3.7 Chronocoulometry and chronoamperometry investigation.....	61
2.3.8 The stability of the network complex.....	65
2.4 Conclusion .....	67
2.5 References.....	68

### **Chapter 3 Bis(terpyridine)iron network complex-carbon nanotube hybridized**

<b>materials.....</b>	<b>71</b>
3.1 Introduction.....	72
3.2 Experimental section.....	73
3.2.1 Materials.....	73
3.2.2 Instruments .....	73
3.3 Results and discussion .....	74
3.3.1 Preparation of carbon nanotube electrode.....	74
3.3.2 The electrochemical synthesis of the complex network on the carbon nanotube electrode .....	77
3.3.3 Electrochemical evaluation of the hybridized material of the network complex and carbon nanotube .....	78
3.3.4 The capacity analyzed by chronocoulometry.....	82
3.3.5 The stability test of the hybridized material.....	84
3.4 Conclusion .....	86
3.5 References.....	87

### **Chapter 4 Electrochemical syntheses of ultra-long bis(terpyridine)metal complex**

<b>wires covalently bound to carbon.....</b>	<b>89</b>
4.1 Introduction.....	90
4.2 Experimental section.....	91
4.2.1 Materials.....	91
4.2.2 Instruments .....	91
4.3 Results and discussion .....	92
4.3.1 The syntheses of extremely long molecular wires .....	92
4.3.2 The anchor group of the electrochemically synthesized molecular wire .....	95

4.3.3 The structure of the electrochemical synthesized molecular wire .....	97
4.3.4 The surface structure of the molecular wire modified electrode.....	100
4.3.5 The formation mechanism of the molecular wire .....	102
4.3.6 Surface coverage of the molecular wire on the electrode .....	103
4.3.7 Synthesis of the longest bis(terpyridine)iron molecular wire .....	107
4.3.8 Characterization of the longest molecular wire.....	109
4.3.9 Hetero metal wires .....	111
4.4 Conclusion .....	114
4.5 References.....	115
<b>Chapter 5 Concluding remarks.....</b>	<b>117</b>
<b>Acknowledgement.....</b>	<b>121</b>



# **Chapter 1**

## **General introduction**

## 1.1 Bis(terpyridine)metal complexes

Bis(terpyridine)metal complexes are regarded as one of the best building blocks of molecular devices and supermolecules. The reasons are that first, bis(terpyridine) complexes show very high stability in harsh conditions, such as low pH solutions and oxidizing or reducing environments. Second, the syntheses of bis(terpyridine)metal complexes are often easy and quick, and a very wide spectrum of terpyridine ligands are available. Third, bis(terpyridine)metal complexes possess very unique physical and chemical properties.<sup>1</sup> Therefore, after 1990, more and more researches are focused on them. (Figure 1-1 & Figure 1- 2)<sup>2, 3</sup>

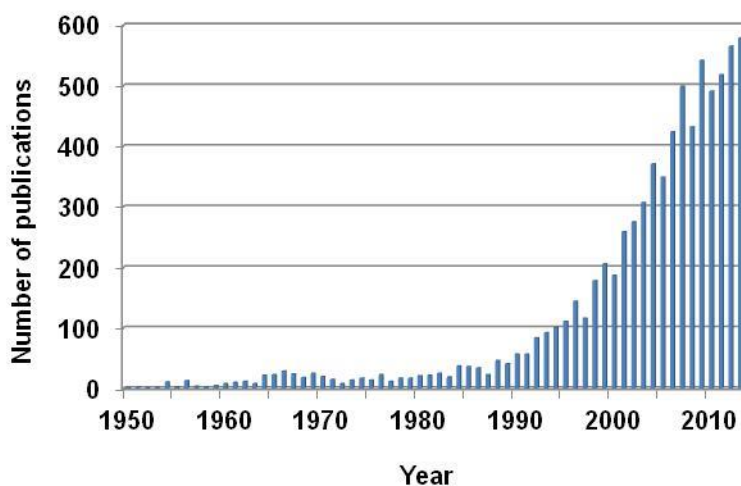


Figure 1-1 Publications related to terpyridine from 1950 to 2013.

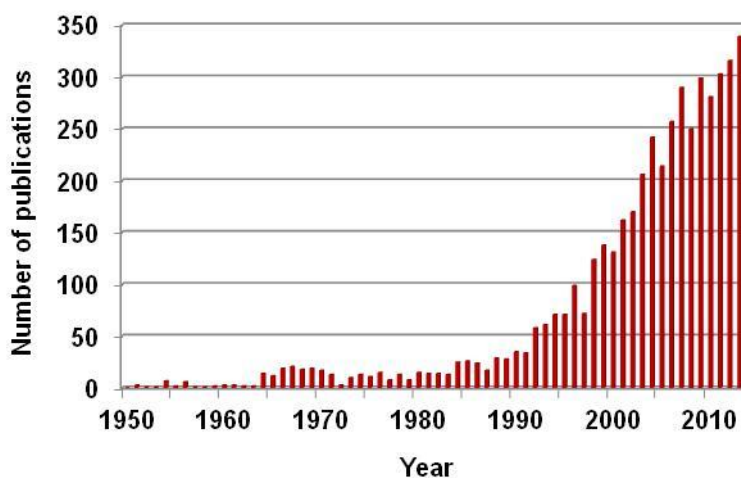
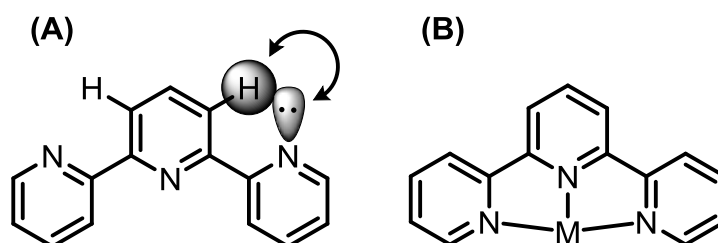


Figure 1- 2 Publications related to terpyridine complexes from 1950 to 2013.

### 1.1.1 Chemical properties of terpyridines and bis(terpyridine) metal complexes

2,2':6',6-Terpyridine is a tridentate chelating ligand consisting of three pyridines linked through carbon atoms on the ortho positions of the nitrogen atom in the aromatic ring (**Figure 1-3**). It is one of the most commonly used polypyridine ligands. Most terpyridines in the solid state have a *trans, trans*-configuration<sup>4</sup> because of the intramolecular C-H...N hydrogen bonding.<sup>5</sup> However, when it coordinates to a metal ion, the structure will change to a *cis, cis*-configuration and three nitrogen atoms will chelate to the same metal center.<sup>6</sup>



**Figure 1-3** The intramolecular hydrogen bonding of terpyridine and chemical structures of a terpyridine complex.

Pyridine is a common sub-structure in organic compounds, bio-active molecules and metal complexes.<sup>7</sup> Pyridine is a relatively weak base but a good catalyst for many reactions,<sup>8</sup> because of its reversible reactions with electrophiles. On the other hand, in coordination chemistry, pyridine is a relatively weak  $\sigma$ -donor but a good  $\pi$ -accepter.<sup>9</sup> From the molecular orbital diagram (**Figure 1-4** & **Figure 1-5**),<sup>10</sup> the lowest unoccupied orbital of pyridine  $\psi_4$  can fit to the  $d_{yz}$  orbital of a metal and form a suitable overlap. Therefore, in the complexes, the transition metal center can strongly back donate through the  $d$ - $\pi^*$  back bonding.

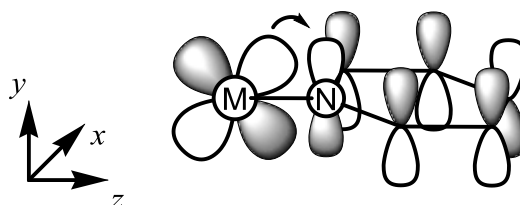


**Figure 1-4** The  $d$ - $\pi^*$  back bonding in a transition metal pyridine complex.

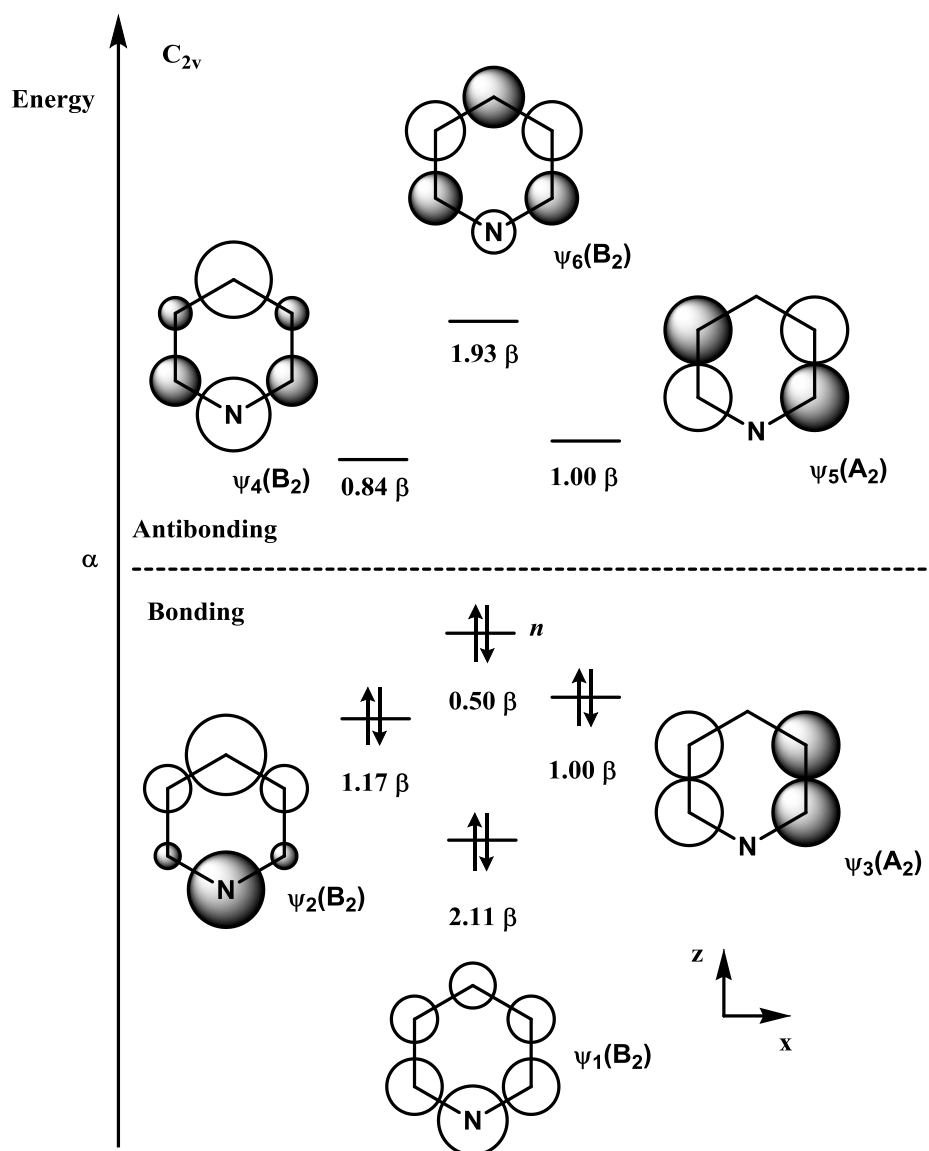


Figure 1-5 Orbitals of pyridine.<sup>10</sup>

The back bonding effect is the first reason why terpyridine complexes can be so stable. The other reason is a chelating effect. The stability constants of various bipyridine and terpyridine metal complexes are shown in **Table 1-1**.<sup>11</sup> Bipyridine and terpyridine ligands are regarded to have similar physical and chemical properties. However, when the coordination ligand changes from bidentate to tridentate, the stability constant  $K$  increase to a large extent, especially in the cases of  $\text{Fe}^{2+}$ ,  $\text{Co}^{2+}$  and  $\text{Ni}^{2+}$ . This indicates that terpyridine can stabilize metal ions much better than bipyridine.

Terpyridines can not only coordinate to normal valence transition metals, but also can stabilize metal species with lower or higher oxidation states. From electrochemical measurements, bis(terpyridine)metal complexes can show multi-electron redox reactions in solution (**Table 1-2**).<sup>12,13</sup> These complexes can remain stable from  $\text{M}^{3+}$  to  $\text{M}^{1-}$  state, and sometimes metals with much lower oxidation states such as  $\text{M}^{2-}$  and  $\text{M}^{3-}$  can also be observed. On the other hand, a series of  $\text{Cr}(\text{tpy})_2(\text{PF}_6)_n$  complexes with  $n = 3-0$  were prepared and isolated in the Wieghardt group in 2012.<sup>14</sup> Moreover, two extra zero valence bis(terpyridine)metal complexes using Ti and V were synthesized successfully in 2013.<sup>15</sup>

The reason why these unusual low valence complexes are stable is that the strong back bonding causes extra electron density to be located on terpyridine ligands from the metal ion. Therefore, electrochemical reductions involving low valence complexes are often regarded as terpyridine ligand reductions rather than metal center reductions.

**Table 1-1 Thermodynamic data of bipyridine and terpyridine complexes at 25°C<sup>11</sup>**

Metal ion	Ligand	Log K <sub>1</sub>	ΔH	Log β <sub>n</sub> <sup>a</sup>
Mn <sup>2+</sup>	bipy	2.6	3.5	
	terpy	4.4	5.6	
Fe <sup>2+</sup>	bipy	4.3	(6.0) <sup>b</sup>	17.5
	terpy	7.1	8	20.9
Co <sup>2+</sup>	bipy	5.7	8.2	16.1
	terpy	8.4	10.7	18.3
Ni <sup>2+</sup>	bipy	7.1	9.6	20.1
	terpy	10.7	9.5	21.8
Zn <sup>2+</sup>	bipy	5.2	7.1	
	terpy	6	10.1	
Cd <sup>2+</sup>	bipy	4.3	5.1	
	terpy	5.1	5.5	

<sup>a</sup> β<sub>n</sub> = K<sub>1</sub>K<sub>2</sub>K<sub>3</sub> for bipy and K<sub>1</sub>K<sub>2</sub> for terpy. <sup>b</sup> Estimated.

**Table 1-2 The redox potential of bis(terpyridine)metal complexes<sup>12,13</sup>**

	3+/2+	2+/1+	1+/0	0/-1	-1/-2	-2/-3
Cr(tpy <sup>1</sup> ) <sub>2</sub> <sup>b</sup>	-0.414	-0.834	-1.334	-2.254	-2.514	-2.714
Mo(tpy <sup>1</sup> ) <sub>2</sub> <sup>b</sup>	0.426	-0.604	-1.064			
W(tpy <sup>1</sup> ) <sub>2</sub> <sup>b</sup>	0.116	-0.464	-0.864			
Mn(tpy <sup>2</sup> ) <sub>2</sub> <sup>c</sup>	0.922	-1.378	-1.678	-2.228	-2.378	
Fe(tpy <sup>2</sup> ) <sub>2</sub> <sup>c</sup>	0.782	-1.488	-1.608	-2.258	-2.538	
Ru(tpy <sup>2</sup> ) <sub>2</sub> <sup>c</sup>	0.982	-1.498	-1.738	-2.148	-2.498	
Ni(tpy <sup>2</sup> ) <sub>2</sub> <sup>c</sup>	1.312	-1.498	-1.698	-2.158	-2.318	
Co(tpy <sup>2</sup> ) <sub>2</sub> <sup>c</sup>	-0.018	-1.028	-1.848	-2.198	-2.288	
tpy <sup>1</sup> <sup>b</sup>				-2.434	-2.944	
tpy <sup>2</sup> <sup>c</sup>				-2.278	-2.678	

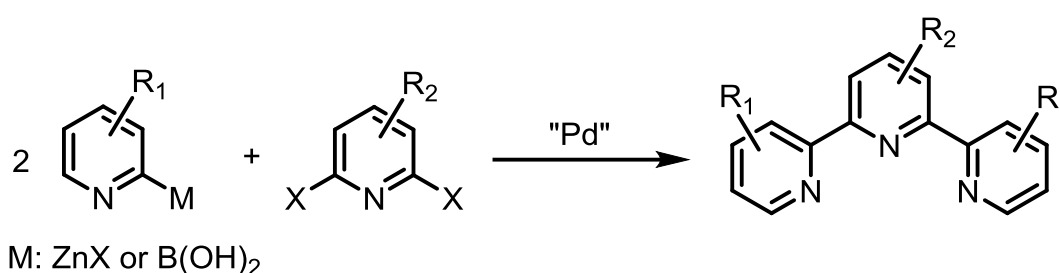
a. Potential (V) vs Ag/Ag<sup>+</sup>.

b. Reference 12; tpy<sup>1</sup>: 2,2':6',2''-terpyridine

c. Reference 13; tpy<sup>2</sup>: 4'-(*p*-tolyl)-2,2':6',2''-terpyridine

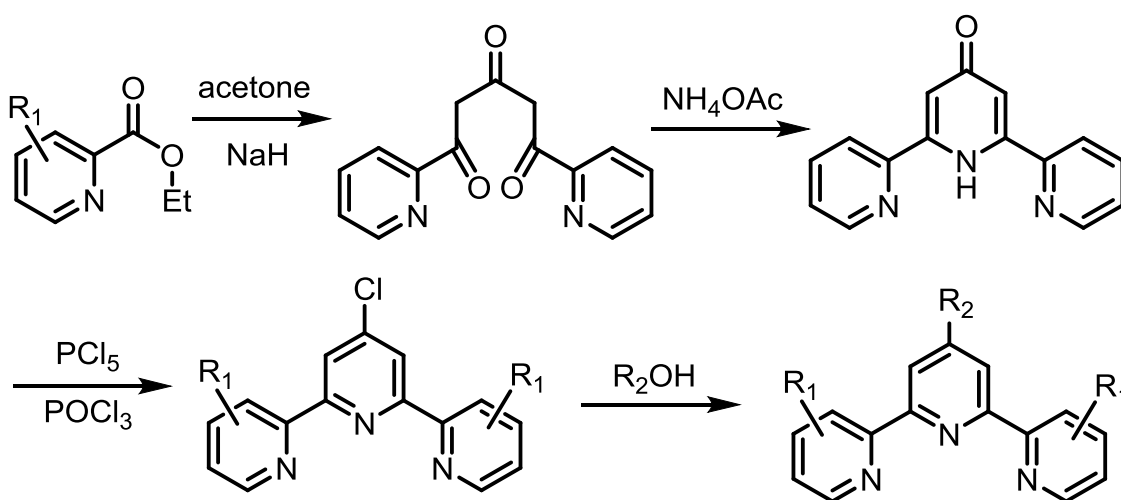
## 1.1.2 Terpyridine syntheses

Terpyridine can be synthesized from several methods.<sup>2,16</sup> First, they can be prepared using two equivalents of 2-halopyridine with one equivalent of 2,6-dihalopyridine by Suzuki or Stille coupling reactions (**Scheme 1-1**).<sup>17</sup> The 2-halopyridine is converted to boronic acids or organozinc complexes. These reagents then are coupled with 2,6-dihalopyridine with palladium catalysts. As the preparation of 2-halopyridine and 2,6-dihalopyridine are not so easy, this method is not the most popular way to synthesize terpyridine.



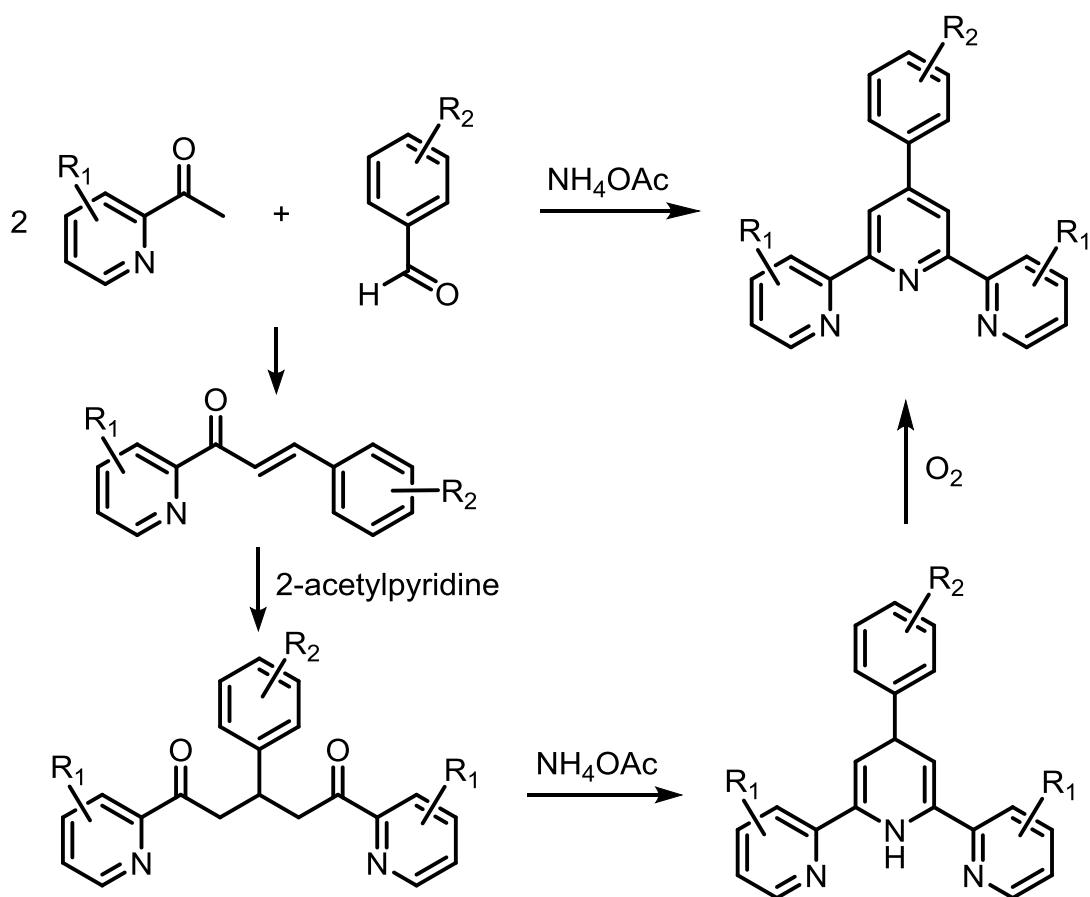
**Scheme 1-1** Syntheses of terpyridine via cross-coupling.

The second way is that ethyl picolinate reacts with acetone to form a 1,3,5-trione (**Scheme 1-2**).<sup>18</sup> This trione then is cyclized by treatment with ammonium acetate to produce pyridone. Finally, 4'-chloro-2,2':6,2''-terpyridine can be generated by reacting with PCl<sub>5</sub> and POCl<sub>3</sub>. 4'-Chloro-terpyridine is a useful intermediate for the preparation of other terpyridine with substituent groups on the center pyridine ring.



**Scheme 1-2** Syntheses of terpyridine through pyridone.

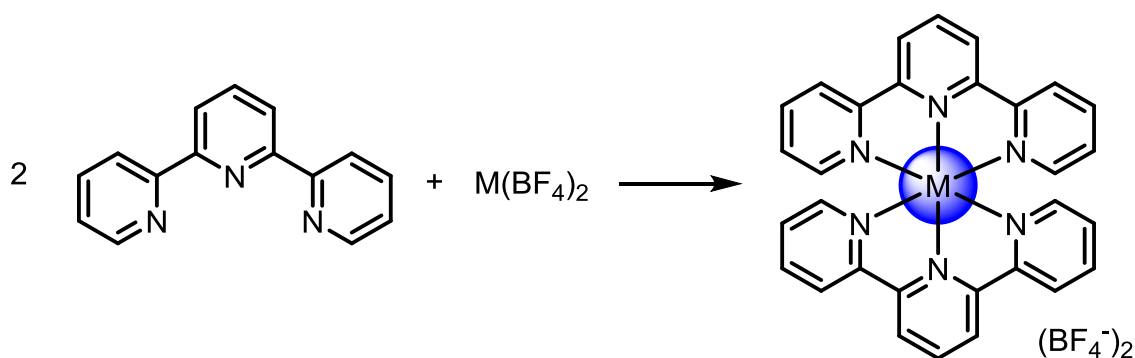
The third method is the most commonly used and has the shortest synthetic route (**Scheme 1-3**).<sup>19</sup> It can be carried out by treating two equivalents of 2-acetylpyridine and one equivalent of aromatic aldehyde with ammonium acetate at high temperature. This reaction also can be done by first treating with strong bases, such as sodium hydride or sodium hydroxide, followed by an excess amount of ammonia solution. Mechanistically, 2-acetylpyridine will be deprotonated and attack the aromatic aldehyde in an aldol condensation reaction. Then, 1,4-addition reaction will occur on the resulting intermediate by attacking 2-acetylpyridine again to form a dione. This dione will be cyclized by ammonia and oxidized by atmospheric oxygen to generate the center pyridine. The advantage of this reaction is that 4'-aryl-terpyridine can be readily prepared. However, the downside of this reaction is that only aromatic aldehydes can be easily incorporated. Therefore, if the target ligand is a terpyridine without a 4'-aryl substitution, it should be synthesized from the other two methods.



**Scheme 1-3** Syntheses of terpyridines from 2-acetylpyridines and arylaldehydes.

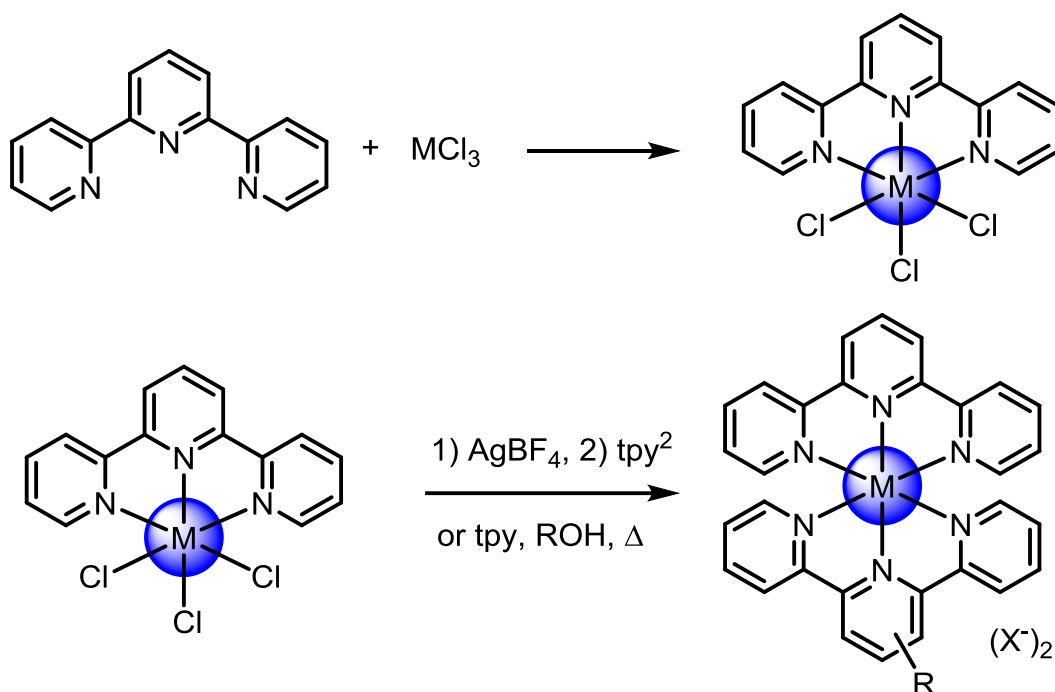
### 1.1.3 Bis(terpyridine)metal complex syntheses

Bis(terpyridine)metal complexes can be synthesized using two major methods.<sup>20,21</sup> One is by using metal salts with low coordination affinity counter anions, such as  $\text{BF}_4^-$  and  $\text{NO}_3^-$ , reacted with two equivalents of terpyridine in solution (**Scheme 1-4**).<sup>22</sup> In the reaction, terpyridine displaces these anions or solvent molecules from the metal center directly without the assistance of other reagents or heating. This method can provide bis(terpyridine)metal complexes efficiently in one step. However, it is impossible to stop the reaction at the mono-terpyridine coordinated intermediate and to prepare hetero-ligand bis(terpyridine) complexes.



**Scheme 1-4 One-step syntheses of bis(terpyridine)metal complexes.**

The other method is by employing metal salts with ligands having strong coordination affinity, for example,  $\text{RuCl}_3$  and  $\text{FeCl}_3$  (**Scheme 1-5**).<sup>23</sup> As chloride bonds strongly to the metal centers, when these salts react with terpyridine, only solvent molecules coordinated to the metals will be displaced, and mono-terpyridine complexes,  $(\text{tpy})\text{MCl}_3$ , will form. These complexes are stable and can be isolated and used. Therefore, they are often used to synthesize hetero-ligand bis(terpyridine)complexes.<sup>23b</sup> However, because the coordination affinity of the chloride ions on trivalent metals is too high to be displaced directly, stronger reaction conditions or reagents are necessary.



**Scheme 1-5 Two-steps syntheses of bis(terpyridine)metal complexes.**

As with most metal halide coordination compounds,  $(tpy)MCl_3$  can be activated by removing the coordinated chloride by treatment with silver reagents such as  $AgBF_4$  or  $AgNO_3$ .<sup>24</sup> After removing silver chloride by filtration, the activated complexes can react with one more equivalent of terpyridine to generate bis(terpyridine)complexes. The other way is by treating these mono-terpyridine complexes with another equivalent of terpyridine in methanol or ethanol under higher temperature.<sup>24b</sup> Under this condition, the trivalent metal centers will be reduced to divalent, decreasing the bond strength of  $M-Cl$ . This facilitates the substitution of coordinated chloride with terpyridine to form bis(terpyridine) complexes. These two methods can be employed to prepare complexes which have no metal sources with weakly coordinated ligands. They are also suitable for preparing hetero-ligand bis(terpyridine) metal complexes, because the mono-terpyridine complexes can be obtained easily by these methods.

### 1.1.4 Applications of bis(terpyridine)metal complexes

Bis(terpyridine)metal complexes have unique physical and chemical properties. Therefore, they have high application potential in photosensitizers,<sup>25,26</sup> sensors,<sup>27</sup> catalysts,<sup>28</sup> molecular electronic components<sup>29,30</sup> and so on. In practical applications, tris(bipyridine)metal complexes show higher luminescence quantum yield than bis(terpyridine) complexes. However, when complexation reactions are carried out, several isomers of tris(bipyridine) complexes are produced, including diastereomers and enantiomers (**Figure 1-6**).<sup>31</sup> They are sometimes difficult to separate from one another. The preparation of optical pure complexes usually requires some special chiral templates.<sup>32</sup> This makes molecular design and construction difficult. Therefore, bis(terpyridine)complexes are considered better building blocks for photo-active molecules.

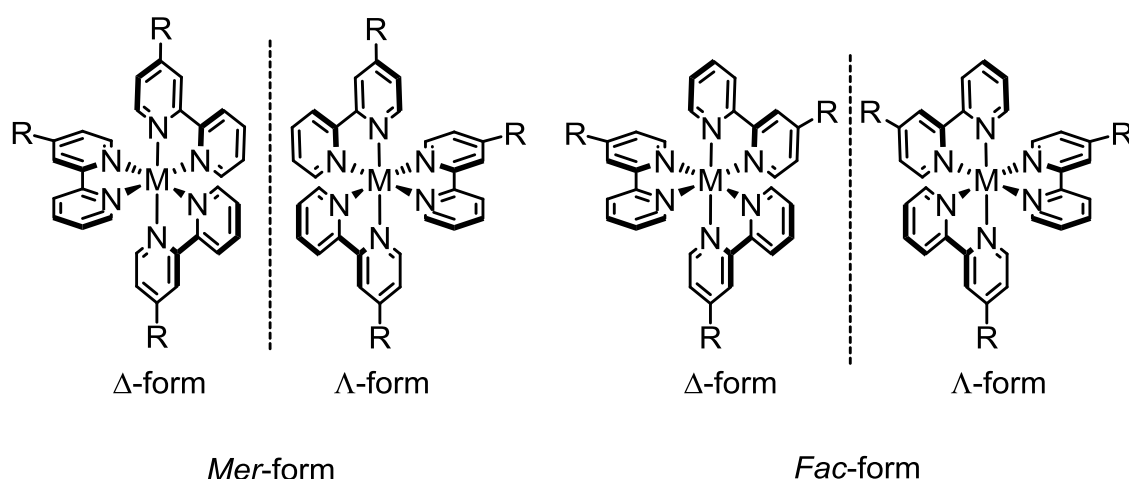


**Figure 1-6** Isomers of tris(bipyridine)metal complexes.

In bis(terpyridine)metal complexes, ruthenium, osmium and iridium<sup>33</sup> complexes are the most promising for applications, because they show good stability, reversible redox responses and relatively high luminescence quantum yields. All these three complexes can be synthesized readily by the two-step method from their chloride salts (**Scheme 1-5**). As this method can offer hetero-ligand bis(terpyridine) complexes without other isomers, the design and construction of a complicated molecule becomes much easier compared to tris(bipyridine) complexes.

These complexes have been incorporated into many molecular systems as light harvesting components. For example, the Åkermark group and the Sun group employed a bis(terpyridine)ruthenium complex as a photosensitizer in a modeling system of iron hydrogenase (**Figure 1-7**).<sup>34,35</sup>

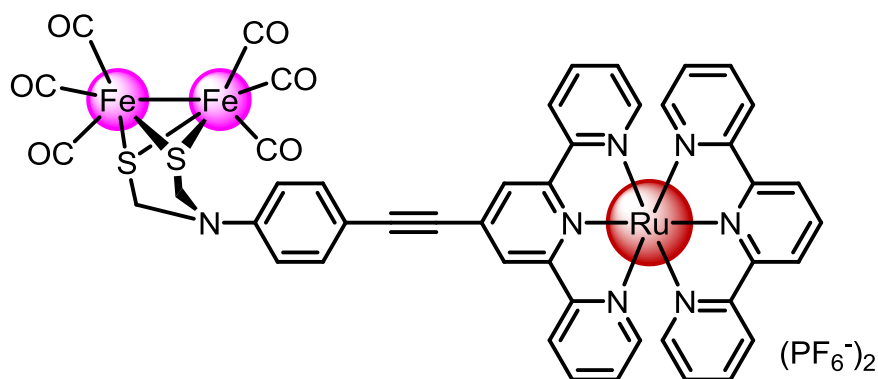


**Figure 1-7** A model molecule of iron hydrogenase with ruthenium photosensitizer.

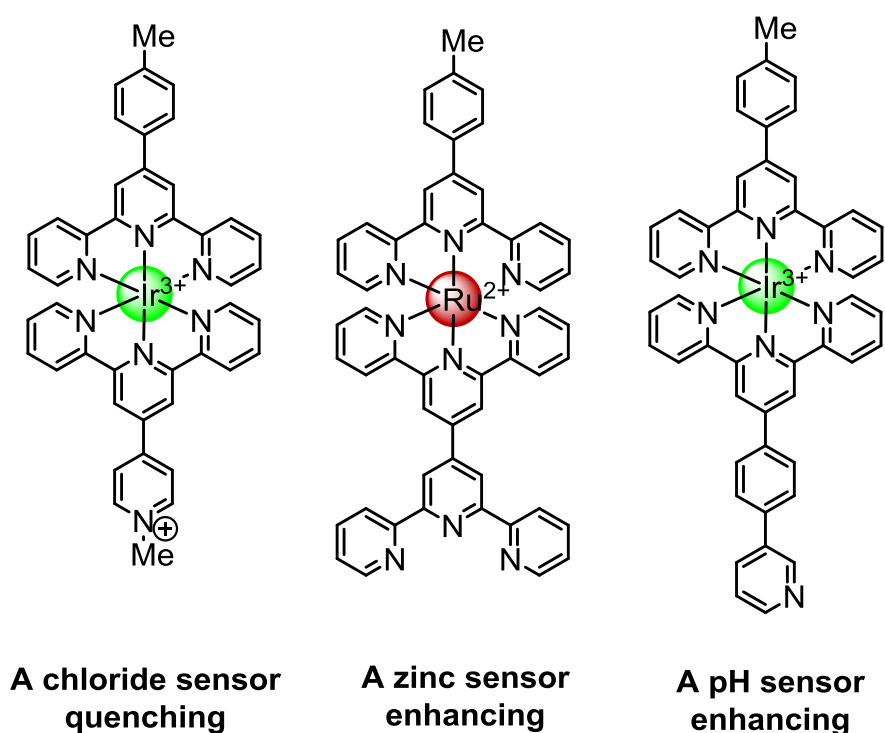


**Figure 1-8** Bis(terpyridine)metal complex-based ion sensors.

The luminescence properties also can be used to design molecular sensors for cations,<sup>36</sup> anions,<sup>37</sup> and pH.<sup>38</sup> This is because the association of some ions can cause changing in luminescence behavior (**Figure 1-8**). For instance, bis(terpyridine)iridium-methylpyridine salt was used as a chloride ion detector.<sup>37</sup> This complex exhibits luminescence quenching when treated with chloride. A bis(terpyridine)ruthinium-terpyridine can function as a zinc ion sensor, because this compound shows increased luminescence when zinc coordinates to the terpyridine moiety.<sup>36d</sup> The final example is a bis(terpyridine)iridium-pyridine. Its proton responsiveness allows it to be a pH sensor.<sup>38</sup>

Another important application of terpyridine is a component of molecular electronics. Because of their special electronic properties, bis(terpyridine)metal complexes can be used in molecular wires, molecular transistors, memories and spintronics. The bis(terpyridine)metal complex molecular wire is one of the best demonstration of their applications in molecular electronics. These complex wires show much better electron transport abilities than organic backbone wires and wires using other types of complexes. Due to these reasons, bis(terpyridine)metal complexes can not only be good frameworks for molecular architectures, but are also excellent functional centers for molecular devices.

## 1.2 Molecular engineering and surface modification

Molecular engineering is a fundamental research to construct and control molecular scale systems.<sup>39</sup> This topic relates to a very wide spectrum of research from traditional chemical syntheses to single molecule manipulations. In the recent decades, nano-functional material construction has become more and more popular than others, because of the pursuit of realizing molecular scale computers<sup>40</sup> and highly efficient molecular devices.<sup>41</sup> Therefore, many new physical and chemical methods have been developed for applications in synthesizing and controlling nano-systems.

The reason why molecular engineering is important in achieving high performance material is the synergistic effect of a well designed molecular structure and intramolecular arrangement (**Figure 1-9**).<sup>41</sup> In traditional polymers and convention molecular devices, molecules are only in random arrangement, because of the limitation in their preparation processes. In this situation, unique single-molecule properties are often cancelled out by other identical molecules. In order to improve the performance and show the special single molecule behaviors for particle applications, rendering material with an ordered nano-structure is critical. This is also the reason why finding an efficient method of controlling molecules at nanoscale is highly desirable.

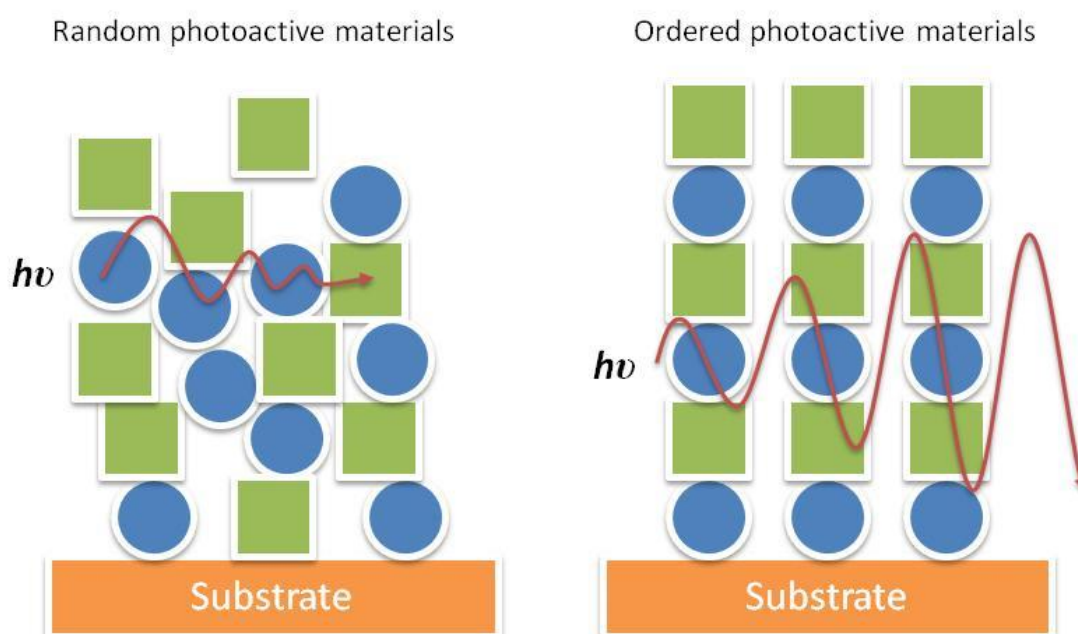


**Figure 1-9** Illustration of the synergistic effect of an ordered material.

To achieve molecular scale systems, there are two methods: one is the top-down method<sup>42</sup> and the other is the bottom-up method (**Figure 1-10**).<sup>43</sup> Top-down methods have been well developed in silicon-based integrated circuit processes. They use photolithoetching to construct micro- to nano-scale circuits. This technique enables all existing computing devices to allow high calculation speed. However, due to the optical limitation of lithography and gate leakage, fabricating circuits smaller than ten nanometers is almost impossible.<sup>44</sup>

On the other hand, bottom-up methods use atoms and molecules to assemble nano-sized devices and functional materials.<sup>45</sup> In this method, some efficient chemical reactions and physical techniques are employed to build up and control molecular groups. Although these technologies have been developed since a long time ago, with the invention of scanning probe microscopy (SPM) scientists can observe the three dimensional structure of these nano-systems and manipulate single molecules at the nanoscale.<sup>46</sup>

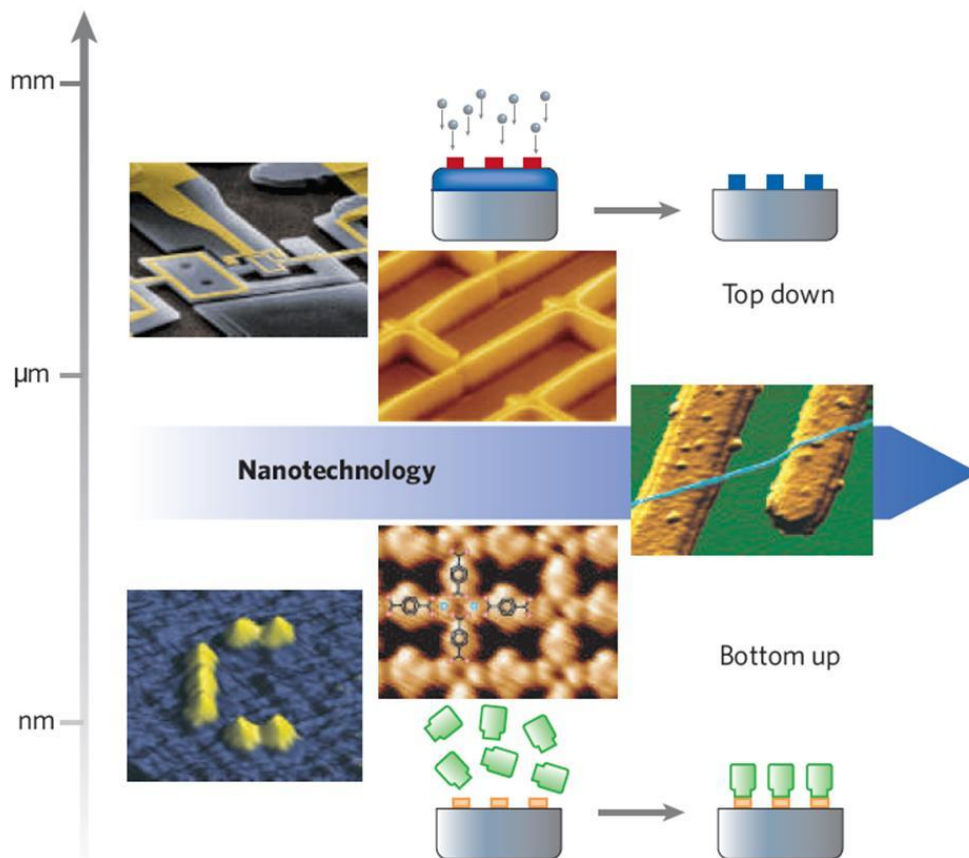


**Figure 1-10** The achievement of top-down and bottom-up techniques.<sup>43</sup>

## 1.2.1 Molecular self-assembly

One of the most commonly used methods to fabricate a well ordered nano-system on a large surface is self-assembly.<sup>47</sup> Self-assembly is a very unique natural phenomenon, especially at the interface. Among them, one of the most focused systems is the interface of a solid substrate. Usually, the substrate used for self-assembling systems should be materials which can bond reversibly with a required surface modification molecule.<sup>48</sup> This is because reversible coordination reactions allow reorganization of the adsorbed molecules. Materials having this property are metals, such as copper,<sup>49</sup> silver,<sup>50</sup> gold<sup>51</sup> or platinum,<sup>52,53</sup> metal oxides, such as aluminum oxide,<sup>54</sup> titanium oxide, zirconium oxide<sup>55</sup> or indium tin oxide,<sup>56</sup> and semiconductors, for instance, gallium arsenide.<sup>57</sup> On the other hand, some molecules which can form covalent linkages with the substrate surface are also used to fabricate self-assembled monolayers. For example, organotrimeoxysilane and organotrichlorosilane are used to modify glass, metal oxide<sup>58</sup> and silicon surface.<sup>59</sup> However, because these organosilane compounds react with not only the substrate, but also water to be hydrolyzed to form organosilicate materials on the surface, sometimes multi-layer or defect structures are generated.

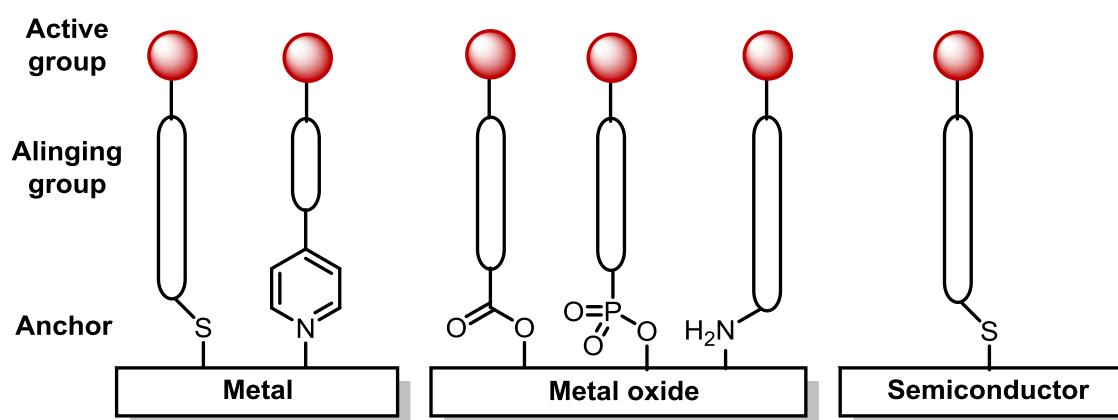


**Figure 1-11** The active functional groups for self-assembling on substrates.

On the other hand, the molecules used in the self-assembly process usually have an anchor part, such as a thiol or a pyridine group for metal substrates and carboxylic acid and phosphoric acid for metal oxide; an aligning group, for example a long alkyl chain; in some cases, a active group will also be incorporated in it, such as electrochemically-active molecules, photo-active groups and so on (**Figure 1-11**).<sup>48</sup> The molecular monolayer can be generated on a clean substrate surface by simply immersing the substrate in a diluted solution of the molecule for self-assembly. In some

cases, more than one type of surface molecules are required to generate special functions. Therefore, the treated substrate will probably be treated by another solution of functional molecules. From this method, a surface containing one or more type of molecules immobilized on it can be easily prepared. Furthermore, by altering the process, different surface structures can also be achieved.

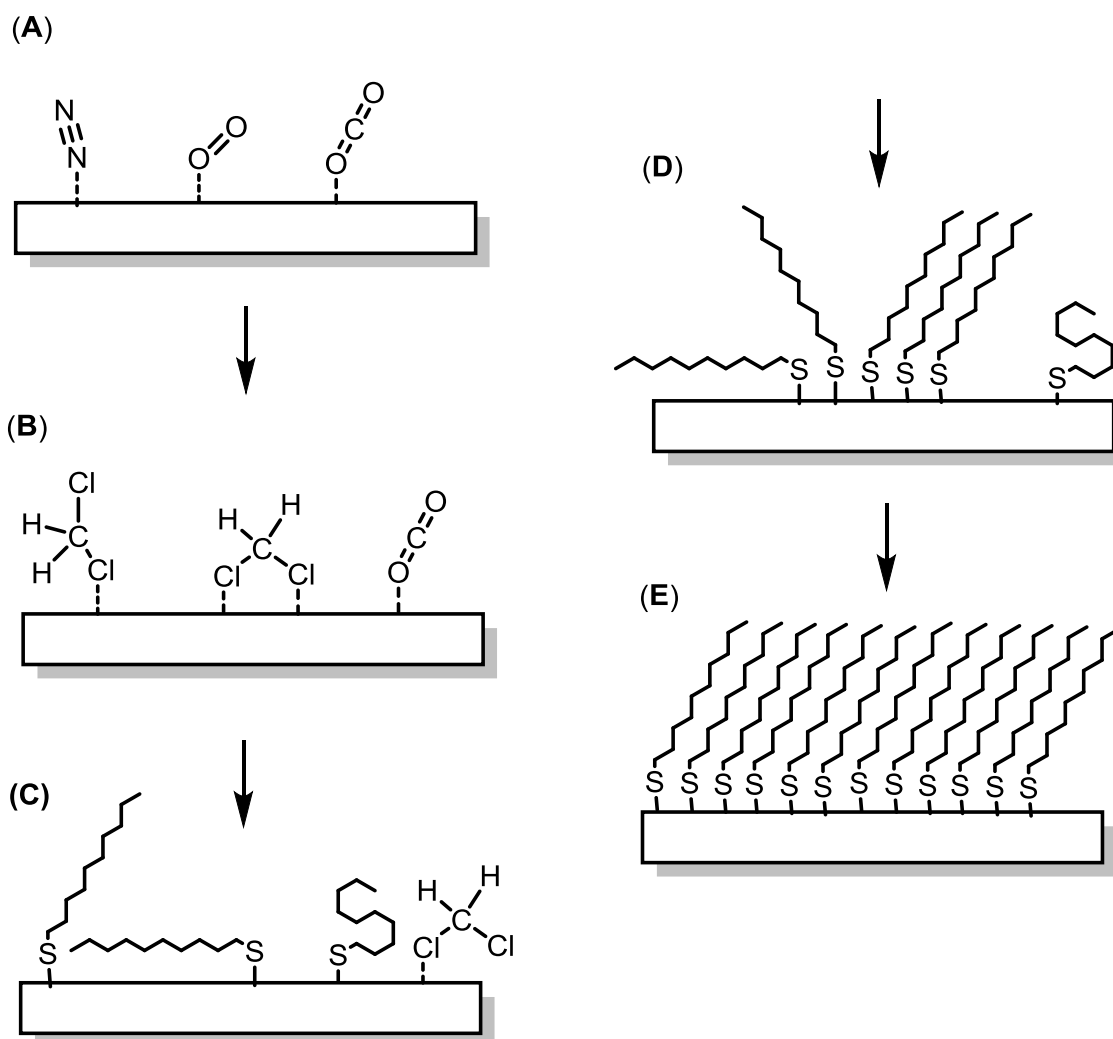


**Figure 1-12 The formation mechanism of self-assembled monolayer on substrate surface.**

In the formation of self-assembled monolayers, the most important aspect is having a reversible coordination reaction on the substrate surface. In this way, a wrongly oriented or coordinated molecule can be redirected and moved to the correct position during the process. If we observe the formation process of a self-assembled monolayer in greater

detail, the mechanism can be considered as following (**Figure 1-12**).<sup>60,61</sup> First, solvent molecules coordinate onto the bare substrate or displace adsorbed air molecules to form a solvated surface. Second, a small amount of the required molecule comes to the surface and kicks out the adsorbed solvent to generate a surface with randomly coordinated molecules. Third, more and more molecules reach the surface and occupy more coordination site of the substrate. As the surface density of the molecule increases, they start to orient vertically, and also due to the interaction between adjacent molecules, a well ordered array structure appears. Finally, almost the entire surface is covered by the molecule and a ligand exchanging steady state is reached.

## 1.2.2 Stepwise surface modifications

Self-assembled monolayers not only modify the nano structure of a surface, which alters substrate properties, but also they can be the foundation of other surface molecular architectures to fabricate more complicated functional molecular systems. Among them, stepwise surface reactions are one of the most useful processes to construct and control a functional nano-system based on a self-assembling molecular layer.<sup>62</sup> They are elegant bottom-up construction techniques of nano-structures. Stepwise methods can elongate the surface structure efficiently. Also, the properties of the surface nano-systems can be changed easily by using different monomer units. Therefore, surface molecular systems can be designed and fabricated smoothly by this method.

There are two main groups of stepwise synthetic methods. One is based on organic reactions.<sup>63</sup> The other is based on coordination reactions.<sup>64</sup> The difference between these two methods is not only the reaction types they employ but also where the connection points are between two molecular units. In organic stepwise syntheses, one of the most used reaction types is condensation reactions (**Figure 1-13**). This is because condensation reactions can proceed under mild conditions and water is the sole byproduct. Moreover, the resulting linkage structure is usually a double bond conjugated to the  $\pi$  systems of both wire component units. This is important for connecting the electronic systems of both molecules adjacent to the bond to one another.

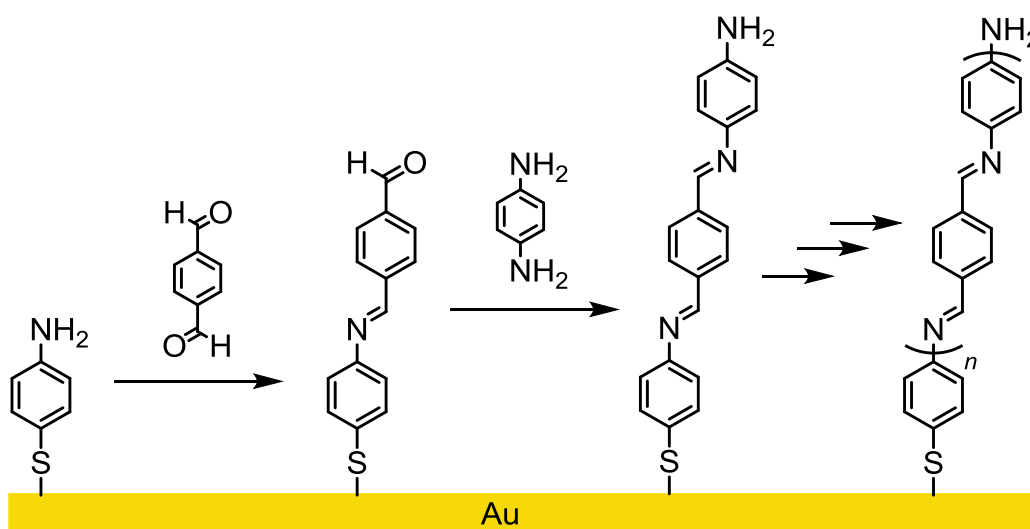


**Figure 1-13** A stepwise condensation reaction to synthesize organic backbone wires.<sup>63</sup>

On the other hand, stepwise coordination methods use coordination reactions to generate new bonds between bridging ligands and metal species to build up a larger molecular system (**Figure 1-14**). The function of surface nano-systems can be changed easily by simply modifying bridging ligands and altering metal species or their oxidation states. One advantage of stepwise coordination methods is that much more types of coordination bonds can be generated in stepwise constructions than in condensation reactions. The other advantage is that the complexes formed by stepwise coordination reactions can also act as functional centers in the nano-system, but the bonds generated in condensation reactions can only function as a simple connection between two molecules.

Generally, stepwise syntheses using organic condensation methods and coordination methods are similar. They can all be done by simply dipping a substrate into one reactant solution, washing, and then changing to another reactant solution. This process is repeated several times in these two solutions or in other solutions to produce the desired structure. The difference between these two methods is that organic condensation reactions usually use at least two types of monomers containing functional groups which can react with each other, but the coordination methods usually use one metal salt solution and one bridging ligand solution. In these methods, either linear or branched bridging ligands or monomers can be used to construct the desired structure. In this way, the structure of surface molecules can be extended to form a linear or branched wire or connected in a network to form a molecular circuits and functional molecular systems. They are important for linking functional molecules to achieve practical applications.

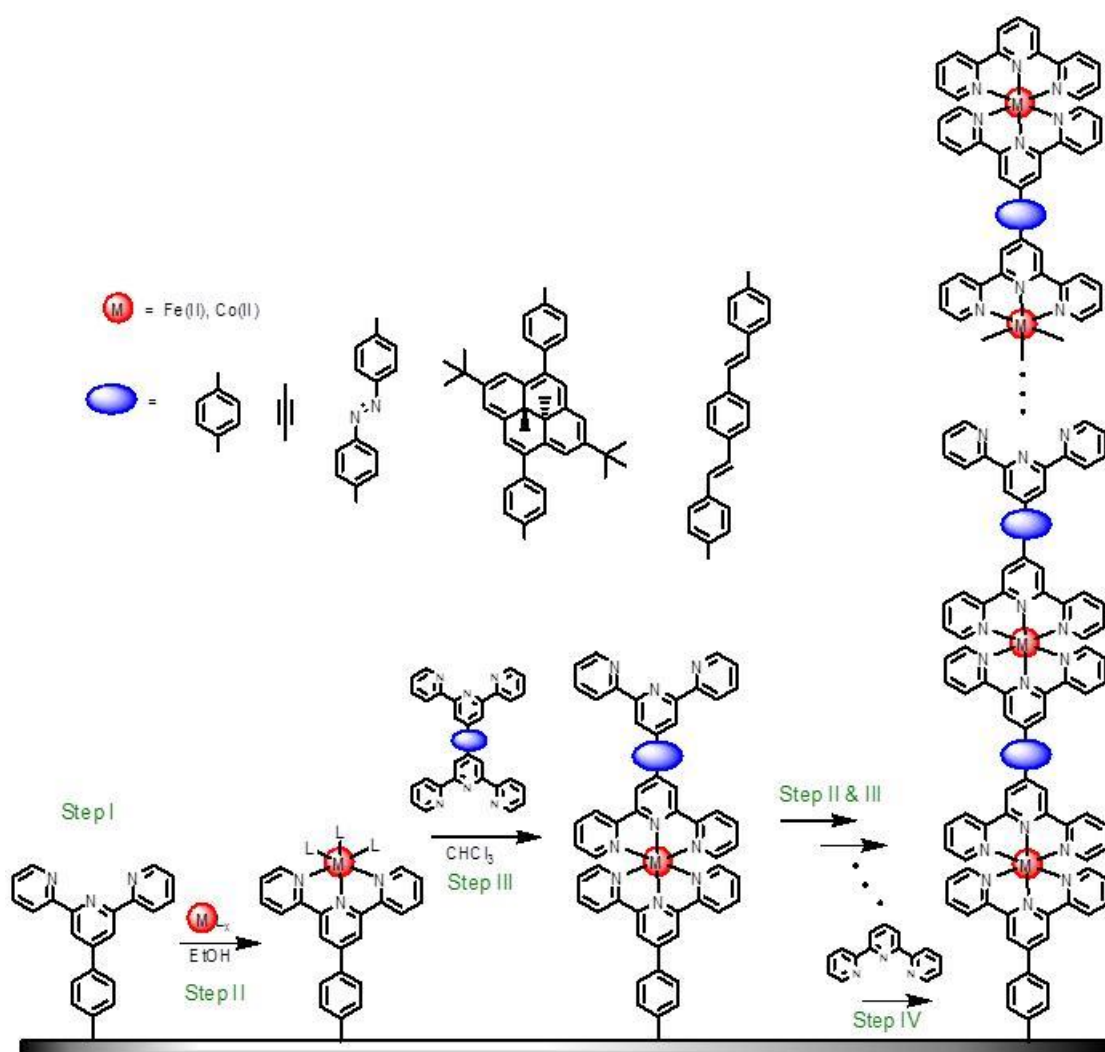
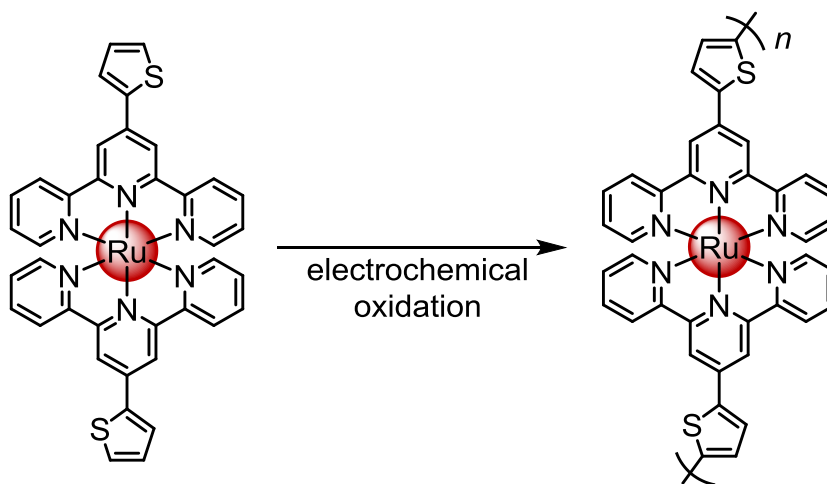


Figure 1-14 Stepwise coordination syntheses of molecular wires.

### 1.2.3 Electrochemical polymerizations

The third method to modify an electrode surface utilizes electrochemical procedures. Applying a suitable potential to an electrode immersed in a material precursor solution can coat the surface with a thin layer of the material. Electroplating is one of the most ancient applications of this method, which is usually used for coating a layer of metal on a substrate to change its exterior or to passivate it.

On the other hand, electrochemical treatments also can be used to generate a layer of organic material on a substrate.<sup>65</sup> Electrochemical polymerization is one type of these treatments, which can immobilize organic polymers on the electrode surface by electrochemical induction. These methods are especially useful for preparing conducting polymer films. To carry out these reactions, monomers are dissolved in an electrolyte solution and set in an electrochemical cell with a required substrate as the working electrode. Then a selected potential or a potential region is applied on the working electrode to produce a conducting polymer film on it.



**Scheme 1-6 Electrochemical polymerization of a thiophene complex.<sup>66</sup>**

The monomers used in electrochemical polymerizations usually have one or more active groups. When these molecules are subjected to an applied potential, the active group will convert to a cation, anion or free-radical which is immobilized on the electrode and reacts with other monomers. Finally, a polymer film will be formed and attached on the working electrode surface.

Active groups of the monomers which can be used in electrochemical polymerization are usually redox active groups such as alkene, alkyne, aniline, pyrrole and thiophene. One of the most commonly used active groups is thiophene, because its polymer exhibits high conductivity and after polymerization the thiophene group still exhibits redox active behavior (**Scheme 1-6**).<sup>66</sup>

As the generation of polymers is very efficient using electrochemical polymerization and the properties of the polymer can be controlled easily by altering electrochemical conditions, it is a very promising method for conducting molecular engineering of the electrode surface.

### 1.3 Supercapacitors

Supercapacitors are regarded as promising next generation energy storage devices, because they can keep relatively larger amounts of charge than traditional capacitors and can work at higher charging and discharging rates than secondary batteries.<sup>67</sup> Supercapacitors are a sub-group of capacitors. In traditional capacitors, they store energy by means of static electricity between two large area parallel electrodes. These two electrodes are separated by a thin insulating film or paper to prevent contact and discharge. However, when a charging potential which is too high is applied on the device, it will cause electric penetration and break the separation layer. Therefore, only a limited amount of charge can be kept within these capacitors.<sup>68</sup>

To overcome this problem, an electrolyte solution is placed between two electrodes and the separation layer is also changed to an ion-penetrable film.<sup>69</sup> Furthermore, a pair of porous carbon electrodes is used to replace aluminum electrodes. These changes bring forth a big increase of capacity, because during charging, electrolytes can adsorb on porous electrode surface to neutralize the static electricity and assist in keeping more charge on them. This layer of ions adsorbed on the electrodes is called the electrical double layer, which occurs in all electrochemical cells. This type of capacitors is named as double layer capacitor, which is a branch of supercapacitors.

The other branch of supercapacitors is pseudocapacitor, also called redox capacitor. The difference between double layer capacitor and pseudo capacitor is that there is a layer of redox active material on the electrode surface of pseudo capacitor.<sup>70</sup> This type of capacitor is a battery-like device, but it can be charged and discharged much faster than batteries. This is because the particle size or film thickness of this electrochemical active material is much smaller and the distance between two electrode is much shorter. Therefore, electrons can be transported with lower resistance between the supporting electrode and the redox material. Furthermore, the electrolyte migration in the electrode material becomes much efficient. In most cells, if the conductivity of electrode materials is good enough, electrolyte transportation will be the rate determining step and hinder the performance of batteries. Therefore, due to the efficient migration of electrolyte, redox capacitors can work much faster than normal batteries.

However, the electrodes of most conventional supercapacitors, which are porous active carbon, do not have well designed nano-structures. Therefore, in the electrode, the existence of too much dead volume, which are the inaccessible parts for electrolytes,

decreases their specific capacity. The random chemical structure of active carbon disturbs the electrode conductivity, and therefore, the performance of capacitors will decrease. This means that making a electrode with suitable nano-structure is valuable to construct a better supercapacitor.

### 1.3.1 Carbon nanotube based supercapacitors

In recent decades, two novel carbon materials with excellent electrical properties have been discovered. One is the carbon nanotube, which is a tube-like one dimensional material which consists of graphite-like  $sp^2$  carbon.<sup>71</sup> The other is graphene, a two dimensional material, which is a single layer graphite sheet.<sup>72</sup> Because of high specific surface area and high electrical conductivity, carbon nanotubes (CNTs) and graphenes are regarded as good electrode material for supercapacitors. However, the application of these materials has met some difficulties. Because of the strong  $\pi$ - $\pi$  interaction of graphite structure, carbon materials tend to form aggregated structures. This property brings forth some difficulties to the treating processes and reduces the specific surface area. Therefore, efficient treatment processes are important for employing these materials for supercapacitor electrodes.

Recently, from the viewpoint of molecular engineering, scientists found that solution processing methods would become feasible for treating carbon nanotubes and graphenes, if they can alter the surface property of carbon materials. One possible way is the physical absorption treatment which is much suitable for one dimensional material, due to the much smaller contact surface area between the tubes. In this method, surfactants are used to change the surface properties of carbon nanotubes.<sup>73</sup> The hydrophobic end of surfactants can attach to the surface of carbon nanotubes via van der Waals interaction, and the hydrophilic end will be exposed on the tube surface to increase their solubility in water and prevent undesirable aggregation. The advantage of this method is that this treatment is a reversible process: the surfactants on the carbon nanotubes can be washed away easily after solution processing.

Many different processes are suitable to prepare porous carbon nanotube electrodes, such as drop casting method,<sup>74</sup> filtration method<sup>75</sup> and paper coating method.<sup>76</sup> Drop casting method uses a CNT dispersion solution to drop on a spinning substrate or putting the solution on a stationary substrate and then waiting for the solution to dry or washing it out by clean solvent. This method can form a stable carbon nanotube film on the supporting substrate. On the other hand, filtration method is employing a micro-porous filter paper to filter the CNT solution. In this way, the thickness of CNT film can be controlled easily by changing the amount of CNT in solution. After filtering and drying, the CNT film can be removed from the paper to form a free standing film. The third method is paper coating, which uses a paper as a supporting material, and then the CNT suspension solution is covered on the paper to form a paper-CNT hybridized material. All

these three methods can provide electrodes high with conductivity and porosity for supercapacitors.

### 1.3.2 Graphene based supercapacitors

In graphene processing, the surfactant treatment is not suitable, because surface treatment with molecules absorbing by van der Waals force is not stable for separating materials with high intermolecular interaction. Therefore, chemical treatment becomes important in processing this two-dimensional material.<sup>77</sup> Covalent linkages are much stronger than physical absorption and can offer a much stable modification of the surface. However, a disadvantage of this process is that most of the chemical reactions on the material surface are irreversible. This means that after processing, the behaviors of materials may be changed forever. In order to overcome this problem, many scientists have been trying to find an efficient but reversible modification reaction for graphenes. One of the most promising methods is the graphite oxidation reaction which can generate graphene oxide and help their separation.<sup>78</sup> Graphene oxide is a type of two-dimensional compound in which some oxygen atoms covalently link to graphene to form some epoxy, alcohol, ketone, aldehyde and carboxylic acid groups on it.<sup>79</sup> These groups can increase the affinity of graphene to polar solvents and also destroy the large  $\pi$  surface to prevent strong stacking interaction. Although the oxygen atoms are chemically bound to graphene, because of the aromatic stabilization effect, when graphene oxide is treated by heat, light or reducing agents, it will be reduced to recover the original graphite structure in a mono-sheet state.<sup>80</sup>

In the case of graphene processing, graphene oxide film can also be prepared by similar methods with those of carbon nanotube. However, when regenerated from the oxidized form, single layer graphene can attach to each other easily. Hence, the reduction process is certainly the key factor to decide the specific surface area of the resulting graphene film. In 2012, Kaner group provided an efficient way to prepare extremely high specific surface area graphene electrode for supercapacitors (**Figure 1-15**).<sup>81</sup> They used a commercial available DVD driver to reduce and exfoliate a graphene oxide film. The resulting material was a well exfoliated graphene film on a supporting substrate. The films were also used as electrodes to construct flexible thin film supercapacitors. The devices not only show high power density and better energy density than traditional ones, but also have nice resistance for continuous application of mechanical forces to cause capacitor bending. This is because even if the electrode possesses well porosity, the physical junctions between sheets are still sufficient and offer good path for electron conductivity and mechanical strength.

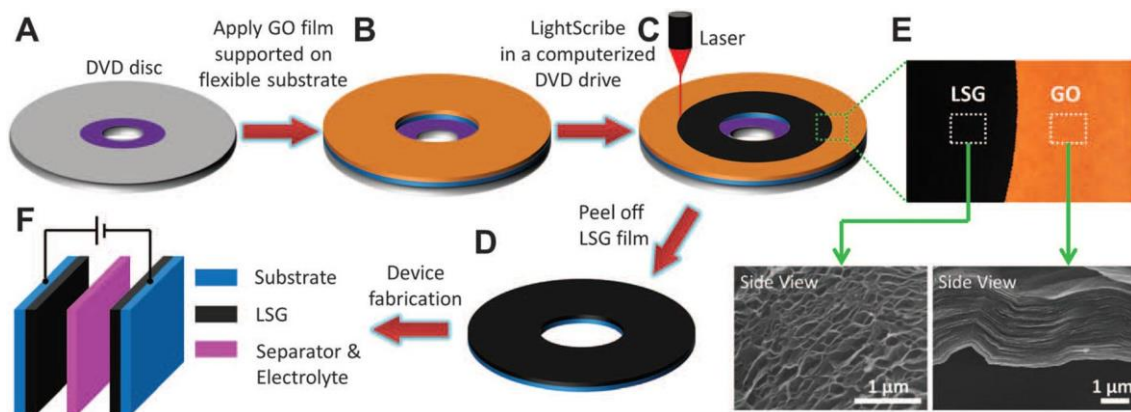


**Figure 1-15 The preparation of laser-scribed exfoliated graphene electrodes and supercapacitors composed of them.<sup>81</sup>**

## 1.4 Molecular scale electronics

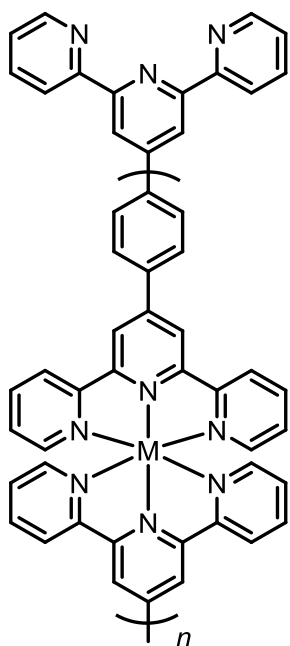
The other important goal of molecular engineering is to fabricate electronic components at molecular scale, such as molecular wires, molecular transistors and molecular rectifiers (**Figure 1-16**).<sup>82</sup> Molecular wires are the molecular scale substitution of electrical conducting wires in integrated circuits.<sup>83</sup> Usually, they are only around 1 nm in width or less. One of the best examples is signal-walled metallic carbon nanotubes, which are considered as the most conductive and robust molecular wires, but because of their inertness for chemical reactions, it is very difficult to integrate them with other molecular devices. Moreover, handling single carbon nanotube at nanoscale is also a big challenge.

Molecular transistors are the nano-scale counterpart of normal transistors.<sup>84</sup> They have similar functions in an electric circuit being current controllers with responses to external stimulations. However, because most of the molecular transistors can only allow one electron path through at one time, they only have two switching states, ON or OFF. They are different from traditional transistors in which the current flowing through them have a quadratic relationship with the applying gate voltage.

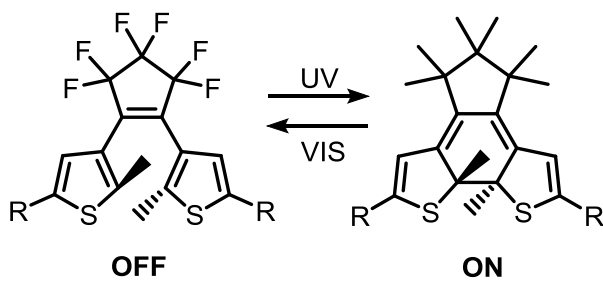
Molecular rectifiers are usually donor-acceptor-type molecules.<sup>85</sup> Because the orbital energy levels of these two ends are different and electrons can be pushed into the acceptor end much easily, they can resemble diode devices to control the current direction. These three devices are the main components of computing systems. Therefore, to construct and control them in the molecular scale is the groundwork of realizing molecular computation.

During these decades, these molecular devices have all been well designed and demonstrated in solution systems. However, a single component operation is still far from practical application, and constructing a stable and compact system in solution is almost impossible. Therefore, to develop a method to fabricate an integrated molecular scale circuit is a pivotal step toward molecular computers.

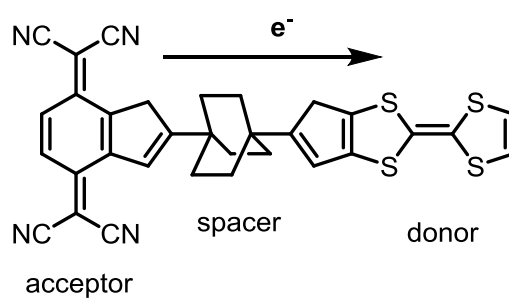
(A) wires



(B) switch



(C) rectifier



(D) transistor

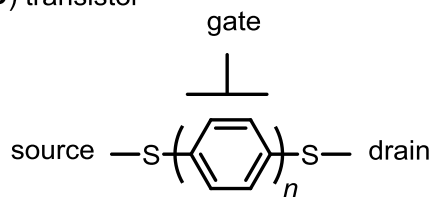


**Figure 1-16 Electronic components in the molecular scale.**

## 1.6 The aim of this thesis

Electrochemical polymerization reactions are very efficient methods to prepare surface immobilized polymers with random or ordered structures. In this thesis, two types of electrochemical reactions are used to prepare bis(terpyridine)metal complex networks and wires for energy storage applications and molecular electronics components respectively.

In Chapter 2 of this thesis, bis(terpyridine)iron complex network modified carbon electrode for high power density electric energy storage applications are focused. First, bis(terpyridine)metal complexes have very good electrochemical properties and high stability. Second, the electron transportability of bis(terpyridine)metal complex wires are regarded as one of the best among metal complex wires. Third, the nanostructure of bis(terpyridine)metal complex polymers can efficiently increase the surface area of electrode.

In Chapter 3 of this thesis, bis(terpyridine)iron complex network-carbon nanotube hybridized material for supercapacitor electrode is investigated. Carbon nanotubes are a group of material having high electric conductivity and high specific surface area. Therefore, the hybridization of these two materials can efficiently improve the areal capacity of the bis(terpyridine)iron complex network modified electrode.

In Chapter 4 of this thesis, ultra-long homo and hetero metal bis(terpyridine) complex wires are synthesized for potential electronics components.

## 1.7 References

---

1. Wild, A.; Winter, A.; Schlütter, F.; Schubert, U. S. *Chem. Soc. Rev.* **2011**, *40*, 1459.
2. Constable, E. C. *Chem. Soc. Rev.*, **2007**, *36*, 246.
3. SciFinder, 2014.
4. Constable, E. C.; Lewis, J.; Liptrot, M. C.; Raithby, P. R. *Inorg. Chim. Acta* **1990**, *178*, 47.
5. (a) Taylor, R.; Kennard, O. *J. Am. Chem. Soc.* **1982**, *104*, 5063. (b) Desiraju, G. R. *Acc. Chem. Res.* **1991**, *24*, 290. (c) Desiraju, G. R. *Acc. Chem. Res.* **1996**, *29*, 441.
6. Rall, J.; Weingart, F.; Ho, D. M.; Heeg, M. J.; Tisato, F.; Deutsch, E. *Inorg. Chem.* **1994**, *33*, 3442.
7. (a) Varela, J. A.; Saá, C. *Chem. Rev.* **2003**, *103*, 3787. (b) Heller, B.; Hapke, M. *Chem. Soc. Rev.* **2007**, *36*, 1085. (c) Desimoni, G.; Faita, G.; Quadrelli, P. *Chem. Rev.* **2003**, *103*, 3119. (d) Foster, J. W.; Moat, A. G. *Microbiol. Rev.* **1980**, *44*, 83. (e) Kaiser, J. P.; Feng, Y.; Bollag, J. M. *Microbiol. Rev.* **1996**, *60*, 483.
8. Eric, F. V. *Chem. Soc. Rev.* **1983**, *12*, 129.
9. (a) Lavalley, D. K.; Baughman, M. D.; Phillips, M. P. *J. Am. Chem. Soc.* **1977**, *99*, 718. (b) Figard, J. E.; Paukstelis, J. V.; Byrne, E. F.; Petersen, J. D. *J. Am. Chem. Soc.* **1977**, *99*, 8417. (c) Gill, N. S.; Nuttall, R. H.; Scaife, D. E.; Sharp, D. A. *J. Inorg. Nucl. Chem.* **1961**, *18*, 79.
10. (a) Fleming, I. *Molecular Orbitals and Organic Chemical Reactions*; John Wiley & Sons, **2009**. (b) Jones, T. E.; Zuo, C.; Jagodzinski, P. W.; Eberhart, M. E. *J. Phys. Chem. C* **2007**, *111*, 5493.
11. Holyer, R. H.; Hubbard, C. D.; Kettle, S. F. A.; Wilkins, R. G. *Inorg. Chem.* **1966**, *5*, 622.
12. Scarborough, C. C.; Lancaster, K. M.; DeBeer, S.; Weyhermüller, T.; Sproules, S.; Wieghardt, K. *Inorg. Chem.*, **2012**, *51*, 3718.
13. Collin, J. P.; Jouaiti, A.; Sauvage, J. P. *J. Electroanal. Chem.*, **1990**, *286*, 75.

- 
14. Scarborough, C. C.; Lancaster, K. M.; DeBeer, S.; Weyhermüller, T.; Sproules, S.; Wieghardt, K. *Inorg. Chem.* **2012**, *51*, 3718.
  15. Wang, M.; Weyhermüller, T.; England, J.; Wieghardt, K. *Inorg. Chem.*, **2013**, *52*, 12763.
  16. (a) Halcrow, M. A. *Coord. Chem. Rev.* **2005**, *249*, 2880. (b) Thompson, A. M. C. *Coord. Chem. Rev.* **1997**, *160*, 1. (c) Jameson, D. L.; Guise, L. E. *Tetrahedron Lett.* **1991**, *32*, 1999.
  17. Heller, M.; Schubert, U. S. *J. Org. Chem.* **2002**, *67*, 8269.
  18. (a) Michael, D. *J. Chem. Soc. Dalton Trans.* **1990**, 1405. (b) Wieprecht, T.; Xia, J.; Heinz, U.; Dannacher, J.; Schlingloff, G. *J. Mol. Catal. A: Chem.* **2003**, *203*, 113.
  19. (a) Tu, S.; Jia, R.; Jiang, B.; Zhang, J.; Zhang, Y.; Yao, C.; Ji, S. *Tetrahedron* **2007**, *63*, 381. (b) Zeng, L. Y.; Cai, C. *Synth. Commun.* **2013**, *43*, 705.
  20. Hofmeier, H.; Schubert, U. S. *Chem. Soc. Rev.* **2004**, *33*, 373.
  21. Medlycott, E. A.; Hanan, G. S. *Coord. Chem. Rev.* **2006**, *250*, 1763.
  22. (a) Kanaizuka, K.; Murata, M.; Nishimori, Y.; Mori, I.; Nishio, K.; Masuda, H.; Nishihara, H. *Chem. Lett.* **2005**, *34*, 534. (b) CargilláThompson, A. M. *J. Chem. Soc., Dalton Trans.* **1992**, 2947.
  23. (a) Chow, H. F.; Chan, I. Y. K.; Fung, P. S.; Mong, T. K. K.; Nongrum, M. F. *Tetrahedron* **2001**, *57*, 1565. (b) Lohmeijer, B. G.; Wouters, D.; Yin, Z.; Schubert, U. S. *Chem. Commun.* **2004**, 2886.
  24. (a) Ohba, Y.; Kanaizuka, K.; Murata, M.; Nishihara, H. *Macromol. Symp.* **2006**, *235*, 31. (b) Joester, D.; Gramlich, V.; Diederich, F. *Helv. Chim. Acta* **2004**, *87*, 2896.
  25. Medlycott, E. A.; Hanan, G. S. *Chem. Soc. Rev.*, **2005**, *34*, 133.
  26. Baranoff, E.; Collin, J. P.; Flamigni, L.; Sauvage, J. P. *Chem. Soc. Rev.* **2004**, *33*, 147.
  27. Wong, W. L.; Huang, K. H.; Teng, P. F.; Lee, C. S.; Kwong, H. L. *Chem. Comm.*, **2004**, 384.
  28. Chelucci, G.; Thummel, R. P. *Chem. Rev.* **2002**, *102*, 3129.
  29. Perrine, T. M.; Dunietz, B. D. *J. Phys. Chem. A*, **2008**, *112*, 2043.
  30. Nishimori, Y.; Kanaizuka, K.; Murata, M.; Nishihara, H. *Chem. Asian J.*, **2007**, *2*, 367.
  31. Brown, R. T.; Fletcher, N. C.; Nieuwenhuyzen, M.; Keyes, T. E. *Inorg. Chim. Acta* **2005**, *358*, 1079.

- 
32. Liu, C. F.; Liu, N. C.; Bailar Jr, J. C. *Inorg. Chem.* **1964**, *3*, 1085.
33. Flamigni, L.; Collin, J.-P.; Sauvage, J.-P. *Acc. Chem. Res.*, **2008**, *41*, 857.
34. Ott, S., Kritikos, M., Åkermark, B. and Sun, L. *Angew. Chem. Int. Ed.*, **2003**, *42*, 3285.
35. Ott, S.; Borgström, M.; Kritikos, M.; Lomoth, R.; Bergquist, J.; Åkermark, B.; Hammarström, L.; Sun, L. *Inorg. Chem.*, **2004**, *43*, 4683.
36. (a) Padilla-Tosta, M. E.; Lloris, J. M.; Martónez-Máñez, R.; Benito, A.; Soto, J.; Pardo, T.; Miranda, M. A.; Marcos, M. D. *European J. Inorg. Chem.* **2000**, *2000*, 741. (b) Hong, Y.; Chen, S.; Leung, C. W. T.; Lam, J. W. Y.; Liu, J.; Tseng, N.-W.; Kwok, R. T. K. *ACS Appl. Mater. Interfaces* **2011**, *3*, 3411. (c) Barigelletti, F.; Flamigni, L.; Calogero, G.; Hammarström, L.; Sauvage, J. P.; Collin, J. P. *Chem. Commun.* **1998**, 2333.
37. Goodall, W.; Williams, J. G. *J. Chem. Soc., Dalton Trans.* **2000**, 2893.
38. Arm, K. J.; Leslie, W.; Williams, J. G. *Inorg. Chim. Acta* **2006**, *359*, 1222.
39. (a) Guo, S.; Dong, S. *Chem. Soc. Rev.* **2011**, *40*, 2644. (b) Qiu, S.; Zhu, G. *Coord. Chem. Rev.* **2009**, *253*, 2891. (c) Whitesides, G. M.; Kriebel, J. K.; Love, J. C. *Sci. Prog.* **2005**, *88*, 17. (d) Zhang, H.; Wang, X.; Zhang, K.; Teo, B. K. *Coord. Chem. Rev.* **1999**, *183*, 157. (e) Barth, J. V. *Annu. Rev. Phys. Chem.* **2007**, *58*, 375.
40. (a) De Silva, A. P.; Uchiyama, S.; Vance, T. P.; Wannalorse, B. *Coord. Chem. Rev.* **2007**, *251*, 1623. (b) Katz, E.; Privman, V. *Chem. Soc. Rev.* **2010**, *39*, 1835. (c) Credi, A. *Angew. Chem. Int. Ed.* **2007**, *46*, 5472. (d) De Silva, A. P.; Uchiyama, S. *Nat. Nanotechnol.* **2007**, *2*, 399. (e) Andréasson, J.; Pischel, U. *Chem. Soc. Rev.* **2010**, *39*, 174.
41. (a) Tanaka, T.; Osuka, A. *Chem. Soc. Rev.* **2015**, *44*, 943. (b) Park, J. H.; Kim, S.; Bard, A. J. *Nano Lett.* **2006**, *6*, 24. (c) Baughman, R. H.; Zakhidov, A. A.; de Heer, W. A. *Science* **2002**, *297*, 787. (d) Qi, P.; Vermesh, O.; Grecu, M.; Javey, A.; Wang, Q.; Dai, H.; Peng, S.; Cho, K. J. *Nano Lett.* **2003**, *3*, 347. (e) Rueckes, T.; Kim, K.; Joselevich, E.; Tseng, G. Y.; Cheung, C. L.; Lieber, C. M. *Science* **2000**, *289*, 94. (f) Yu, J.; Mathew, S.; Flavel, B. S.; Johnston, M. R.; Shapter, J. G. *J. Am. Chem. Soc.* **2008**, *130*, 8788. (g) Yang, Z. P.; Ci, L.; Bur, J. A.; Lin, S. Y.; Ajayan, P. M. *Nano Lett.* **2008**, *8*, 446. (h) Rao, A. M.; Jacques, D.; Haddon, R. C.; Zhu, W.; Bower, C.; Jin, S. *Appl. Phys. Lett.* **2000**, *76*, 3813. (i) Li, J.; Hu, L.; Wang, L.; Zhou, Y.; Grüner, G.; Marks, T. J. *Nano Lett.* **2006**, *6*, 2472.
42. Koch, C. C. *Rev. Adv. Mater. Sci.* **2003**, *5*, 91.
43. Barth, J. V.; Costantini, G.; Kern, K. *Nature*, **2005**, *437*, 671.
44. (a) Okazaki, S. *J. Vac. Sci. Technol. B* **1991**, *9*, 2829. (b) Xia, Y.; Whitesides, G. M.

---

*Annu. Rev. Mater. Sci.* **1998**, 28, 153.

45. (a) von Freymann, G.; Kitaev, V.; Lotsch, B. V.; Ozin, G. A. *Chem. Soc. Rev.* **2013**, 42, 2528. (b) Ruiz-Hitzky, E.; Aranda, P.; Darder, M.; Ogawa, M. *Chem. Soc. Rev.* **2011**, 40, 801.
46. (a) Giessibl, F. J. *Rev. Mod. Phys.* **2003**, 75, 949. (b) Gewirth, A. A.; Niece, B. K. *Chem. Rev.* **1997**, 97, 1129.
47. Love, J. C., Estroff, L. A., Kriebel, J. K., Nuzzo, R. G., & Whitesides, G. M. *Chem. Rev.*, **2005**, 105, 1103.
48. Ulman, A. *Chem. Rev.*, **1996**, 96, 1533.
49. Jennings, G. K.; Yong, T.-H.; Munro, J. C.; Laibinis, P. E. *J. Am. Chem. Soc.*, **2003**, 125, 2950.
50. Zhang, S.; Sun W.-l.; Zhang, W.; Jin, L.-T.; Yamamoto, K.; Tao, S.; Jin, J. *Anal. Lett.*, **1998**, 31, 2159.
51. Rouhana, L. L.; Moussallem, M. D.; Schlenoff, J. B. *J. Am. Chem. Soc.*, **2011**, 133, 16080.
52. Dreesen, L.; Humbert, C.; Celebi, M.; Lemaire, J. J.; Mani, A. A.; Thiry, P. A.; Peremans, A. *Appl. Phys. B*, **2002**, 74, 621.
53. Figgemeier, E.; Merz, L.; Hermann, B. A.; Zimmermann, Y. C.; Housecroft, C. E.; GuIntherodt, H.-J.; Constable, E. C. *J. Phys. Chem. B*, **2003**, 107, 1157.
54. Vogelson, C. T.; Keys, A.; Edwards, C. L.; Barron, A. R. *J. Mater. Chem.*, **2003**, 13, 291.
55. Pawsey, S.; McCormick, M.; De Paul, S.; Graf, R.; Lee, Y. S.; Reven, L.; Spiess, H. W. *J. Am. Chem. Soc.*, **2003**, 125, 4174.
56. Oh, S.-Y.; Yun, Y.-J.; Kim, D.-Y.; Han, S.-H. *Langmuir*, **1999**, 15, 4690.
57. Marshall, G. M.; Lopinski, G. P.; Bensebaa, F.; Dubowski, J. J. *Langmuir*, **2009**, 25, 13561.
58. Cho, Y.-J.; Ahn, T. K.; Song, H.; Kim, K. S.; Lee, C. Y.; Seo, W. S.; Lee, K.; Kim, S. K.; Kim, D.; Park, J. T. *J. Am. Chem. Soc.*, **2005**, 127, 2380.
59. Ito, Y.; Virkar, A. A.; Mannsfeld, S.; Oh, J. H.; Toney, M.; Locklin, J.; Bao, Z. *J. Am. Chem. Soc.* **2009**, 131, 9396.
60. Poirier, G. E.; Pylant, E. D. *Science*, **1996**, 272, 1145.
61. Schwartz, D. K. *Annu. Rev. Phys. Chem.*, **2001**, 52, 107.

- 
62. (a) Sakamoto, R.; Katagiri, S.; Maeda, H.; Nishihara, H., *Coord. Chem. Rev.* **2013**, 257, 1493. (b) George, S. M. *Chem. Rev.* **2009**, 110, 111. (c) Zacher, D.; Shekhah, O.; Wöll, C.; Fischer, R. A. *Chem. Soc. Rev.* **2009**, 38, 1418.
63. (a) Choi, S. H.; Kim, B.S.; Frisbie, C. D. *Science*, **2008**, 320, 1482. (b) Choi, S. H.; Risko, C.; Delgado, M. C. R.; Kim, B.; Brédas, J. L.; Frisbie, C. D. *J. Am. Chem. Soc.* **2010**, 132, 4358. (c) Luo, L.; Frisbie, C. D. *J. Am. Chem. Soc.* **2010**, 132, 8854.
64. Haga, M. A.; Kobayashi, K.; Terada, K. *Coord. Chem. Rev.* **2007**, 251, 2688.
65. (a) Sadki, S.; Schottland, P.; Brodie, N.; Sabouraud, G. *Chem. Soc. Rev.* **2000**, 29, 283. (b) Roncali, J. *Chem. Rev.* **1992**, 92, 711. (c) Li, C.; Bai, H.; Shi, G. *Chem. Soc. Rev.* **2009**, 38, 2397.
66. Hjelm, J.; Constable, E. C.; Figgemeier, E.; Hagfeldt, A.; Handel, R.; Housecroft, C. E.; Mukhtar, E.; Schofield, E. *Chem. Comm.* **2002**, 284.
67. (a) Miller, J. R.; Simon, P. *Science*, **2008**, 321, 651. (b) Simon, P.; Gogotsi, Y. *Nat. Mater.* **2008**, 7, 845. (c) Winter, M.; Brodd, R. J. *Chem. Rev.* **2004**, 104, 4245. (d) Miller, J. R.; Simon, P. *Electrochem. Soc. Interface* **2008**, 17, 31. (e) Simon, P.; Gogotsi, Y. *Nat. Mater.* **2008**, 7, 845.
68. Zhu, Y.; Murali, S.; Stoller, M. D.; Ganesh, K. J.; Cai, W.; Ferreira, P. J.; Pirkle, A.; Wallace, R. M.; Cychosz, K. A.; Thommes, M.; Su, D.; Stach, E. A.; Ruoff, R. S. *Science*, **2011**, 332, 1537.
69. (a) Largeot, C.; Portet, C.; Chmiola, J.; Taberna, P. L.; Gogotsi, Y.; Simon, P. *J. Am. Chem. Soc.* **2008**, 130, 2730. (b) Sato, T.; Masuda, G.; Takagi, K. *Electrochim. Acta* **2004**, 49, 3603. (c) Yoon, S.; Lee, J.; Hyeon, T.; Oh, S. M. *J. Electrochem. Soc.* **2000**, 147, 2507. (d) Arulepp, M.; Permann, L.; Leis, J.; Perkson, A.; Rumma, K.; Jänes, A.; Lust, E. *J. Power Sources* **2004**, 133, 320. (e) Osaka, T.; Liu, X.; Nojima, M.; Momma, T. *J. Electrochem. Soc.* **1999**, 146, 1724.
70. (a) Hu, C. C.; Chang, K. H.; Lin, M. C.; Wu, Y. T. *Nano Lett.* **2006**, 6, 2690. (b) Wang, H.; Casalongue, H. S.; Liang, Y.; Dai, H. *J. Am. Chem. Soc.* **2010**, 132, 7472. (c) Brezesinski, T.; Wang, J.; Tolbert, S. H.; Dunn, B. *Nat. Mater.* **2010**, 9, 146. (d) Chang, J. K.; Tsai, W. T. *J. Electrochem. Soc.* **2003**, 150, A1333. (e) Yang, L.; Cheng, S.; Ding, Y.; Zhu, X.; Wang, Z. L.; Liu, M. *Nano Lett.* **2011**, 12, 321. (f) Li, H. B.; Yu, M. H.; Wang, F. X.; Liu, P.; Liang, Y.; Xiao, J.; Wang, C. X.; Tong, Y. X.; Yang, G. W. *Nat. Commun.* **2013**, 4, 1894. (g) Yang, S.; Wu, X.; Chen, C.; Dong, H.; Hu, W.; Wang, X. *Chem. Commun.* **2012**, 48, 2773.
71. (a) An, K. H.; Kim, W. S.; Park, Y. S.; Choi, Y. C.; Lee, S. M.; Chung, D. C.; Bae, D. J.; Lim, S. C.; Lee, Y. H. *Adv. Mater.* **2001**, 13, 497. (b) Terrones, M. *Annu. Rev. Mater. Res.* **2003**, 33, 419. (c) Ajayan, P. M. *Chem. Rev.* **1999**, 99, 1787. (d)

- 
- Dresselhaus, M. S.; Dresselhaus, G.; Jorio, A. *Annu. Rev. Mater. Res.* **2004**, *34*, 247. (e) Karousis, N.; Tagmatarchis, N.; Tasis, D. *Chem. Rev.* **2010**, *110*, 5366. (f) Britz, D. A.; Khlobystov, A. N. *Chem. Soc. Rev.* **2006**, *35*, 637. (g) Guldi, D. M.; Rahman, G. A.; Sgobba, V.; Ehli, C. *Chem. Soc. Rev.* **2006**, *35*, 471. (h) Tasis, D.; Tagmatarchis, N.; Bianco, A.; Prato, M. *Chem. Rev.* **2006**, *106*, 1105.
72. (a) Neto, A. C.; Guinea, F.; Peres, N. M. R.; Novoselov, K. S.; Geim, A. K. *Rev. Mod. Phys.* **2009**, *81*, 109. (b) Allen, M. J.; Tung, V. C.; Kaner, R. B. *Chem. Rev.* **2009**, *110*, 132. (c) Georgakilas, V.; Otyepka, M.; Bourlinos, A. B.; Chandra, V.; Kim, N.; Kemp, K. C.; Hobza, P.; Zboril, R.; Kim, K. S. *Chem. Rev.* **2012**, *112*, 6156. (d) Huang, X.; Qi, X.; Boey, F.; Zhang, H. *Chem. Soc. Rev.* **2012**, *41*, 666. (e) Sarma, S. D.; Adam, S.; Hwang, E. H.; Rossi, E. *Rev. Mod. Phys.* **2011**, *83*, 407. (f) Chen, D.; Tang, L.; Li, J. *Chem. Soc. Rev.* **2010**, *39*, 3157. (g) Guo, S.; Dong, S. *Chem. Soc. Rev.* **2011**, *40*, 2644.
73. (a) Hu, L.; Hecht, D. S.; Gruner, G. *Chem. Rev.* **2010**, *110*, 5790. (b) Cao, Q.; Rogers, J. A. *Adv. Mater.* **2009**, *21*, 29. (c) Nirmalraj, P. N.; Lyons, P. E.; De, S.; Coleman, J. N.; Boland, J. J. *Nano Lett.* **2009**, *9*, 3890. (d) Gong, X.; Liu, J.; Baskaran, S.; Voise, R. D.; Young, J. S. *Chem. Mater.* **2000**, *12*, 1049.
74. (a) Kymakis, E.; Alexandou, I.; Amaratunga, G. A. J. *Synth. Met.* **2002**, *127*, 59. (b) Harris, P. J. F. *Int. Mater. Rev.* **2004**, *49*, 31.
75. Wu, Z.; Chen, Z.; Du, X.; Logan, J. M.; Sippel, J.; Nikolou, M.; Kamaras, K.; Reynolds, J. R.; Tanner, D. B.; Hebard, A. F.; Rinzler, A. G. *Science* **2004**, *305*, 1273.
76. Hu, L.; Choi, J. W.; Yang, Y.; Jeong, S.; La Mantia, F.; Cui, L. F.; Cui, Y. *Proc. Natl. Acad. Sci.* **2009**, *106*, 21490.
77. (a) Chen, D.; Feng, H.; Li, J. *Chem. Rev.* **2012**, *112*, 6027. (b) Chua, C. K.; Pumera, M. *Chem. Soc. Rev.* **2014**, *43*, 291. (c) Dreyer, D. R.; Todd, A. D.; Bielawski, C. W. *Chem. Soc. Rev.* **2014**, *43*, 5288. (d) Jiang, K.; Ma, L.; Wang, J.; Chen, W. *Rev. Nanoscience Nanotechnol.* **2013**, *2*, 171. (e) Jiang, K.; Ma, L.; Wang, J.; Chen, W. *Rev. Nanosci. Nanotechnol.* **2013**, *2*, 171. (f) Chua, C. K.; Pumera, M. *Chem. Soc. Rev.* **2013**, *42*, 3222.
78. Becerril, H. A.; Mao, J.; Liu, Z.; Stoltenberg, R. M.; Bao, Z.; Chen, Y. *ACS Nano* **2008**, *2*, 463.
79. Dreyer, D. R.; Park, S.; Bielawski, C. W.; Ruoff, R. S. *Chem. Soc. Rev.* **2010**, *39*, 228.
80. Eda, G.; Fanchini, G.; Chhowalla, M. *Nat. Nanotechnol.* **2008**, *3*, 270.
81. El-Kady, M. F.; Strong, V.; Dubin, S.; Kaner, R. B. *Science*, **2012**, *335*, 1326.
82. Joachim, C.; Gimzewski, J. K.; Aviram, A. *Nature*, **2000**, *408*, 541.

- 
83. (a) Nitzan, A.; Ratner, M. A. *Science* **2003**, *300*, 1384. (b) Davis, W. B.; Svec, W. A.; Ratner, M. A.; Wasielewski, M. R. *Nature* **1998**, *396*, 60. (c) Reed, M. A.; Zhou, C.; Muller, C. J.; Burgin, T. P.; Tour, J. M. *Science* **1997**, *278*, 252. (d) Tao, N. J. *Nat. Nanotechnol.* **2006**, *1*, 173.
84. (a) Mitra, A.; Aleiner, I.; Millis, A. J. *Phys. Rev. B* **2004**, *69*, 245302. (b) Tans, S. J.; Dekker, C. *Nature* **2000**, *404*, 834. (c) Liang, W.; Shores, M. P.; Bockrath, M.; Long, J. R.; Park, H. *Nature* **2002**, *417*, 725.
85. (a) Aviram, A.; Ratner, M. A. *Chem. Phys. Lett.* **1974**, *29*, 277. (b) Dhirani, A.; Lin, P. H.; Guyot-Sionnest, P.; Zehner, R. W.; Sita, L. R. *J. Chem. Phys.* **1997**, *106*, 5249. (c) Troisi, A.; Ratner, M. A. *Nano Lett.* **2004**, *4*, 591. (d) Majumder, C.; Mizuseki, H.; Kawazoe, Y. *J. Phys. Chem. A* **2001**, *105*, 9454. (e) Scheib, S.; Cava, M. P.; Baldwin, J. W.; Metzger, R. M. *J. Org. Chem.* **1998**, *63*, 1198.



## **Chapter 2**

### **Electrochemical syntheses of bis(terpyridine)iron network complex covalently bound to glassy carbon**

## 2.1 Introduction

Supercapacitors are one of the most important next generation energy storage devices.<sup>1,2,3,4</sup> First, supercapacitors can tolerate much higher current density operation with lower capacity loss than secondary batteries.<sup>5</sup> In other words, the charging time of portable energy storage devices can be reduced greatly and they will be much suitable to drive electric automobiles which require high power for speeding up. Second, supercapacitors have longer life span than most batteries and almost no battery memory effect, which is the main culprit for decreasing battery capacities.<sup>6</sup> Therefore, supercapacitors are regarded to be much environmentally friendly and economical devices. Third, supercapacitors can store much more energy than traditional capacitors.<sup>7</sup> This makes their applications in energy storage for portable devices possible. Therefore, recently, supercapacitors are studied intensively.

Although supercapacitors have many advantages, there is still a big problem in practical applications. The energy kept in each mass unit (specific capacitance) or volume unit (volumetric capacitance) of supercapacities<sup>8</sup> is much lower than that of secondary lithium batteries<sup>9</sup> and cannot fulfill the requirement of existing portable electric devices. This is because the energy storage ability of supercapacities mainly comes from the double layer capacity effect of electrodes. This is the result of the adsorption of electrolytes on electrode surface to neutralize the surface charge, when a potential is applied on the electrode. Therefore, the specific surface area of an electrode material limits the maximum energy storage capacity.<sup>10</sup> However, the density of a porous material is inversely proportional to its specific surface area.

To overcome this problem, a layer of a redox active material was used to modify the electrode surface of supercapacitors to increase their charge storage capacities. This group of supercapacitors is known as pseudocapacitors or redox capacitors.<sup>11</sup> The active material, such as metal oxides,<sup>12</sup> metal salts<sup>13</sup> or organic polymers,<sup>14</sup> bonded on the electrodes provide extra energy storage ability by means of redox reactions other than electrolyte adsorption. However, the linkage between the porous electrodes and this redox active material is sometimes weak, which causes the charging and discharging efficiency to be cancelled out by this imperfect linkage.<sup>15</sup> Therefore, a direct covalent modification of the redox active material is necessary for high power systems.

In our group, a series of bis(terpyridine)metal complex wires were synthesized on gold and silicon electrodes by stepwise coordination methods.<sup>16</sup> They have high

electrical conductivity and high stability. Moreover, the redox reactions of the complex backbone show high reversibility and their nanostructures can increase surface area of the electrodes. As these properties are important not only for molecular electronics but also for supercapacitors, bis(terpyridine)metal complex polymers are expected as good modifier of the electrode of supercapacitors.

In this research, glassy carbon electrodes are used as a model electrode of porous carbon electrodes. This is because the properties of glassy carbon electrodes are much better understood than porous carbon electrodes and the glassy carbon electrode preparation is also much easily reproduced.<sup>17</sup>

The modification of carbon with perfect graphite structure is more difficult than those of other materials, because this structure is inert for most chemical reagents.<sup>18</sup> The most efficiently and well established method to modify carbon electrode is free-radical addition reactions.<sup>19</sup> Free-radicals can easily add to graphite surface and form stable bonds to immobilize themselves. Diazonium salt single electron reduction reactions are one of the most commonly used methods to generate aryl free-radicals.<sup>20</sup> In this reaction, a free-radical and a dinitrobenzene can be generated immediately. However, diazonium salts are unstable reagents under ambient condition.<sup>21</sup> Therefore, in this research, another free-radical precursor, hydrazine terminated complex, was selected. Aryl hydrazines, a reduced form of aryl diazonium salts, can be oxidized to form free-radical via a common intermediate with diazonium salt reduction reaction.<sup>22</sup>

Moreover, bis(terpyridine)iron complex was used as the monomer unit of the network complex. First, iron is a high abundance, low price and low toxicity element. This is, this compound is much economical and environment friendly. Second, the redox potential of bis(terpyridine)iron(III)/(II) couple is high,<sup>23</sup> so the energy storage devices using this network complex as electrode can have high operation potential. In other words, these devices can keep much more energy than that with lower operation potential. Third, one of the most stable bis(terpyridine)metal complexes is iron complex.<sup>24</sup> It has much higher formation constant and can remain stable under oxidation and reduction conditions. Therefore, in this study, bis(terpyridine)iron complex is selected.

On the glassy carbon electrode, bis(terpyridine)iron network complexes were prepared using electrochemical polymerization with bis(4'-hydrazine-terpyridine)iron complex as a monomer. This hydrazine terminated complex was selected as a strong reagent, such as free-radical, is needed to modify the carbon surface, which is a one of

the most inert substrates. Diazonium salts are one of the most commonly used reagents in electrochemical process to generate free-radicals, but these compounds are not stable and usually decompose during experiments. Compared with diazonium salts, hyrazine compounds, which can be regarded as the reduced counterparts of diazonium salts, are much stable free-radical precursors and can also convert to free-radical easily by electrochemical oxidation.<sup>25</sup> Therefore, the complex with hydrazine terminated groups is employed as the monomer.

## 2.2 Experimental section

### 2.2.1 Materials

#### 4'-Hydrazinyl-2,2':6',2''-terpyridine

4'-Hydrazinyl-2,2':6',2''-terpyridine was prepared according to literature methods,<sup>26</sup> but the method used to remove excess hydrazine after the reaction was changed from washing the precipitating product with a few drop of water to extract the chloroform solution of product with bigger amount of water. 4'-Chloro-2,2':6',2''-terpyridine (1.641 g, 6.14 mmol) was mixed with isobutanol (12 mL) and hydrazine monohydrate (4 mL). The mixture was heated to reflux in isobutanol for 12 h under nitrogen. After cooling to room temperature, the mixture was diluted by chloroform and then washed with deionized water to remove excess hydrazine. The solution was then dried over anhydrous magnesium sulfate and evaporated to offer a pure product (1.52 g, 94 % yield). <sup>1</sup>H NMR (500 MHz; CDCl<sub>3</sub>): δ = 8.68 (d, *J* = 4.0 Hz, 2 H), 8.62 (d, *J* = 8.0, 2 H), 7.85 (dd, *J* = 1.6, 15.0 Hz, 2 H), 7.86 (s, 2H), 7.33(dd, *J* = 5.0, 6.5 Hz, 2 H), 5.80 (s, 1 H), 3.82 (d, *J* = 3, 2 H). <sup>13</sup>C NMR (125 MHz, *d*<sub>6</sub>-DMSO): δ = 158.87, 156.13, 154.68, 148.85, 136.91, 123.71, 120.55, 102.83. MS (MALDI TOF): *m/z*: 264.56 [M+H]<sup>+</sup>.

#### Bis(4'-hydrazinyl-2,2':6',2''-terpyridine)iron(II) tetrafluoroborate

Two equivalents of 4'-hydrazinyl-2,2':6',2''-terpyridine and one equivalent of iron(II) tetrafluoroborate hexahydrate were mixed in acetonitrile. Upon mixing, the solution became purple immediately. The purple mixture was then stirred for 1 h and used for electrochemical reaction directly. The pure complex can be obtained by removing solvent under vacuum and without any further purification. <sup>1</sup>H NMR (500 MHz; CD<sub>3</sub>CN): δ = 8.23 (d, *J* = 7.5 Hz, 2 H), 8.07 (s, 2 H), 7.80 (t, *J* = 7.5 Hz, 2 H), 7.23 (d, *J* = 4.6 Hz, 2 H), 7.04 (t, *J* = 6.3 Hz, 2 H), 6.10 (s, 2 H). <sup>13</sup>C (125 MHz, *d*<sub>6</sub>-DMSO): δ = 158.71, 158.38, 157.96, 152.83, 138.04, 127.05, 122.68, 105.84.

### 2.2.2 Instruments

Electrochemical measurements were carried out using ALS 750A and 650DT electrochemical analyzers (BAS. Co., Ltd.). All measurements were conducted in a three-electrodes cell with a glassy carbon working electrode sealed in glass tube, a platinum coil counter electrode and an Ag/Ag<sup>+</sup> reference electrode (0.01 M AgClO<sub>4</sub> in

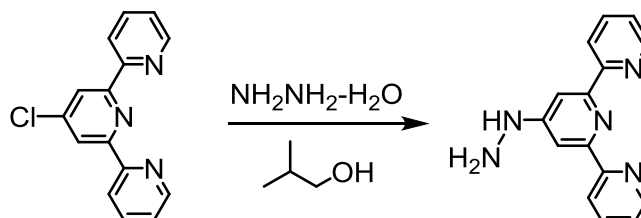
0.1 M-Bu<sub>4</sub>NClO<sub>4</sub>/acetonitrile).

The working electrode was made from a glassy carbon rod purchased from Tokai Carbon Co. Ltd. The glassy carbon rod was cut to about 4 mm long pieces, washed with water and acetone and dried in 110°C oven. The glassy carbon was then sealed in a Pyrex glass tube by gas-oxygen flame. The sealed glassy carbon electrode was polished by #240, #500, #1000, #2000 waterproof abrasive papers (Fuji Star, Sankyo Rikagaku Co., Ltd.) successively. After that, the electrode was polished by 0.3 μm Al<sub>2</sub>O<sub>3</sub>. The counter electrode was prepared by sealing platinum wire in a soda-lime glass.

AFM was conducted using an Agilent Technologies 5500 Scanning Probe Microscope, under ambient conditions. AFM was performed in the dynamic contact mode (AC mode), with a silicon cantilever PPP-NCL (Nano World).

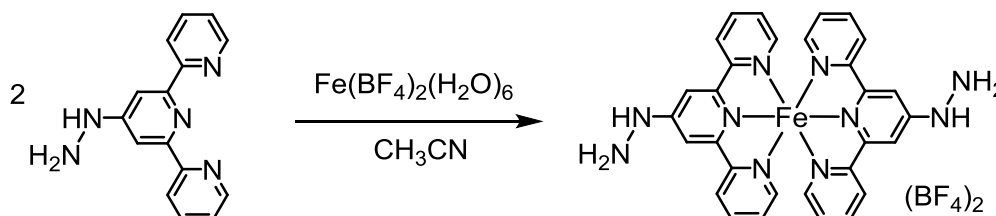
## 2.3 Results and discussion

### 2.3.1 Synthesis of the monomer complex for electrochemical polymerization



**Scheme 2-1** The synthesis of 4'-2,2':6',2''-terpyridine.

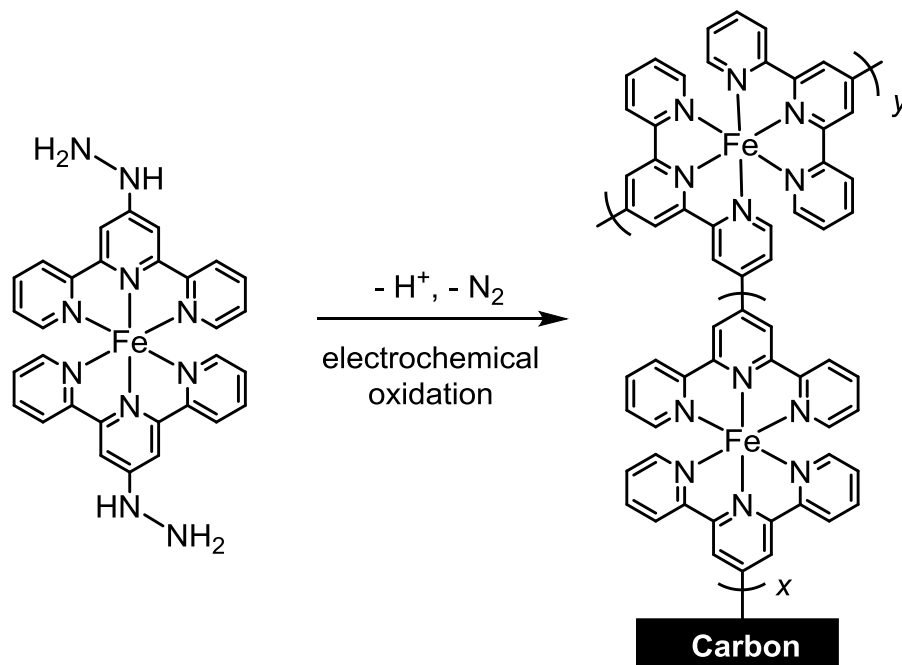
As shown in **Scheme 2-1**, a hydrazine substituted ligand, 4'-hydrazinyl-2,2':6',2''-terpyridine, was prepared from 4'-chloro-2,2':6',2''-terpyridine treated with an excess amount of hydrazine to offer high chemical yield and purity.<sup>26</sup> The reaction undergoes as a simple aromatic nucleophilic substitution from chloride to hydrazine on an electron deficient pyridine ring. Because of the high reactivity of the chloro-substituted pyridine, the substitution reaction can proceed efficiently.



**Scheme 2-2** The synthesis of bis(4'-hydrazinyl-terpyridine)iron(II) tetrafluoroborate.

On the other hand, as shown in **Scheme 2-2**, the bis(4'-hydrazinyl-terpyridine)iron complex was synthesized by mixing two equivalent of the substituted terpyridine ligand and one equivalent of iron(II) tetrafluoroborate hexahydrate in acetonitrile under ambient condition. Because the formation constants of bis(terpyridine)iron(II) complexes are very high, and the precursor is a bare iron(II) cation, the complexation reaction completes with a very short time without the assistance of other reagents and provides a product with high purity. Therefore, the bis(terpyridine)iron complex can be obtained directly without further purification.

### 2.3.2 Electrochemical synthesis of the network complex on a glassy carbon electrode



**Scheme 2-3** The electrochemical polymerization of bis(terpyridine)iron complex networks on glassy carbon.

The electrochemical synthesis was carried out with bis(4'-hydrazinyl-terpyridine)iron(II) tetrafluoroborate in a tetrabutylammonium perchlorate (TBAP) acetonitrile solution (**Scheme 2-3**). A glassy carbon sealed in a glass tube was used as the working electrode for the modification. The experiment was carried out by cyclic voltammetry with potential sweep between 1.5 V and -1.5 V versus a Ag/Ag<sup>+</sup> reference electrode. During the electrochemical polymerization, the solution was agitated by a small argon stream in the semi-closed system which allows a small amount of oxygen entering.

In the first scan for the cyclic voltammogram of the electrochemical synthesis (**Figure 2-1**), two irreversible and two reversible waves can be found. From the potential end of this sweeping, a pair of waves at 0.8 V are redox reactions with high reversibility derived from the bis(terpyridine)iron(III)/(II) couple.<sup>27</sup> The second and the third peak at 0.38 V and 0.77 V are two irreversible reactions ascribe to stepwise oxidation of the hydrazine group of the complex.<sup>28</sup> The final signal at -1.2 V is a quasi-reversible reaction corresponding to the O<sub>2</sub>/O<sub>2</sub><sup>-</sup> couple.<sup>29</sup>

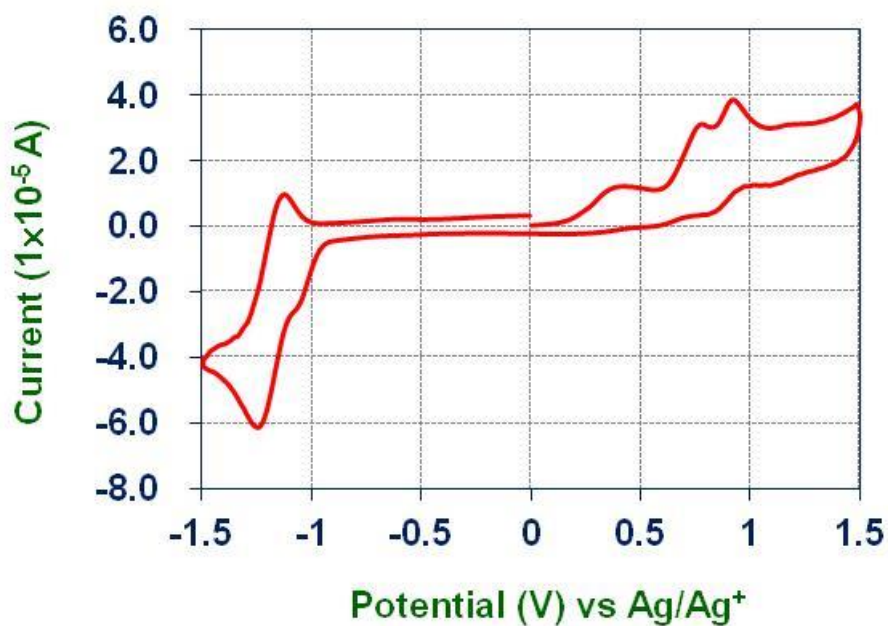
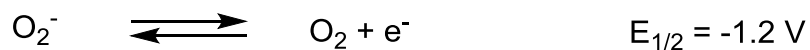
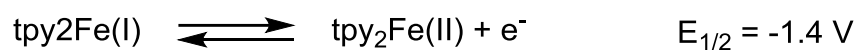
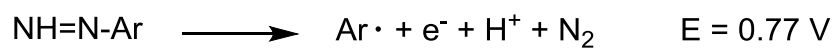


**Figure 2-1** The first scan cycle of a cyclic voltammogram of the electrochemical synthesis of the bis(terpyridine)iron network complex



In the whole modification process (**Figure 2-2**), the cyclic voltammograms show a growing tendency of the bis(terpyridine)iron complex redox waves; the redox pair continuously growing around 0.8 V is the bis(terpyridine)iron(III)/(II) couple. Another gradually increasing broad peak around -1.3 V is from one electron redox reaction of the terpyridine ligand. Other than these signals, a far separated redox pair appears at 0.7 V and -1.1 V, which can be attributed to charge trapping peaks of redox active species with the redox potential between 0.8 V and -1.3 V. One possible specie is molecular oxygen of which reduction potential is -1.2V.

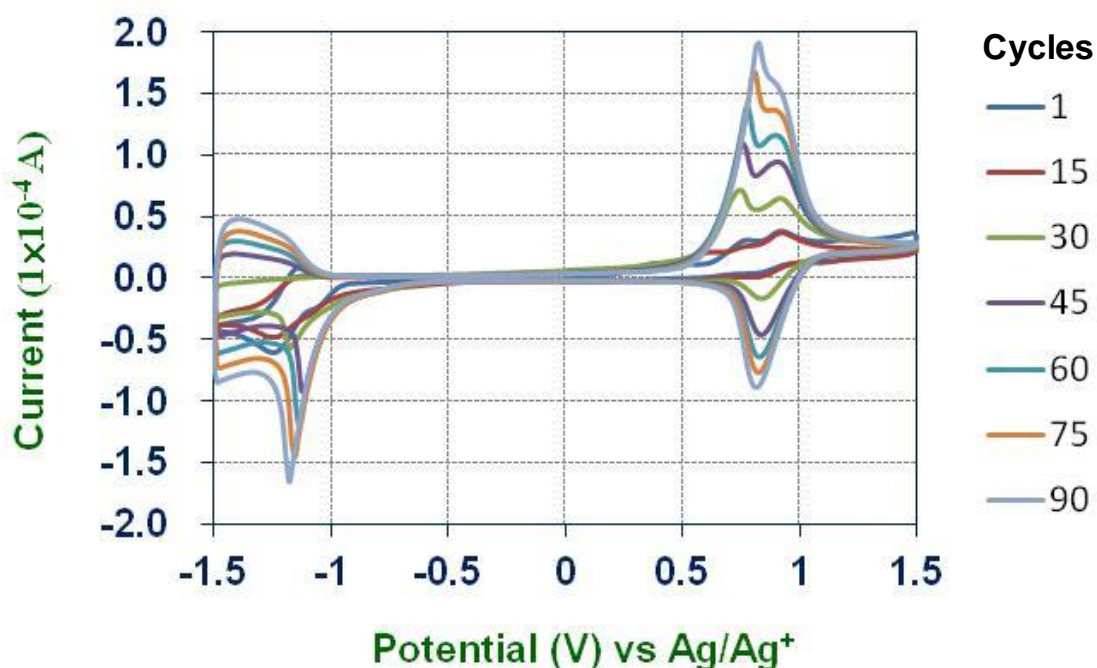


**Figure 2-2** The cyclic voltammograms of the electrochemical synthesis of the bis(terpyridine)iron complex network

### 2.3.3 The investigation of the role of oxygen in the electrochemical polymerization

Presence of oxygen in an electrochemical measurement often causes undesired reactions. Therefore, most of the cases, an oxygen-free system is important for getting a good spectrum. However, in the electrochemical synthesis of the bis(terpyridine)iron network, oxygen seems to play an important role for making a thick polymer film.

In order to evaluate the role of oxygen in the reaction, an experiment was conducted under an oxygen-free system with argon continuously bubbling (**Figure 2-3**). Under this condition, the signal of oxygen reduction cannot be found in voltammograms. Initially, an increase of bis(terpyridine)iron complex redox signals is observed. This indicates that a thin layer of the network complex was immobilized on the glassy carbon. However, the film growth did not continue as the potential scan number increased. The amount of the immobilized bis(terpyridine)iron complex reached a limit corresponding to several layers under this condition.

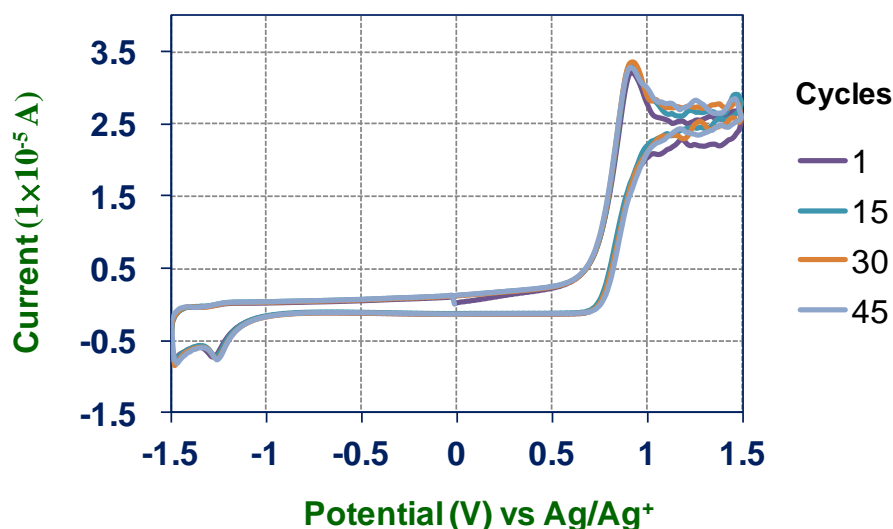


**Figure 2-3** The cyclic voltammograms of the electrochemical synthesis of the bis(terpyridine)iron complex network without oxygen

From this experiment, only the fact can be known that the presence of oxygen in this system is important. However, whether oxygen itself or superoxide produced from oxygen electrochemical reduction plays the key role is still unclear. This is because both substances do not exist in the testing system. To check whether superoxide anion is essential, another experiment was carried out under the presence of oxygen but without

superoxide generation. The potential sweep of cyclic voltammogram was therefore changed to scan between 1.5 V and 0 V (**Figure 2-4**). The resulting voltammograms were similar to those of the oxygen-free experiments and no thicker film was generated.

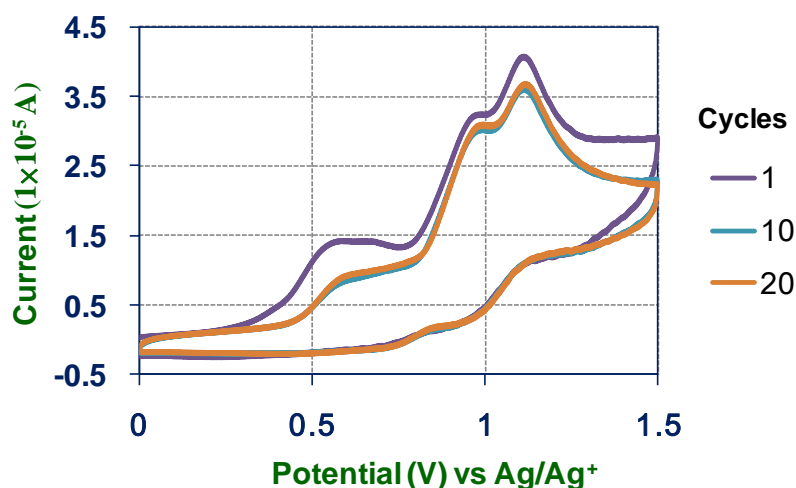


**Figure 2-4** The cyclic voltammograms of the electrochemical synthesis of the bis(terpyridine)iron complex network between 0 V and 1.5 V

From these results, it can be concluded that oxygen is essential for elongating the network complex on the electrode surface. However, only including oxygen in the reaction still cannot increase the complex loading amount. From the second control experiment, it is found that superoxide generation is another key point for synthesizing a thicker network film.

A possible reason is that the direct electrode oxidation of hydrazine only happens near the electrode surface. Although the network complex can transport electrons efficiently in most cases, because the hydrazine oxidation reaction requires three-electron oxidation and atom reorganization to generate a free-radical, the electron transfer through the network associating with oxidation become inefficient. Therefore, when the network grows thicker, the oxidation of hydrazine on the network surface will slow down and stop the film growth. On the other hand, oxygen can assist this oxidative electrochemical polymerization because it can be converted to superoxide by electrochemical reduction, which is a strong oxidation reagent for hydrazine. Superoxide can then be an efficient co-oxidant to remove electrons from hydrazine and help the film grow thicker. In short, this electrochemical polymerization mainly occurs through direct electrochemical oxidation, when the network is thinner. However, when the network becomes thicker, superoxide is adopted as the major oxidant of hydrazine.

### 2.3.4 The mechanism of the electrochemical polymerization reaction

According to literature and the electrochemical measurements,<sup>22</sup> aryl-hydrazine compounds can be converted to aryl-free radicals by two pathways. One is a direct electrooxidation, while the other is a chemical oxidation reaction by superoxide. The former predominates the stage of thinner film growth, while the latter predominates as the film grows thicker.

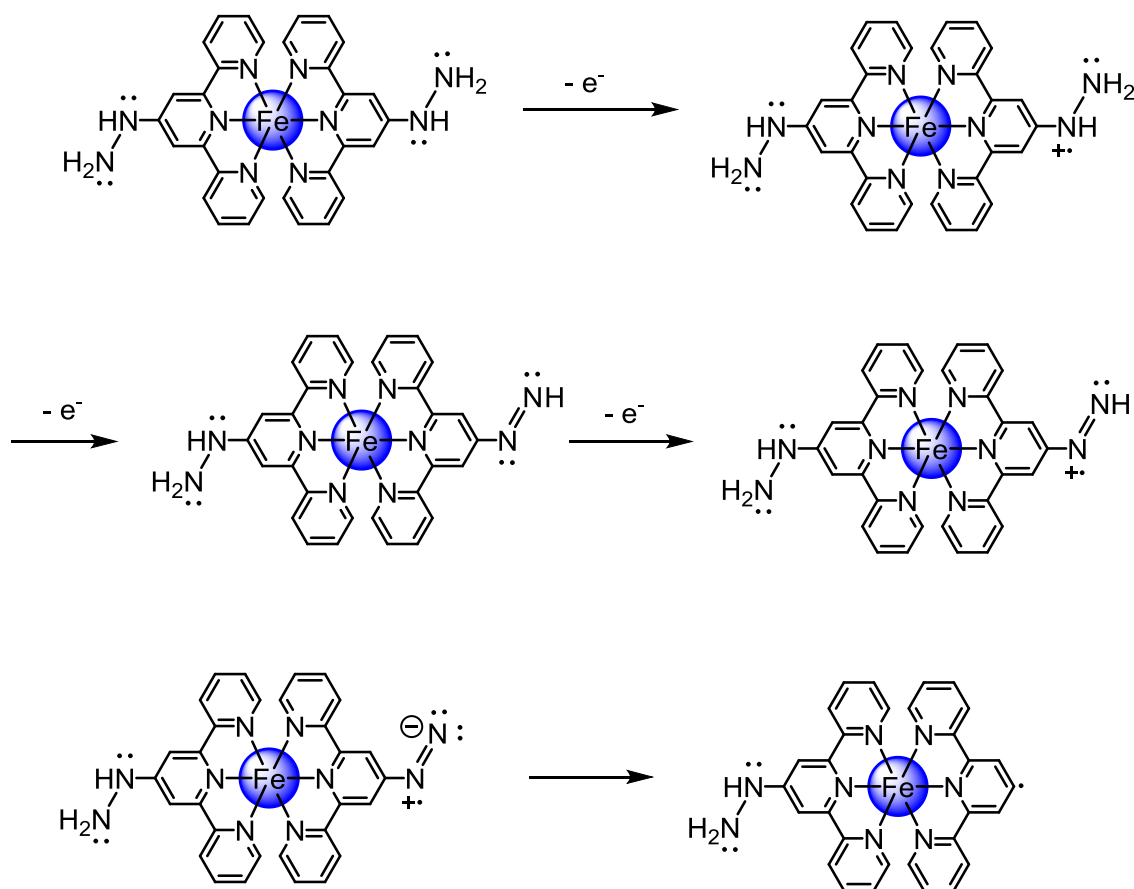


**Figure 2-5** the oxidation mechanism of hydrazine.

The detailed mechanism of oxidation is shown in **Figure 2-5**. First, an aryl-diazeno group is formed from a hydrazine group through a two-electron oxidation process. This is a stable intermediate as the oxidation process is separated from the next oxidation in the cyclic voltammogram. The aryl-diazeno group will be further oxidized at the electrode to form an aryl-diazeno radical or a diazonium like compound. As this intermediate is unstable, a dinitrogen will be immediately released from the compound and an aryl free-radical will then be generated near the electrode surface. This

free-radical will attack the carbon electrode surface to immobilize itself via a free radical addition reaction to the unsaturated conjugated  $\pi$ -bond of the surface graphite-like structure.

After immobilization, the other hydrazine group of the complex will also be oxidized and converted to free radical. This immobilized free radical can couple with another free radical to form a carbon-carbon bond. The surface immobilized molecule is also possibly attacked by another free-radical complex in solution to proceed a radical addition reaction on a pyridine ring of the complex. This addition will cause a branch structure or form cross linking between wires. After repeating these processes several times, the immobilized complex will grow thicker and thicker to form a network structure on the surface (**Figure 2-6**).

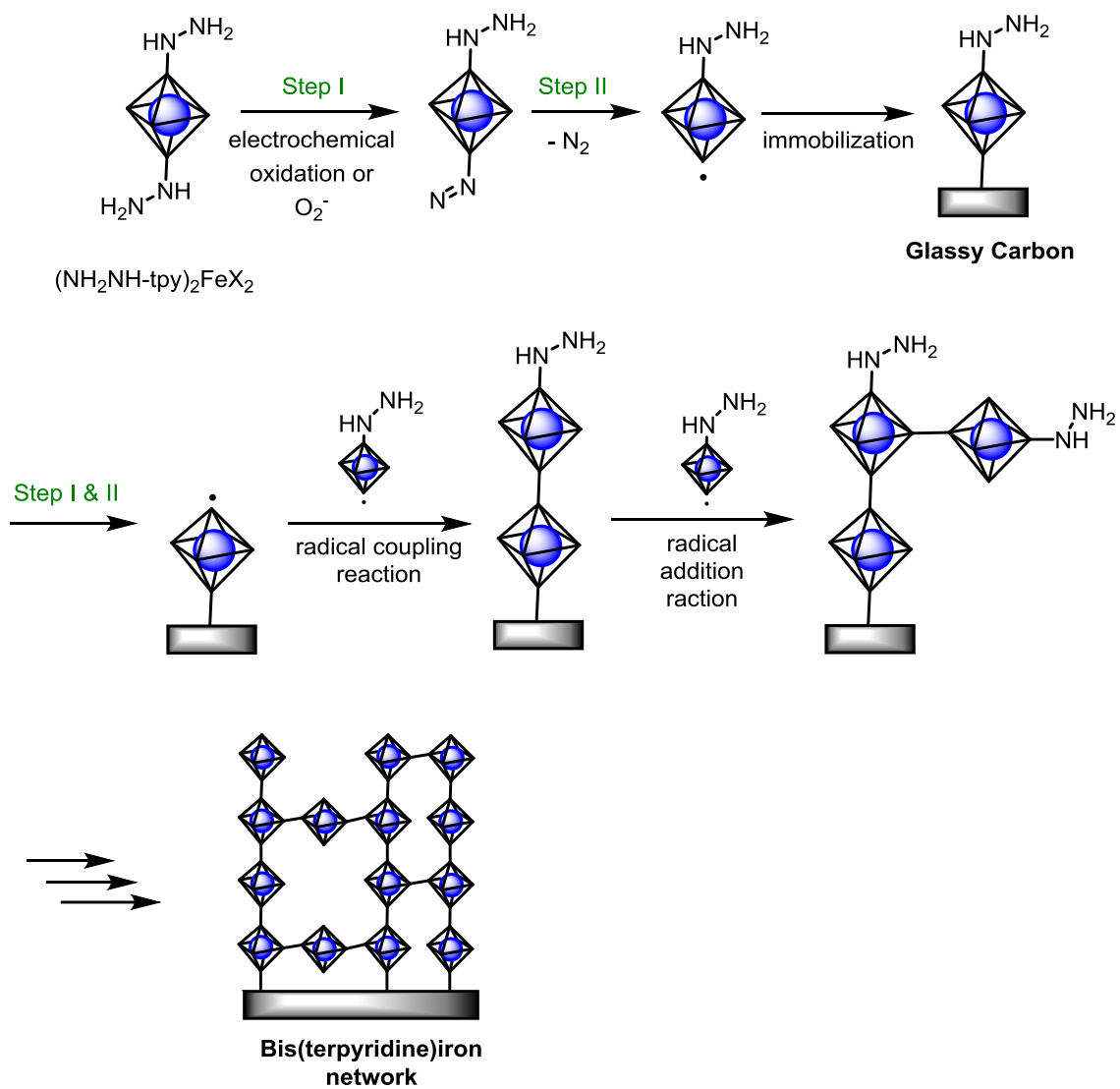


**Figure 2-6** The formation mechanism of the bis(terpyridine)iron network on glassy carbon electrode.

### 2.3.5 Surface structure characterization of the network complex

In order to understand the structure of the network complex on a glassy carbon electrode, a piece of well-polished glassy carbon electrode is measured by atomic force microscopy before and after the network complex immobilization (**Figure 2-7**). The AFM measurement is carried out at a  $1\ \mu\text{m}^2$  scan region.

The topography of the pristine glassy carbon electrode shows many small gaps. There are two main reasons causing this rough surface. One is from the inherent glassy carbon structure. In glassy carbon, the carbon atoms form a curved bundle graphite structure and fullerene-like structure which often cause small isolated holes. This imperfect structure prevents the formation of a flat surface. The other comes from the polishing process. Normal physical polishing methods are different from chemical-mechanical planarization techniques and it is difficult to offer a surface with atomic scale flatness.

On the other hand, the surface topography of the modified electrode exhibits a totally different image. This indicates that there is a network film covering the surface. This surface is dominated by many random polymer particles. The size of spherical particles is around 100 nm or bigger, and their height is about 20 to 100 nm.

Moreover, the phase images of the pristine electrode and the modified electrode also show totally different structures. This further proves that this electrochemical polymerization method can produce a film covering the electrode surface totally.

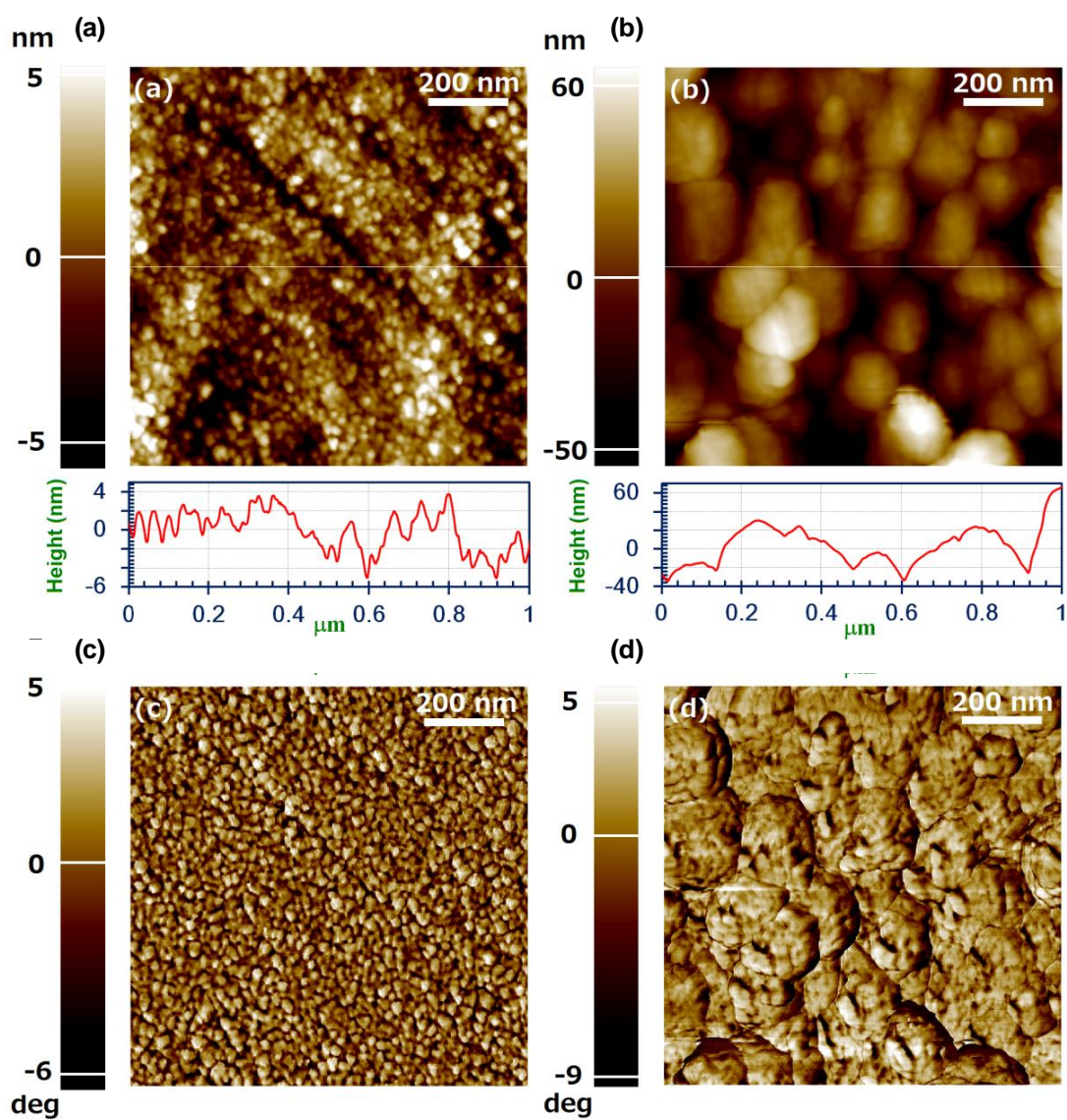


**Figure 2-7 AFM measurements of a pristine glassy carbon electrode (a) topography and (c) phase image and a network complex modified electrode (b) topography and (d) phase image.**

### 2.3.6 Energy storage performance of the network complex

To evaluate the charging and discharging performance of the material, cyclic voltammetry is first employed. Cyclic voltammetry is a good technique to monitor the electrochemical reactions in charging and discharging process. Moreover, this method is also very useful to evaluate the capacity of the material at different scan rates.

In the energy storage testing, the bis(terpyridine)iron(III)/(II) redox reactions are mainly focused. This is because bis(terpyridine)iron(II) and (III) complex are very stable under ambient condition and their self-exchange redox reactions are extremely fast. Therefore, it is expected that when the operation region is selected to be near the potential of the iron(III)/(II) redox couple, this material can exhibit high current density; this is to say, it can be charged and discharged very quickly.

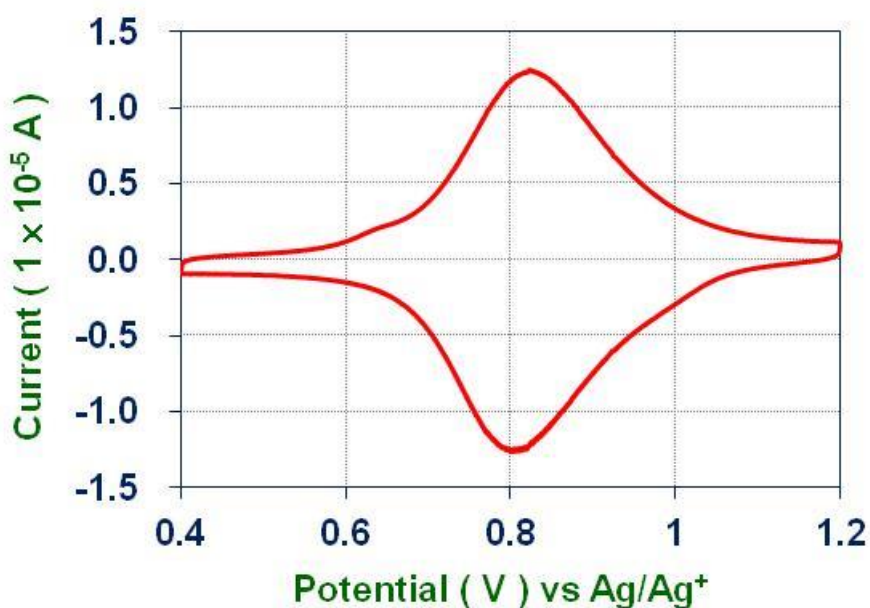


**Figure 2-8** A cyclic voltammogram at a scan rate of 0.1 Vs<sup>-1</sup>.

In a cyclic voltammogram at 0.1 Vs<sup>-1</sup>, the peak potential of the oxidation of bis(terpyridine)iron(II) complex is observed at 0.824 V and the reduction of bis(terpyridine)iron(III) complex is at 0.805 V (**Figure 2-8**). The peak potential difference is only 19 mV. This indicates that this system has very small internal resistance. Therefore, only very small energy will be lost in the cell operation.

The oxidation process, the charging reaction, starts at 0.57 V and finishes at 1.10 V. The reduction process, the discharging reaction, is from 1.10 V to 0.56 V. Both

processes show almost symmetric gaussian curve. Moreover, the capacities of these two process are almost identical. These results indicate that almost no side redox reactions occur during charging and discharging and energy wastage is kept to the minimum. In short, it can be simply concluded that network complex operating in this potential operation region is very stable and suitable for energy storage.

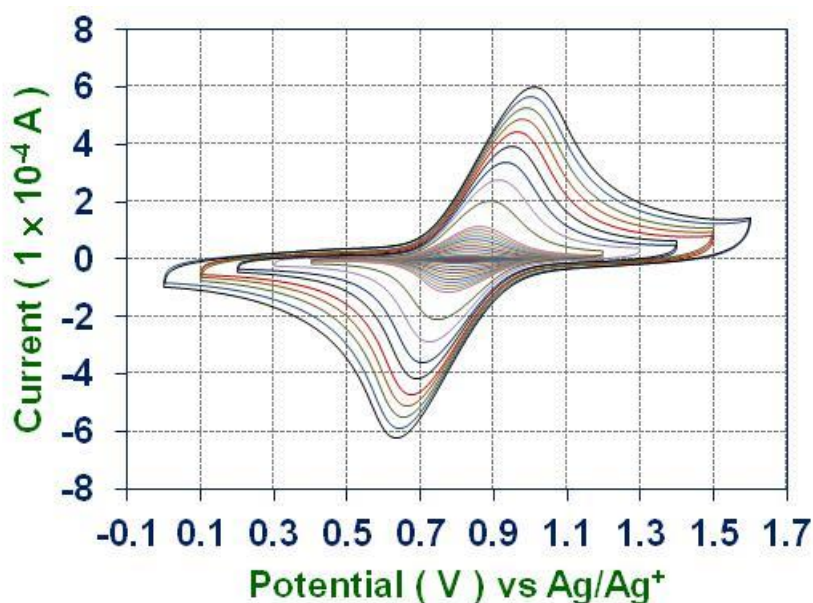


**Figure 2-9** Cyclic voltammograms at various scan rates.

In order to examine the performance of this material under high charging and discharging speeds, cyclic voltammetries are carried out at scan rates from  $0.01 \text{ Vs}^{-1}$  to  $10 \text{ Vs}^{-1}$  (**Figure 2-9**). The cyclic voltammograms of higher scan rates show much higher charging and discharging currents, but their peaks also become much wider. Although the material can offer higher current when operating at higher speeds, the charging and discharging potential difference also become bigger. This means that under high current density operations, the charging process will require much more energy and the discharging will offer less energy.

Furthermore, if the area of these charging and discharging peaks is integrated, capacities of this network complex can be obtained (**Figure 2-10**). At a scan rate of  $0.01 \text{ Vs}^{-1}$ , the charging and discharging capacity are around  $2.5 \times 10^{-5} \text{ C}$ . When the scan rate increases by ten, one hundred and one thousand times, the capacities are about  $2.45 \times 10^{-5} \text{ C}$ ,  $2.23 \times 10^{-5} \text{ C}$  and  $1.75 \times 10^{-5} \text{ C}$  respectively. The decreases of capacities are only 2 %, 10.8 % and 30% correspondingly.

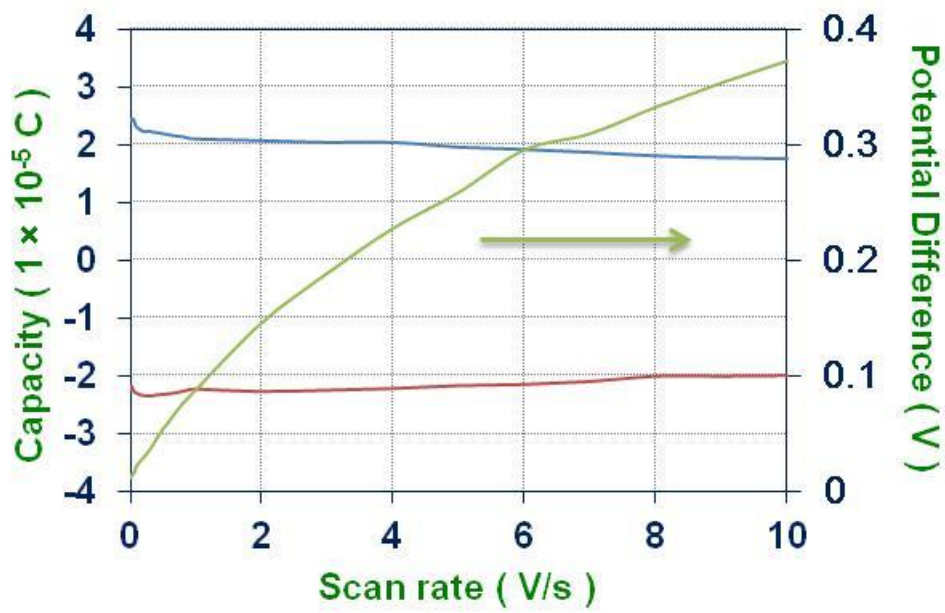
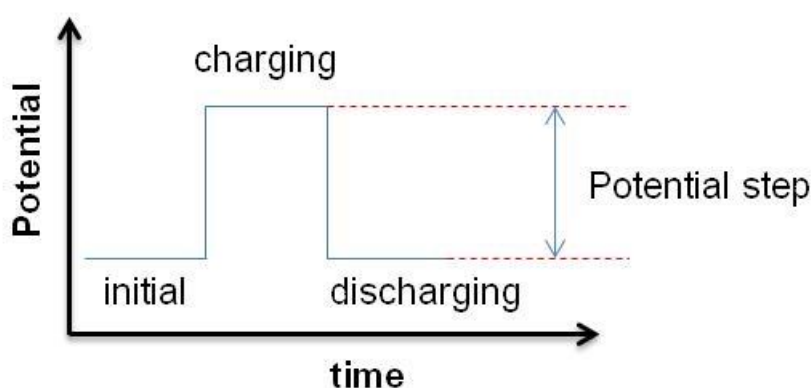


Figure 2-10 The capacities of the network complex at various scan rates.

### 2.3.7 Chronocoulometry and chronoamperometry investigation

In order to understanding the charging and discharging property of the network complex at a constant operation potential, chronocoulometry and chronoamperometry was employed. In these measurements, the potential of working electrode is set at a constant potential to charge the material (**Figure 2-11**). After charging, the potential is reduced to another potential to discharge the material. During these processes, the amount of charge or the magnitude of current are monitored by chronocoulometry and chronoamperometry, respectively.



**Figure 2-11 Potential setting of chronocoulometry and chronoamperometry versus time.**

In measuring the network complex, the charging and discharging potential are set equally apart from the redox potential of bis(terpyridine)iron complex, 0.8 V. For example, in the case of the 0.6 V potential step, the charging potential is fixed at 1.1 V and the discharging potential is set at 0.5 V. Both potentials have 0.3 V difference from the redox potential of bis(terpyridine)iron complex.

In the chronocoulometry measurements, the potential steps are from 0.1 V to 1.0 V (**Table 2- 1 & Figure 2-13**). This means that the charging potentials are from 0.85 V to 1.3 V and the discharging potentials are from 0.75 V to 0.3 V. In the chronocoulomogram with a 0.4 V potential difference, the network complex can be charged to 80% in 0.08 s, 90% in 0.16 s and 95% in 0.35 s. On the other hand, the charged material can be discharged to 80% in 0.08 s, 90% in 0.16 s and 95% in 0.62 s (**Figure 2-12**).

In the measurements of the series of potential differences, when the potential step increases, the capacity of the material also increases. However, the increase is not linear. The increase is bigger in the initial potential increasing steps as compared in the final steps.

**Table 2- 1 Capacities derived from chronocoulometry<sup>a</sup>**

Entry	Potential difference (V)	Charging potential (V)	Discharging potential (V)	Capacity (C)
1	0.10	0.85	0.75	$1.2 \times 10^{-5}$
2	0.20	0.90	0.70	$1.9 \times 10^{-5}$
3	0.30	0.95	0.65	$2.4 \times 10^{-5}$
4	0.40	1.00	0.60	$2.7 \times 10^{-5}$
5	0.50	1.15	0.55	$2.9 \times 10^{-5}$
6	0.60	1.10	0.50	$3.1 \times 10^{-5}$
7	0.70	1.25	0.45	$3.2 \times 10^{-5}$
8	0.80	1.20	0.40	$3.35 \times 10^{-5}$
9	0.90	1.35	0.35	$3.46 \times 10^{-5}$
10	1.00	1.30	0.30	$3.6 \times 10^{-5}$

<sup>a</sup> The potential is referred to Ag/Ag<sup>+</sup> reference electrode.

There are two reasons for causing the capacity increase. One is the redox reaction of bis(terpyridine)metal complex and the other is double layer capacitor effect derived from electrode surface. For smaller potential differences, the capacity increases mainly come from the redox reactions of bis(terpyridine)iron complex. However, for larger potential differences, the capacity increases are mainly due to the double layer capacity effect of the electrode surface.

On the other hand, the chronoamperometry can be used to evaluate the relationship between current density and capacity retention. For example, in the measurement of the 0.4 V potential step, the network complex can retain 80% of its capacity at a discharging rate of 280 A g<sup>-1</sup>, 90% at 60 A g<sup>-1</sup>, 95% at 7.6 A g<sup>-1</sup> (**Figure 2-14**). This indicates that the network has the potential be a high power density material.

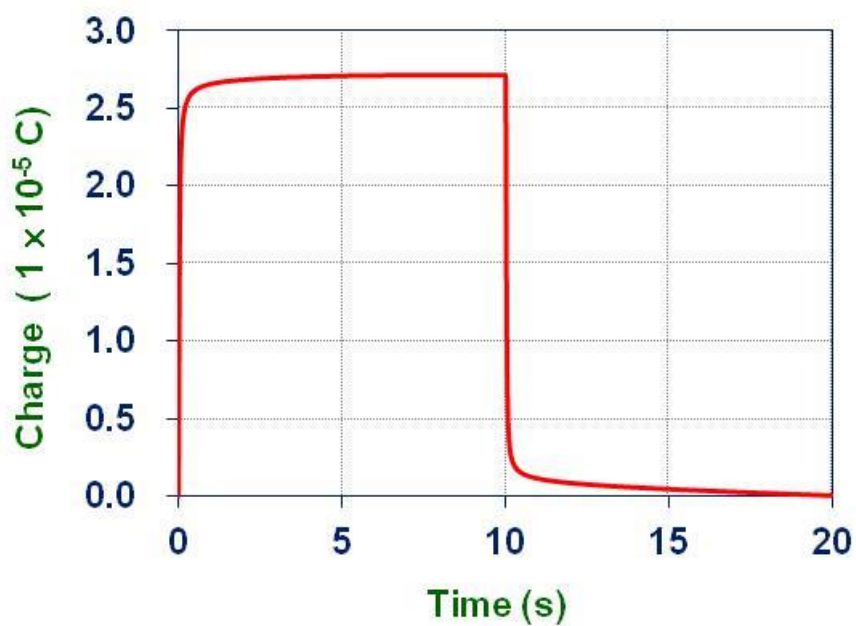


Figure 2-12 A chronocoulammogram of the bis(terpyridine)iron network complex at a potential step of 0.4 V.

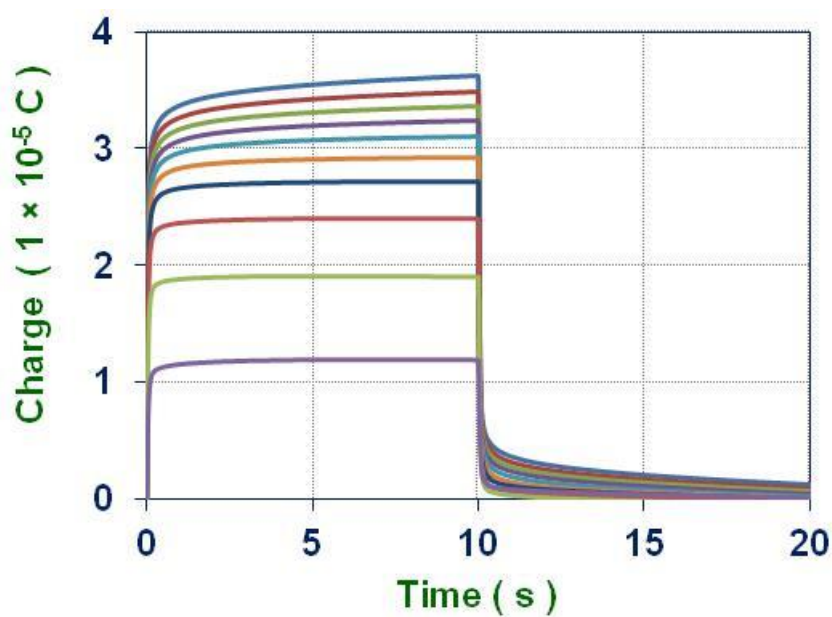
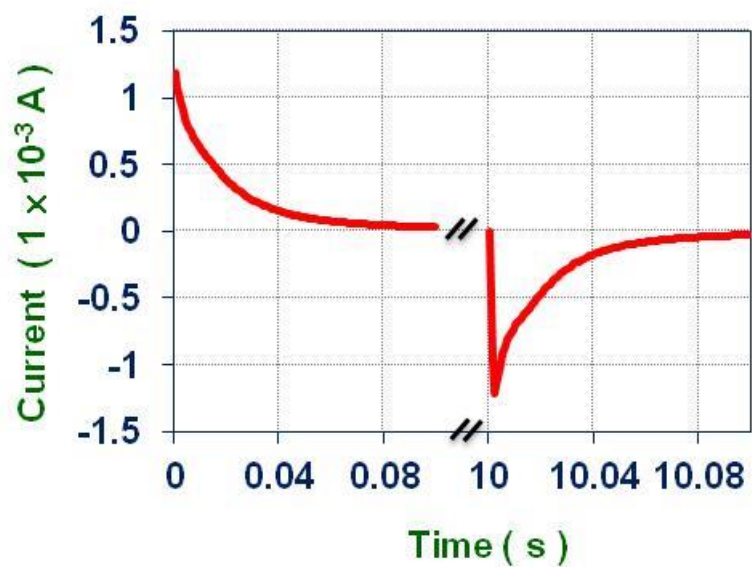


Figure 2-13 Chronocoulammograms of the bis(terpyridine)iron complex at potential steps from 0.1 V to 1.0 V.



**Figure 2-14** A chronoamperogram of the bis(terpyridine)iron complex at a potential step of 0.4 V.

### 2.3.8 The stability of the network complex

To evaluate the stability of the network complex, the modified glassy carbon electrode is subjected to continuous charging and discharging using cyclic voltammetry. The charging and discharging processes are carried out between 0.4 V and 1.2 V at a scan rate of  $1 \text{ V s}^{-1}$ . The voltammograms from the first cycle to the 3000th cycle are shown in **Figure 2-15**. The profiles are almost the same from the initial scan to the final scan. This means that the continuous charging and discharging processes do not cause any electrochemical side reactions or change the structure of the network complex.

Moreover, the charging and discharging capacities of each cycle show only 5 % decay after 3000 cycles (**Figure 2-16**). This indicates that there is almost no decomposition of the network complex during the charging and discharging test.

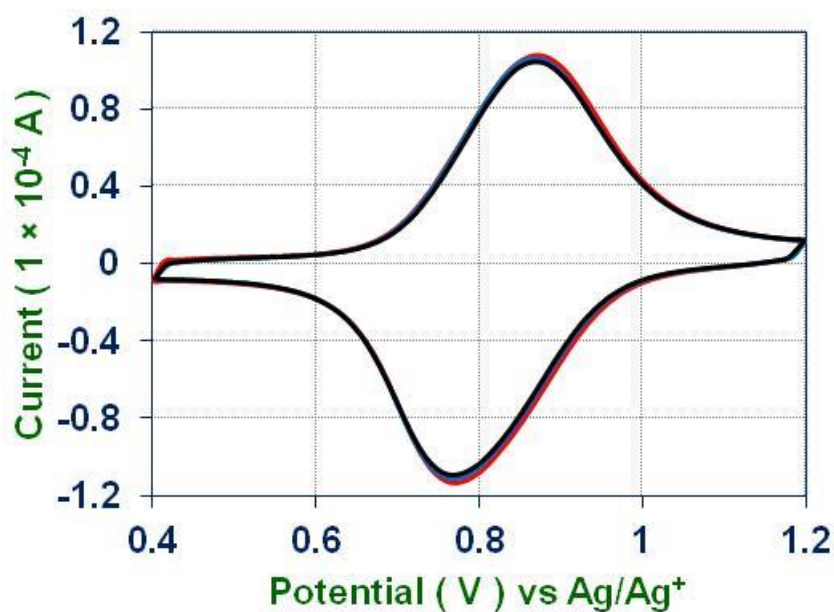


**Figure 2-15** Charging and discharging testing of the network complex from 1st to 3000th cycle.

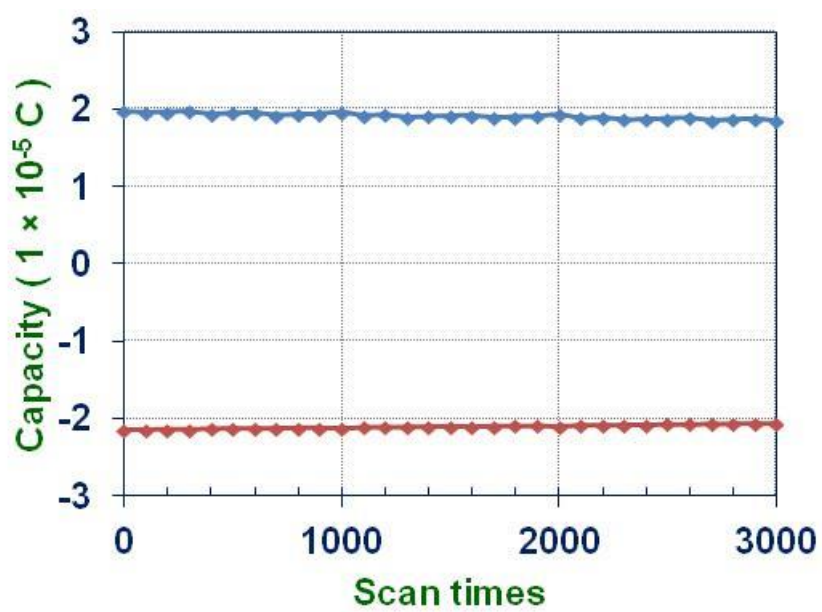


**Figure 2-16** The charging and discharging capacities of the bis(terpyridine)iron complex versus scan cycles.

## 2.4 Conclusion

In this research, a very stable network bis(terpyridine)iron complex was synthesized on a glassy carbon electrode by an electrochemical polymerization method. The network complex shows high compatibility with glassy carbon electrode. The network film can be attached stably to glassy carbon and the electron flow between these two materials occurs smoothly. In the electrochemical investigation of the charging and discharging processes, the capacity of the network complex decreases only moderately when the scan rate increases. Moreover, its capacity increases with a bigger magnitude of potential steps in the chronocoulommograms. This material also shows high stability and can endure high speed charging and discharging processes for three thousands cycles with only 5% capacity decay. Based on these results, it can be concluded that this bis(terpyridine)iron complex network material can be a good candidate for modifying carbon electrodes of supercapacitors to improve their electric capacities. This indicate that redox active metal complex polymers may be a high promising high power density energy storage materials for next generation power sources of automobiles and other portable devices.

## 2.5 References

---

1. Service, R. F. *Science*, **2006**, *313*, 902.
2. Miller, J. R.; Simon, P. *Science*, **2008**, *321*, 651.
3. Simon, P.; Gogotsi, Y. *Science*, **2001**, *334*, 917.
4. Miller, J. R. *Science*, **2012**, *335*, 1312.
5. (a) Kötz, R.; Carlen, M. *Electrochim. Acta* **2000**, *45*, 2483. (b) Burke, A. *J. Power Sources* **2000**, *91*, 37.
6. Du Pasquier, A.; Plitz, I.; Menocal, S.; Amatucci, G. *J. Power Sources* **2003**, *115*, 171.
7. Conway, B. E. *J. Electrochem. Soc.* **1991**, *138*, 1539.
8. Pandolfo, A. G.; Hollenkamp, A. F. *J. Power Sources* **2006**, *157*, 11.
9. (a) Sun, Y. K.; Oh, S. M.; Park, H. K.; Scrosati, B. *Adv. Mater.* **2011**, *23*, 5050. (b) Oh, S. W.; Myung, S. T.; Bang, H. J.; Yoon, C. S.; Amine, K.; Sun, Y. K. *Electrochem. Solid State Lett.* **2009**, *12*, A181.
10. Chmiola, J.; Yushin, G.; Gogotsi, Y.; Portet, C.; Simon, P.; Taberna, P. L. *Science* **2006**, *313*, 1760.
11. Yamazaki, S.; Ishikawa, M. *Encyclopedia of Applied Electrochemistry: Redox Capacitor*, Springer, New York, **2014**, 1779.
12. (a) Brezesinski, T.; Wang, J.; Tolbert, S. H.; Dunn, B. *Nat. Mater.* **2010**, *9*, 146. (b) Yang, L.; Cheng, S.; Ding, Y.; Zhu, X.; Wang, Z. L.; Liu, M. *Nano Lett.* **2011**, *12*, 321.
13. (a) Xiao, J.; Wan, L.; Yang, S.; Xiao, F.; Wang, S. *Nano Lett.* **2014**, *14*, 831. (b) Wu, C.; Lu, X.; Peng, L.; Xu, K.; Peng, X.; Huang, J.; Yu, G.; Xie, Y. *Nat. Commun.* **2013**, *4*, 2431. (c) Lai, C.; Dou, Y. Y.; Li, X.; Gao, X. P. *J. Power Sources* **2010**, *195*, 3676.
14. (a) Zhang, J.; Zhao, X. S. *J. Phys. Chem. C* **2012**, *116*, 5420. (b) Ryu, K. S.; Lee, Y.-G.; Hong, Y.-S.; Park, Y. J.; Wu, X.; Kim, K. M.; Kang, M. G.; Park, N.-G.;

- 
- Chang, S. H. *Electrochim. Acta* **2004**, *50*, 843.
15. Lee, H. Y.; Kim, S. W.; Lee, H. Y. *Electrochem. Solid State Lett.* **2001**, *4*, A19.
16. (a) Nishihara, H.; Kanaizuka, K.; Nishimori, Y.; Yamanoi, Y. *Coord. Chem. Rev.* **2007**, *251*, 2674. (b) Nishimori, Y.; Kanaizuka, K.; Murata, M.; Nishihara, H. *Chem. Asian J.* **2007**, *2*, 367. (c) Kurita, T.; Nishimori, Y.; Toshimitsu, F.; Muratsugu, S.; Kume, S.; Nishihara, H. *J. Am. Chem. Soc.* **2010**, *132*, 4524. (d) Nishimori, Y.; Kanaizuka, K.; Kurita, T.; Nagatsu, T.; Segawa, Y.; Toshimitsu, F.; Muratsugu, S.; Utsuno, M.; Kume, S.; Murata, M.; Nishihara, H. *Chem. Asian J.* **2009**, *4*, 1361. (e) Maeda, H.; Sakamoto, R.; Nishimori, Y.; Sendo, J.; Toshimitsu, F.; Yamanoi, Y.; Nishihara, H. *Chem. Commun.* **2011**, *47*, 8644. (f) Sakamoto, R.; Katagiri, S.; Maeda, H.; Nishihara, H. *Coord. Chem. Rev.* **2013**, *257*, 1493.
17. (a) Engstrom, R. C. *Anal. Chem.* **1982**, *54*, 2310. (b) Engstrom, R. C.; Strasser, V. A. *Anal. Chem.* **1984**, *56*, 136. (c) Hu, F.; Karweik, D. H.; Kuwana, T. *J. Electroanal. Chem. Interfacial Electrochem.* **1985**, *188*, 59.
18. (a) Kinoshita, K. *Carbon: electrochemical and physicochemical properties*. John Wiley Sons, New York, **1988**. (b) Donnet, J. B. *Carbon* **1968**, *6*, 161. (c) Banks, C. E.; Davies, T. J.; Wildgoose, G. G.; Compton, R. G. *Chem. Commun.* **2005**, 829.
19. (a) Saby, C.; Ortiz, B.; Champagne, G. Y.; Bélanger, D. *Langmuir* **1997**, *13*, 6805. (b) Deinhammer, R. S.; Ho, M.; Anderegg, J. W.; Porter, M. D. *Langmuir* **1994**, *10*, 1306.
20. (a) Bahr, J. L.; Yang, J.; Kosynkin, D. V.; Bronikowski, M. J.; Smalley, R. E.; Tour, J. M. *J. Am. Chem. Soc.* **2001**, *123*, 6536. (b) Delamar, M.; Hitmi, R.; Pinson, J.; Saveant, J. M. *J. Am. Chem. Soc.* **1992**, *114*, 5883. (c) Allongue, P.; Delamar, M.; Desbat, B.; Fagebaume, O.; Hitmi, R.; Pinson, J.; Savéant, J. M. *J. Am. Chem. Soc.* **1997**, *119*, 201.
21. Dahmen, S.; Bräse, S. *Angew. Chem. Int. Ed.* **2000**, *39*, 3681.
22. Malmos, K.; Iruthayaraj, J.; Ogaki, R.; Kingshott, P.; Besenbacher, F. Pedersen, S. U.; Daasbjerg, K. *J. Phys. Chem. C*, **2011**, *115*, 13343.
23. (a) Collin, J. P.; Jouaiti, A.; Sauvage, J. P. *J. Electroanal. Chem.*, **1990**, *286*, 75. (b) Scarborough, C. C.; Lancaster, K. M.; DeBeer, S.; Weyhermüller, T.; Sproules, S.;

- 
- Wieghardt, K. *Inorg. Chem.*, **2012**, *51*, 3718.
24. Holyer, R. H.; Hubbard, C. D.; Kettle, S. F. A.; Wilkins, R. G. *Inorg. Chem.* **1966**, *5*, 622.
25. Malmos, K.; Iruthayaraj, J.; Pedersen, S. U.; Daasbjerg, K. *J. Am. Chem. Soc.* **2009**, *131*, 13926.
26. Zhou, Z.; Sarova, G. H.; Zhang, S.; Ou, Z.; Tat, F. T.; Kadish, K. M.; Echegoyen, L.; Guldi, D. M.; Schuster, D. I.; Wilson, S. R. *Chem. Eur. J.*, **2006**, *12*, 4241.
27. Nishimori, Y.; Kanaizuka, K.; Murata, M.; Nishihara, H. *Chem.–Asian J.*, **2007**, *2*, 367.
28. Malmos K.; Iruthayaraj J.; Pedersen S. U.; Daasbjerg K. *J. Am. Chem. Soc.*, **2009**, *131*, 13926.
29. Sawyer, D. T.; Seo, E. T. *Inorg. Chem.*, **1977**, *16*, 499.

## **Chapter 3**

# **Bis(terpyridine)iron network complex-carbon nanotube hybridized materials**

### 3.1 Introduction

Porous carbon electrodes are one of the most important features of supercapacitors.<sup>1,2</sup> This is because electrode surface area is a critical parameter for the size of their capacities.<sup>3</sup> Moreover, the porosity of an electrode can increase ion migration rates around the electrode surface and therefore enhance supercapacitor performance.<sup>4</sup>

The most commonly used porous electrodes for supercapacitors are active carbon electrodes.<sup>5</sup> Active carbon can be obtained from many different preparation methods, such as pyrolysis of carbon containing material or oxygen activation of inactive carbons.<sup>6</sup> They are so commonly used mainly due to their low price and ease of large scale industrial production. Also, they have good conductivity and stability which are suitable for capacitor electrodes. However, active carbons usually have irregular chemical structures and chemically active functional groups on their surface.<sup>7</sup> These are potential problems for the further improvement of supercapacitors. For example, irregular structure on the carbon prevents large current from flowing through the electrode and electrode modification. On the other hand, active functional groups on electrodes may cause some undesired side reactions which reduce the coulomb efficiency. Therefore, a porous carbon electrode with ordered and stable chemical structure is highly desirable.

Two of the most promising novel materials for preparing porous carbon electrodes of supercapacitors are graphene<sup>8,9</sup> and carbon nanotubes.<sup>10</sup> Graphene is monolayer graphite and is usually prepared by oxidation-dispersion-reduction process in a large scale.<sup>11</sup> This method is complicated and sometime cannot offer highly specific surface area electrode easily. On the other hand, carbon nanotubes can be processed much easier by using only ultrasonic assisting dispersing method to form stable and well porous electrodes.<sup>12</sup> Moreover, compared with graphene, carbon nanotubes only have a very small ratio of unstable carbon, such as that at structural edges. Therefore, carbon nanotube electrodes are considered to be a much stable and suitable electrode material.

## **3.2 Experimental section**

### **3.2.1 Materials**

#### **Preparation of carbon nanotube porous electrodes**

Carbon nanotubes and a surfactant (sodium dodecyl sulfate or sodium dodecylbenzene- sulfonate) were mixed in ultra-pure water. The suspension solution was sonicated by probe-type sonicator for 5 min at 150 W. The mixture then became a homogeneous black solution. This solution was dropped onto a clean glassy carbon electrode with 10 mm diameter and dried in a 120°C oven for 30 min. After all water evaporated, a carbon nanotube film is formed on the glassy carbon surface. The film was washed by acetone, ethanol and water to remove surfactant adsorbing on carbon nanotube surface. Finally the electrode was dried again to offer a stable carbon nanotube porous electrode.

#### **Immobilization of the bis(terpyridine)iron network complex on carbon nanotube electrode**

The modification process is almost identical with the method described in Chapter 2. The only exception is that the working electrode was replaced by a carbon nanotube porous electrode.

### **3.2.2 Instruments**

Electrochemical measurements were conducted using the same instruments and conditions as described in Chapter 2.

### 3.3 Results and discussion

#### 3.3.1 Preparation of carbon nanotube electrode

The process to prepare a porous and stable carbon nanotube electrode for the supporting electrode of the network complex is shown in **Figure 3-1**. A 60 nm diameter multi-walled carbon nanotube was dispersed in aqueous surfactant solutions with ultrasonic assistance. The CNT dispersion solution was then dropped on a clean glassy carbon electrode surface and the solvent was dried at 120°C. After drying, the electrode was washed by organic solvents and water to remove surfactants. Then a porous carbon nanotube electrode was immobilized on the surface of glassy carbon.

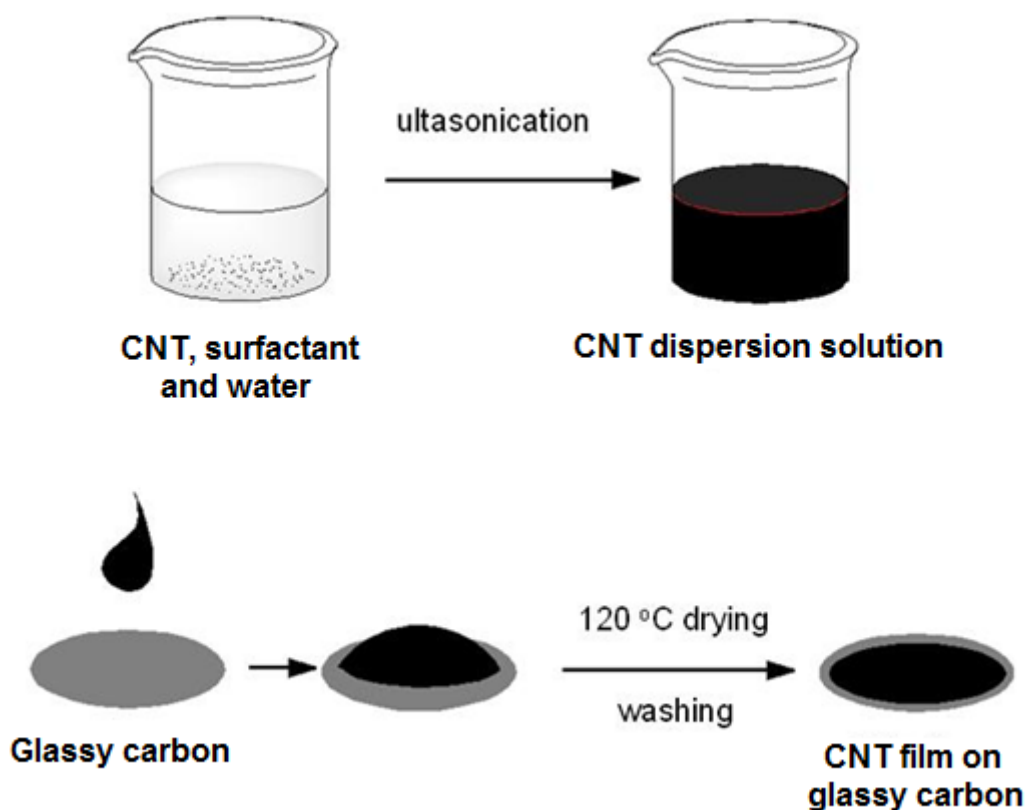


**Figure 3-1** The preparation of porous carbon nanotube film on glassy carbon.

In this preparation process, sodium dodecyl sulfate (SDS) and sodium dodecylbenzene- sulfonate (SDBS) were tested. These two anionic surfactants can both disperse carbon nanotube in water well. However, in the case using sodium dodecyl

sulfate, the just prepared carbon nanotube film is weak against water, because the solubility of carbon nanotubes covered by surfactants in water is significant. Moreover, SDS can be dissolved only in water but not in organic solvents. Therefore, no suitable solvents can be used to remove SDS from the carbon nanotube and keep the film intact at the same time.

On the other hand, compared with SDS, SDBS has a higher solubility in organic solvents, especially in acetone. Therefore, after the carbon nanotube film drying, SDBS can be removed by acetone without damaging the film. This is because only SDBS can be dissolved in acetone but the carbon nanotube coated by SDBS cannot. In short, SDBS was found to be a better dispersion agent for preparing the carbon nanotube film on glassy carbon surface.

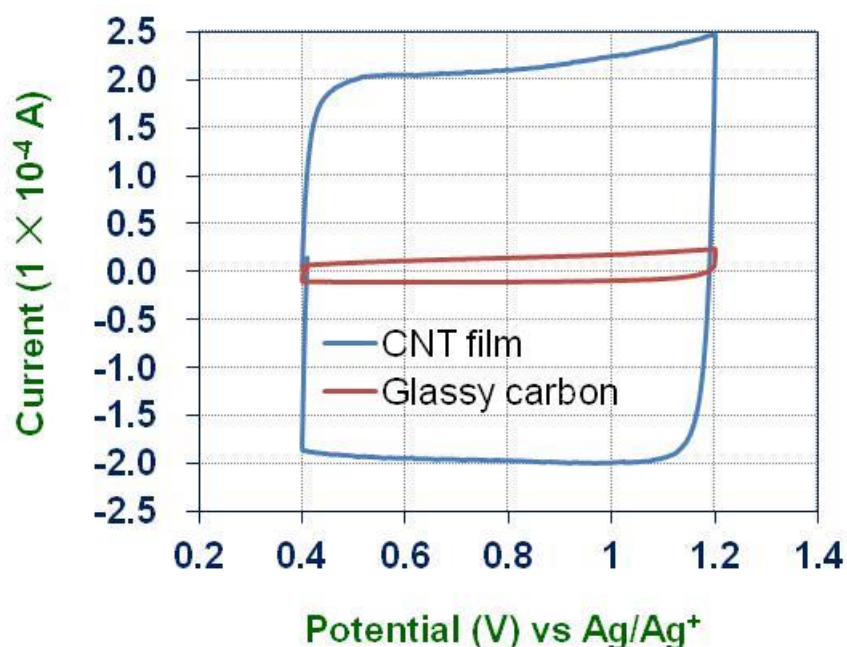


**Figure 3-2** The Cyclic voltammograms of a CNT film on a glassy carbon electrode and the bare glassy carbon electrode.

The resulting carbon nanotube electrode was then investigated by cyclic voltammetry in 0.1 M  $\text{Bu}_4\text{ClO}_4\text{-MeCN}$  solution at a scan rate of  $100 \text{ mVs}^{-1}$  (**Figure 3-2**). The double layer capacity of the carbon nanotube electrode is  $1.55 \times 10^{-3} \text{ C}$  and that of the bare supporting glassy carbon electrode is  $9.2 \times 10^{-5} \text{ C}$ . This means that immobilization of 0.1 mg carbon nanotube increases the surface area about 16 times. From these values, it can be calculated that the effective surface area of the carbon nanotube electrode is  $13.2 \text{ cm}^2$ .

On the other hand, the cyclic voltammogram of the carbon nanotube electrode shows an almost rectangle shape. This indicates that electrolytes in the solution can rapidly reach all tube surfaces, and electrons can easily flow between nanotubes. Although these nanotubes are not linked by covalent bonds, the electrode still has fast response to an external applied potential. This is because high electrical conductivity of carbon nanotube help electrons flow smoothly through a tube and the strong  $\pi$ - $\pi$  stacking interaction reduces distance and hence the electron tunneling energy between nanotubes.

### 3.3.2 The electrochemical synthesis of the complex network on the carbon nanotube electrode

The bis(terpyridine)iron complex network can be immobilized on the carbon nanotube porous electrode by the same condition as the previous research in Chapter 2. However, as the electrode surface is extended to all carbon nanotube surface and many slight surface structure differences exist on the tubes, the rates of oxidation and reduction reactions on these tubes should also be slightly different (**Figure 3-3**). Therefore, the signals in the modification cyclic voltammogram on carbon nanotube electrode become broader than those on the glassy carbon electrode.

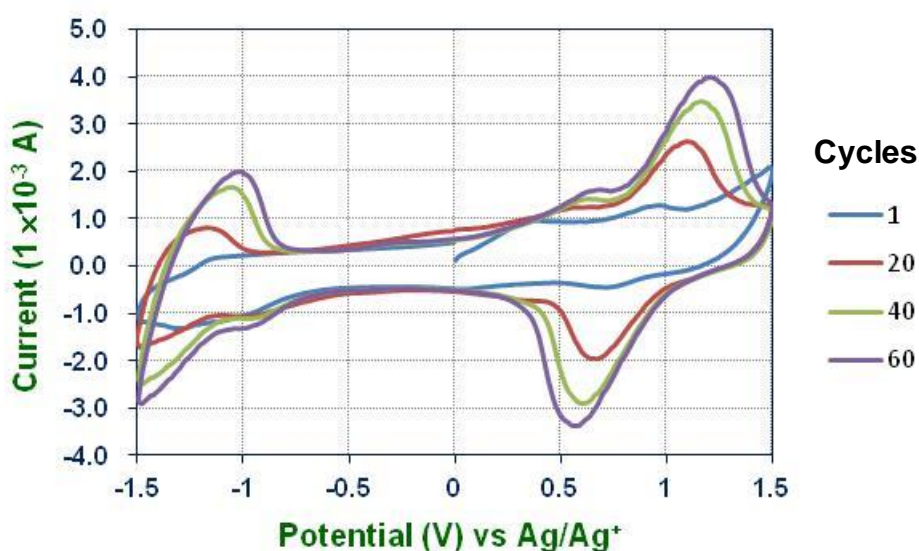


**Figure 3-3** The cyclic voltammograms of electrochemical synthesis of bis(terpyridine)iron complex network on porous carbon nanotube electrode.

### 3.3.3 Electrochemical evaluation of the hybridized material of the network complex and carbon nanotube

A test cell was assembled with the complex network-carbon nanotube hybridized electrode, an Ag/Ag<sup>+</sup> reference electrode and a platinum counter electrode in a button battery like cell configuration. In this configuration, the working and the counter electrodes are set face to face with a small distance between them (**Figure 3-4**). In this cell, the hybridized electrode was set at the bottom of the cell. The counter electrode was at the upper side, and the reference electrode was set at the center of the counter electrode. All electrodes were sealed in a glass tube which was filled with 1.0 M NBu<sub>4</sub>ClO<sub>4</sub>-MeCN solution. This cell configuration decreases the distance between working and counter electrodes and hence reduces the system resistance.

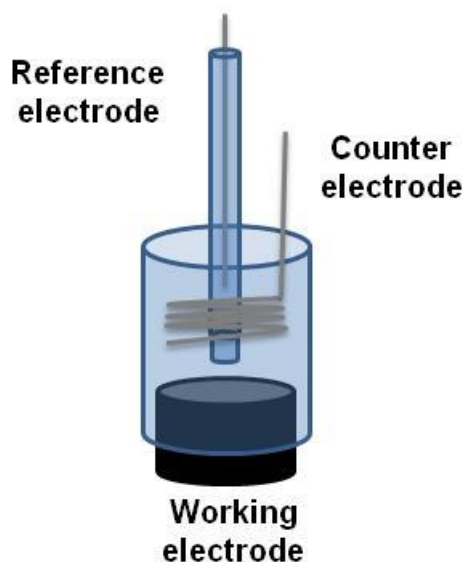


**Figure 3-4** The structure of a test cell for a network complex-carbon nanotube hybridized electrode.

To evaluate the charging and discharging behavior of the cell, cyclic voltammetry was used with changing the scan rate from 10 mVs<sup>-1</sup> to 1000 mVs<sup>-1</sup> (**Figure 3-5**). The potential of the voltammograms was swept from 0.4 V to 1.2 V and then reversed. In this potential region, reversible redox waves were found to be the signals of bis(terpyridine)iron(III)/(II) couple. These anodic and cathodic peaks appeared at almost the same potential of the network complex on glassy carbon electrode described in Chapter 2.

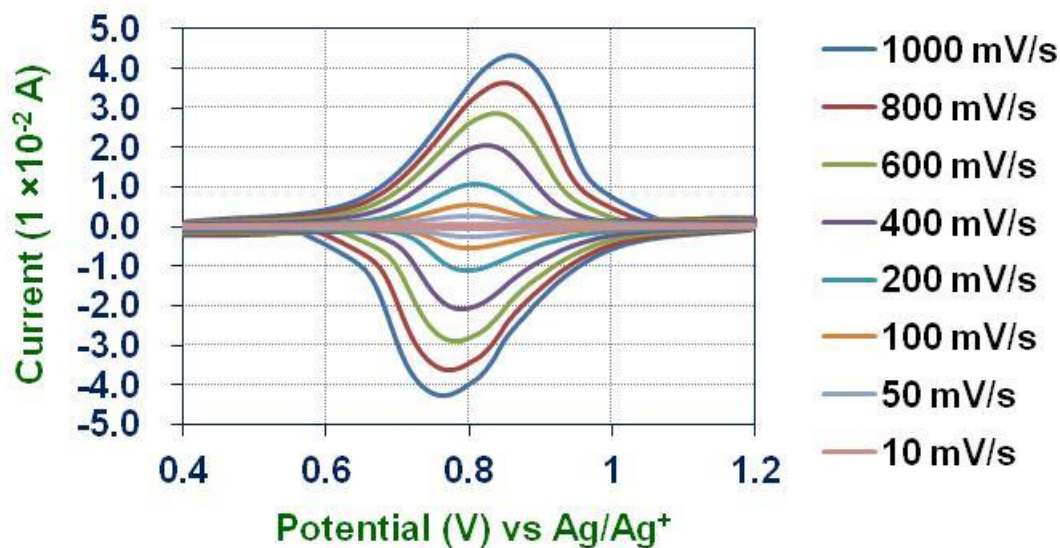


**Figure 3-5** Cyclic voltammograms of the hybridized material at various scan rates.

In the voltammograms at the scan rate of  $10 \text{ mVs}^{-1}$  (**Figure 3-6**), the peak has a highly symmetrical gaussian curve shape. The charging starts at 0.55 V and ends at 1.05 V. The peak current is located at 0.8 V. On the other hand, the discharging signal is from 1.05 V to 0.55 V. The peak current is at 0.79 V. At this scan rate, the charging and discharging signal have almost the same shape and appear at almost the same potential. This means that at such low charging and discharging rates, all redox centers on the electrode might have similar chemical environment, and all redox reactions occur under a steady state, because electrolytes have enough time to diffuse to anywhere around the hybridized electrode.

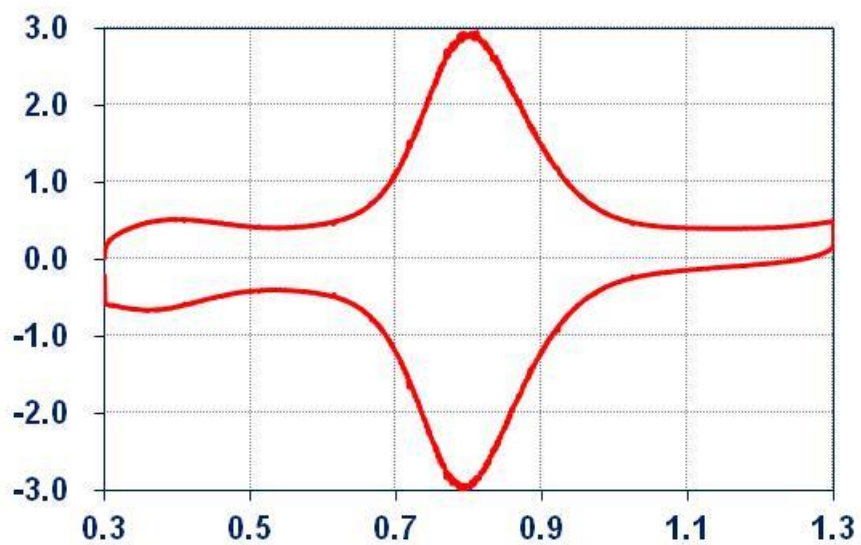


Figure 3-6 Cyclic voltammogram at a scan rate of 10 mVs<sup>-1</sup>.

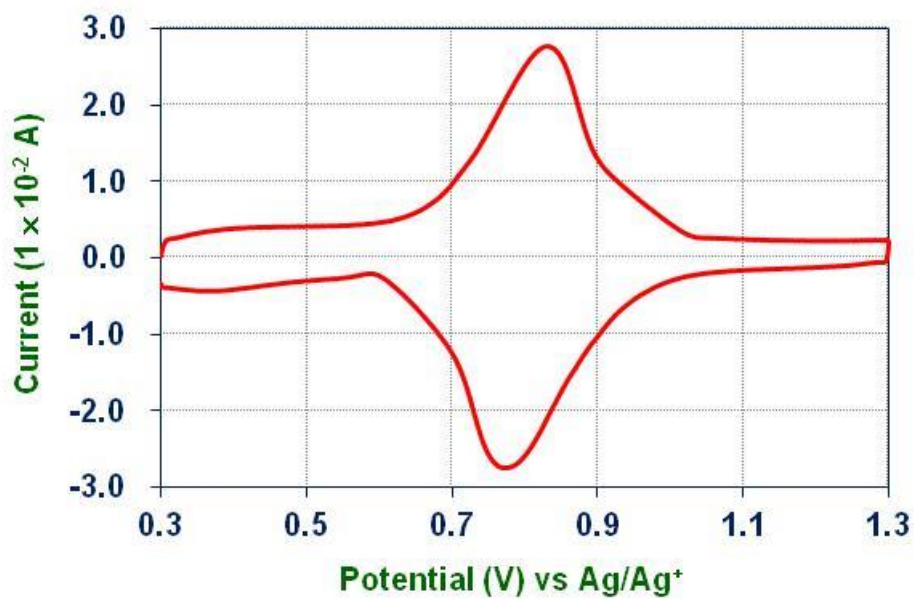


Figure 3-7 Cyclic voltammogram at a scan rate of 1000 mVs<sup>-1</sup>.

When the scan rate increases to  $1000 \text{ mVs}^{-1}$  (**Figure 3-7**), the starting and ending points of charging and discharging process are similar to the case of  $10 \text{ mVs}^{-1}$ . The charging reaction starts at 0.55 V and ends at 1.07 V and the discharging reaction is from 1.09 to 5.58 V. Moreover, the charging and the discharging peaks only shift slightly to 0.83 V and 0.77 V, respectively.

Comparing with the low scan rate result, the peak widths have almost similar and the peak potentials are only shifted by a little. This means that although the operation rate was increased by 100 times, the charging and discharging process do not change too much. However, the peak shapes of the fast charging and discharging voltammogram is no longer a perfect symmetric gaussian peak, but some minor peaks can be found to be part of the main peak.

This difference between high scan process and low scan process comes from the redox centers in different location of the electrode showing different activity. The complexes locating at the surface of the electrode can have much faster electrochemical response, because electrolytes easily migrate there. However, when the redox centers exist in the deeper site of the electrode, electrolyte equilibrium cannot be reached quickly and therefore, the redox response will also be much slower.

Other than slight differences, the capacities of the hybridized material at high scan rates have a much smaller decrease than those at low scan rate. The charging capacity at the scan rate of  $10 \text{ mVs}^{-1}$  is  $4.35 \times 10^{-3} \text{ C}$  and the discharging capacity is  $4.56 \times 10^{-3} \text{ C}$ . When the scan rate increases to  $1000 \text{ mVs}^{-1}$ , the charging and discharging capacity decreases slightly to  $4.06 \times 10^{-3} \text{ C}$  and  $4.45 \times 10^{-3} \text{ C}$  respectively. This scan rate increase causes only 7 % loss and 2.5 % loss of charging and discharging capacity, respectively. In these measurements, the charging capacity is slightly lower than discharging capacity, because the 18-electron bis(terpyridine)iron(II) complex is more stable than the 17-electron iron(III) complex. Therefore, the oxidation rate is slightly lower than the reduction rate. This is also the reason why the discharging capacities decrease by a smaller amount as compared to the charging capacities as the scan rate increases.

From results of these voltammograms, almost no capacity decrease is found when the charging and discharging rate increases. This indicates that the hybridized material has a well porous structure and good connections exist among all components. Therefore, when the scan rate increases, electrolyte migration and electron transportation in this material are able to follow the rate of external potential changing.

### 3.3.4 The capacity analyzed by chronocoulometry

In order to understand the charging and discharging behaviors of the hybridized material under the constant potential, chronocoulometry was employed. The constant potential measurements can offer information about the electrode performance of the initial state of a battery in a real operation situation. Charging and discharging potentials of batteries usually keep at a constant value for a period and then increase or decrease along with the process respectively. This is because the battery internal resistance changes, and charge storage units would be saturated, then exhausted.

The charging and discharging were carried out in a series of potential steps from 0.2 V to 1.0 V. The charging potential is from 0.7 V to 0.3 V and the discharging potential is from 0.9 V to 1.3 V (**Figure 3-8**).

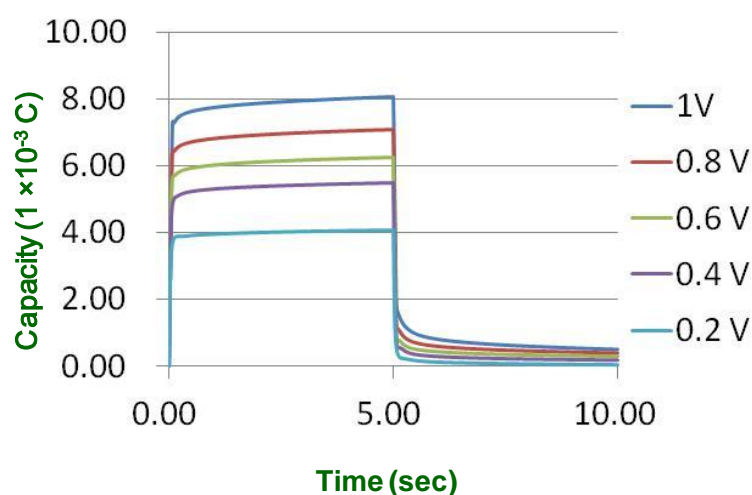


**Figure 3-8 Chronocoulammograms of the complex network-carbon nanotubes hybridized electrode.**

Under the potential step of 0.6 V from 0.5 V to 1.1 V, this hybridized material can be charged to 50% within 0.034s, 60% within 0.040s, 70% within 0.046s, 80% within 0.054s, 90% within 0.080s and 95% within 0.536s. On the other hand, it can be discharged to 50% within 0.034s, 60% within 0.040s, 70% within 0.047s, 80% within 0.057s, 90% within 0.254s and 95% within 4s. From these data, the charging and discharging capacity changings show similar tendencies. Initially, the charging and discharging reactions proceed quickly. After 80% of the processes, the charging and discharging rates slow down. In the cases of operation at other potential steps, the charging and discharging processes have similar capacity changing tendency.

From all measurements of the series of potential steps (**Figure 3- 9**), initially the capacity increases quickly. In the step of 0.1 V, the capacity is  $2.40 \times 10^{-3}$  C, and in the step of 0.2 V, the capacity increases to almost twice,  $4.68 \times 10^{-3}$  C. Then the capacity increase slows down. In the potential step of 0.3 V, the capacity only increases by 7% to  $5.00 \times 10^{-3}$  C. The slow increase continues as the size of potential step increases. Finally, when the potential step is changed to 1.0 V, the capacity is  $8.00 \times 10^{-3}$  C.

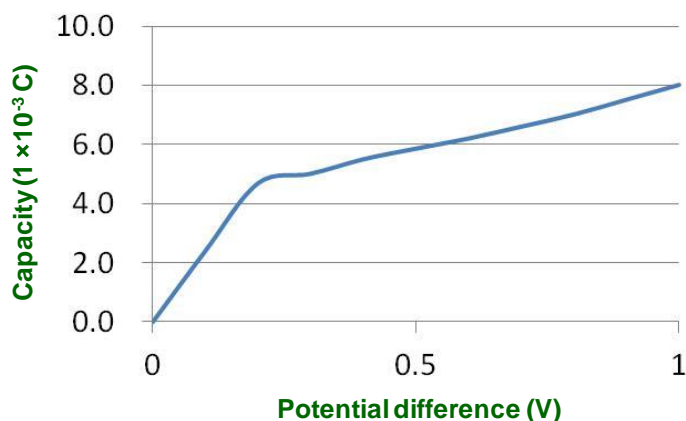


**Figure 3- 9 Capacities of the complex network-carbon nanotubes hybridized electrode versus various potential steps.**

This two-step increasing tendency comes from two different energy storage mechanisms. In the initial step, the capacity increase is mainly from the redox reaction of the bis(terpyridine)iron(III)/(II) couple. It can be proved by the cyclic voltammograms, where this potential region overlaps with the iron(III)/(II) redox peaks. The slope of the second capacity increase is more gentle than that of the first region, because this increase mainly comes from the double layer capacities effect of the surface of carbon nanotubes and network complexes.

To further study these measurements, the electrode energy density can be deduced from these chronocoulometry measurements. Under the potential step of 1.0 V, the specific energy density is  $18 \text{ mAhg}^{-1}$ . About 55% of this energy density comes from faradic current due to the bis(terpyridine)iron complex network, and about 45% is from the nonfaradic double layer capacitor effect.

### 3.3.5 The stability test of the hybridized material

In order to evaluate the life span of the hybridized material, this testing cell was subjected to a continuous charging and discharging process by cyclic voltammetry. The test was carried out in a 1 M  $\text{NBu}_4\text{ClO}_4\text{-MeCN}$  solution with a scan rate of  $1.0 \text{ Vs}^{-1}$  for 2000 cycles (**Figure 3-10 & Figure 3-11**).

From the cyclic voltammograms, a moderate decrease of the capacity is found after the 2000 cycles of charging and discharging. Initially, the charging peak current is  $2.48 \times 10^{-2} \text{ A}$ , the capacity is  $3.78 \times 10^{-3} \text{ C}$ , and the peak potential is 0.829 V. The discharging peak current is  $-2.3 \times 10^{-2} \text{ A}$ , the capacity is  $3.73 \times 10^{-3} \text{ C}$ , and the peak potential is 0.778 V. The potential difference of these two peaks is 0.051 V.

After 1000 cycles of charging and discharging, the charging peak current and the capacity decrease to  $2.16 \times 10^{-2} \text{ A}$  and  $3.29 \times 10^{-3} \text{ C}$  respectively. The peak potential is 0.819 V. The discharging peak current decreases to  $-2.07 \times 10^{-2} \text{ A}$ , and the capacity reduces  $3.29 \times 10^{-3} \text{ C}$ . The peak current is 0.788V. Moreover, the size of peak potential difference shrinks to 0.031 V.

In the final cycle, 2000<sup>th</sup> scan, the charging peak current and the capacity further decrease to  $1.96 \times 10^{-2} \text{ A}$  and  $2.81 \times 10^{-3} \text{ C}$ . The peak potential is still 0.819 V. The discharging peak current and the capacity also decrease to  $-1.86 \times 10^{-2} \text{ A}$  and  $2.87 \times 10^{-3} \text{ C}$ . The peak potential is 0.788 V. The potential difference is also 0.031 V.

From these data, the peak current decreases 13% in the charging process and 10 % in the discharging process after 1000 cycles of operations. Furthermore the peak current shows 21% decrease and 19% in charging and discharging process correspondingly after 2000 cycles. On the other hand, the capacity decreases about 13% after 1000 cycles, and decreases about 26% after 2000 cycles. However, the peak potential difference of charging and discharging peaks was slightly smaller. After 1000 cycles proceeded, the potential difference shows 39% decrease, but the difference was kept constant.

This capacity decreases is supposed to result from carbon nanotubes detachment. As the porous carbon nanotube film only adsorbs on the glassy carbon supporting electrode by physical interaction, the resulting hybridized material is more unstable than the network complex in Chapter 2. Therefore, during charging and discharging processes, the volume hybridized material film changing caused by electrolytes

migration and solvent molecule intercalation results in structure strength decreasing and film detachment.

Although the capacity of this hybridized material shows a moderate decrease during continuous charging and discharging operations, its coulomb efficiency, which is the ratio of the discharging and charging capacity, was kept at almost 100%. This means that almost all charge kept in this material can be taken out efficiently and almost no side redox reactions happen in these processes.

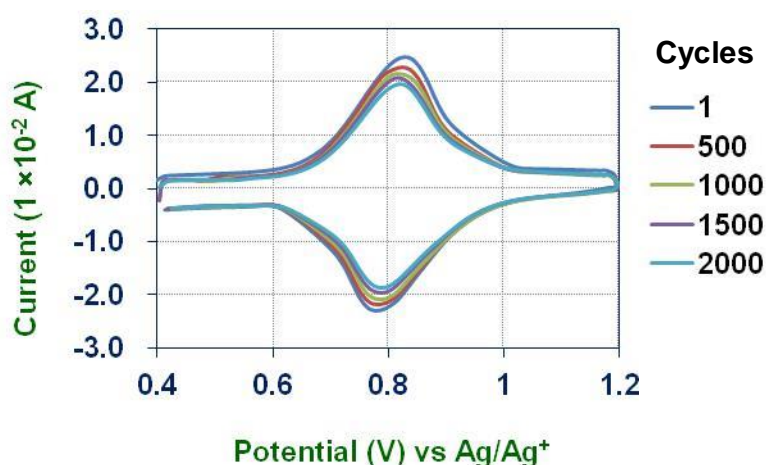


**Figure 3-10** Cyclic voltammograms of a stability test of the network complex-carbon nanotube hybridized material.

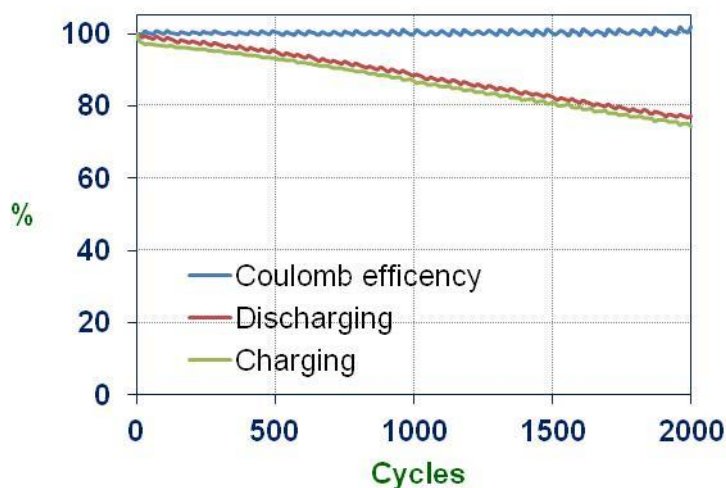


**Figure 3-11** The capacities and coulomb efficiency of the hybridized material versus scan cycles.

### **3.4 Conclusion**

A novel hybridized material of bis(terpyridine)iron network complex with carbon nanotube was prepared by an electrochemical modification reaction. The hybridized material possesses good porosity and conductivity. In the electrochemical measurements, both redox responses of the bis(terpyridine)iron complex network and the double layer capacitance effect of nano structures of network and carbon nanotube can be observed. This indicates that the immobilization of the network complex does not block accessibility of ions to carbon nanotube surface. Moreover, this hybridized material, like the pristine network complex, can be operated under high charging and discharging current with small capacity loss. It also exhibits good stability for continuous charging and discharging operations. In this research, the combination of the network complex and carbon nanotube successfully increases the areal capacity of the electrode and can be a basis of development for high energy supercapacitors.

### 3.5 References

---

1. Zhang, L. L.; Zhao, X. S. *Chem. Soc. Rev.*, **2009**, *38*, 2520.
2. Chmiola, J.; Yushin, G.; Gogotsi, Y.; Portet, C.; Simon, P.; Taberna, P. L. *Science*, **2006**, *313*, 1760.
3. (a) Soffer, A.; Folman, M. *J. Electroanal. Chem. Interfacial Electrochem.* **1972**, *38*, 25. (b) Zheng, C.; Qi, L.; Yoshio, M.; Wang, H. *J. Power Sources* **2010**, *195*, 4406.
4. Xu, F.; Cai, R.; Zeng, Q.; Zou, C.; Wu, D.; Li, F.; Lu, X.; Fu, Y. L. R. *J. Mater. Chem.* **2011**, *21*, 1970.
5. (a) Zhang, L. L.; Zhao, X. S. *Chem. Soc. Rev.* **2009**, *38*, 2520. (b) Wang, G.; Zhang, L.; Zhang, J. *Chem. Soc. Rev.* **2012**, *41*, 797. (c) Wang, Y. G.; Cheng, L.; Xia, Y. Y. *J. Power Sources* **2006**, *153*, 191. (d) Yuan, A.; Zhang, Q. *Electrochem. Commun.* **2006**, *8*, 1173.
6. (a) Ioannidou, O.; Zabaniotou, A. *Renew. Sust. Energy Rev.* **2007**, *11*, 1966. (b) De Jong, K. P.; Geus, J. W. *Catal. Rev.* **2000**, *42*, 481.
7. De Jong, K. P.; Geus, J. W. *Catal. Rev.* **2000**, *42*, 481.
8. Zhu, Y.; Murali, S.; Stoller, M. D.; Ganesh, K. J.; Cai, W.; Ferreira, P. J.; Pirkle, A.; Wallace, R. M.; Cychosz, K. A.; Thommes, M.; Su, D.; Stach, E. A.; Ruoff, R. S. *Science*, **2011**, *332*, 1537.
9. Stoller, M. D.; Park, S.; Zhu, Y.; An, J.; Ruoff, R. S. *Nano. Lett.*, **2008**, *8*, 3498.
10. An, K. H.; Kim, W. S.; Park, Y. S.; Choi, Y. C.; Lee, S. M.; Chung, D. C.; Bae, D. J.; Lim, S. C.; Lee, Y. H. *Adv. Mater.*, **2001**, *13*, 497.
11. Fan, X.; Peng, W.; Li, Y.; Li, X.; Wang, S.; Zhang, G.; Zhang, F. *Adv. Mater.* **2008**, *20*, 4490.
12. Rastogi, R.; Kaushal, R.; Tripathi, S. K.; Sharma, A. L.; Kaur, I.; Bharadwaj, L. M. *J. Colloid Interface Sci.* **2008**, *328*, 421.



## **Chapter 4**

# **Electrochemical syntheses of ultra-long bis(terpyridine)metal complex wires covalently bound to carbon**

## 4.1 Introduction

Conducting wires are essential components in all electronics, because they can not only supply power for operation but also transport calculation information between electric components. In present integrated circuits, nano copper wires fabricated by copper interconnect technology developed by IBM and Motorola in 1997 are used.<sup>1</sup> This technology is suitable to prepare copper wires of any length to connect components, from neighboring logic units to distant computation clusters. However, the stability and conductivity of copper wires dramatically decrease when their widths are smaller than tens of nanometers. Therefore, synthesizing and controlling molecular scale wire is important for next generation computer systems.

There are two major types of molecular wires. One type is metal complex molecular wires<sup>2</sup> and the other is organic back-bond molecular wires.<sup>3</sup> The former is often regarded to be much superior to the latter. First their chemical and physical properties can be easily modified by changing metal species or bridging ligands. Second, the long-range electron transport abilities of complex wires are much better than organic wire.

However, employing a molecular wire system is totally different from the present copper system, because it is difficult to prepare and control the desired length of a long molecular wire.<sup>4</sup> Long molecular wires are usually synthesized by random reactions. For example, carbon nanotubes are produced by gas phase chemical vapor deposition reactions<sup>5</sup> and conducting polymers are prepared by catalyzed polymerization reactions.<sup>6</sup> Generally, wires generated from these reactions have various lengths and properties, and it is almost impossible to separate them accordingly. Furthermore, methods to efficiently control long molecular wire in nano-systems have not yet been established.

To overcome these problems, electrochemical methods are a promising solution. First, electrochemical syntheses can efficiently control and synthesize molecular wires at the same time. Second, long molecular wires with a desired length can be easily prepared in a short time. Third, fabricating a molecular wire with electrochemical methods can ensure that the counter ions of the molecular wires are well distributed among the wires and have enough moving space. This is especially important for molecular devices of wet systems.

## 4.2 Experimental section

### 4.2.1 Materials

4'-(4-Anilino)-2,2':6',2''-terpyridine, bis(4'-(4-anilino)-2,2':6',2''-terpyridine)iron(II) tetrafluoroborate and bis(4'-(4-anilino)-2,2':6',2''-terpyridine)ruthenium(II) hexafluorophosphate were synthesized according to literature procedures.<sup>7</sup> Perchloric acid, 60 %, and acetonitrile, HPLC grade, were purchased from Wako Pure Chemical Industries, Ltd and used without further purification. Water was double purified by millipore water purification systems. Tetrabutylammonium perchlorate was purchased from Tokyo Chemical Industry Co., Ltd. and recrystallized from ethanol before use.

#### Electrochemical syntheses of bis(terpyridine)metal complex wires

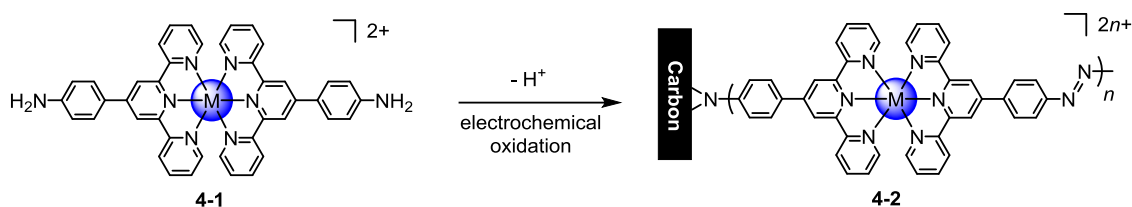
The electrochemical syntheses were carried out in a 0.1 M HClO<sub>4</sub>-MeCN-H<sub>2</sub>O solution (acetonitrile: water = 1: 1) with 0.1 mM of a bis(4'-(4-aniline)-terpyridine)metal complex. The reaction was set in a three electrodes cell: a glassy carbon electrode was used as the working electrode, a platinum coil electrode was used as the counter electrode and a Ag/Ag<sup>+</sup> electrode was used as the reference electrode. The electrochemical reaction was carried out by cyclic voltammetry with potential sweeps between 1.1 V and -0.8 V vs. Ag/Ag<sup>+</sup>.

### 4.2.2 Instruments

Electrochemical measurements and AFM investigations were conducted using the same instruments and conditions as described in Chapter 2. Raman spectroscopy was carried out using NRS-1000N laser Raman spectrophotometer (JASCO).

## 4.3 Results and discussion

### 4.3.1 The syntheses of extremely long molecular wires



**Scheme 4-1** The electrochemical syntheses of bis(terpyridine)metal complexes wires on carbon electrodes.

The fabrication of the long molecular wires was carried out by an electrochemical oxidation (**Scheme 4-1**). Comparing with the synthesis of the networks in Chapter 2, the monomer was changed from the bis(4'-hydrazino-2,2':6',2'')-terpyridine)iron complex to bis(4'-(4-anilino)-2,2':6',2'')-terpyridine)metal complexes. Also the reaction medium is changed from a  $\text{NBu}_4\text{ClO}_4\text{-MeCN}$  solution to a  $\text{HClO}_4\text{-MeCN-H}_2\text{O}$  solution.

There are a number of reasons why the reaction medium was changed. First, addition of water can increase the polarity of the solution to improve solubility of ionic complexes. Therefore, aggregation of complexes and random electrochemical reactions caused by this aggregation can be reduced to offer a more uniformly modified structure on the surface.

Second, addition of acids can efficiently reduce the resistance of solutions, because proton has the highest migration rate in aqueous medium. If the system resistance of an electrochemical cell is high, the electron transfer and redox reactions on the electrodes might not be uniform, and a higher oxidation potential or a lower reduction potential would be necessary to drive the required electrochemical reactions. These are often the main reasons causing partial decomposition of immobilized molecules. Furthermore, acids can protonate the aniline groups of the monomer complex to control the concentration of active molecules in the modification reaction. This can slow down the reaction rate to generate the polymer layer by layer and produce a well ordered structure. As the  $\text{NBu}_4\text{ClO}_4\text{-MeCN}$  solution cannot fulfill the above requirements,  $\text{HClO}_4\text{-H}_2\text{O-MeCN}$  solution was used instead.

The electrochemical syntheses of molecular wires were carried out by cyclic voltammetry (**Figure 4-1**). The potential sweeps were from -0.8 V to 1.1 V versus a Ag/Ag<sup>+</sup> reference. In the first scan, bis(4'-(4-anilino)-2,2':6',2''-terpyridine)iron complex shows one irreversible oxidation wave and one pair of reversible waves. The irreversible peak at 0.63 V is derived from a one-electron oxidation reaction of an amino group to generate a highly reactive amino free-radical. The other reversible signal at 0.8 V is from the tpy<sub>2</sub>Fe(III)/(II) couple.

After several potential sweep cycles, the signal of tpy<sub>2</sub>Fe(III)/(II) couple becomes bigger and bigger. This is an indication of immobilization of the bis(4'-(4-anilino)-2,2':6',2''-terpyridine)iron complex on the carbon electrode surface. However, the oxidation signal of aniline gradually becomes smaller. When the electrode surface is covered by molecular wires, the aniline will not be oxidized electrically but chemically by the tpy<sub>2</sub>Fe(III) complex in the molecular wires. The molecular wires acts as a co-oxidant to oxidize the aniline, and the produced iron(II) complex is then regenerated by electro-oxidation. Therefore, when the wires grow longer, only the signal of tpy<sub>2</sub>Fe complex will be observed, but the oxidation signal of aniline will become less obvious in the cyclic voltammogram.

In the modification process, the size of tpy<sub>2</sub>Fe signal shows an almost linear relationship with the scan cycles after 80 cycles, as shown in **Figure 4-2**. This indicates that the wires grow at a constant rate and it is possible to control the wire length by this method.

However, before 80 cycles, the signals do not grow proportionally. One possible reason is that when the wire is short, its signals are overlapped with solution species. The other possible reason is that the immobilization reaction needs an initiation period to start the wire growth. As the surface of glassy carbon is not totally flat, when approaching to the surface, the complex must find a suitable orientation to have the smallest repulsion from the electrode. The best possible structure should be vertical to the substrate.

From this, the molecular wire growth mechanism can be considered as follows: initially, the aniline free-radical is quickly immobilized on the electrode. The density of the surface molecules then becomes higher and higher. However, the immobilization rate becomes slower due to increasing repulsion and the random orientation of the molecules. After the surface molecules reach a certain concentration, a small portion of the complex starts to immobilize at the top of anchors having the vertical structure. During this period, more and more anchors rotate to the vertical direction and precede

the elongation reaction. Due to this reorientation reaction, almost all wires change to the vertical structure. Therefore, the molecular wire growth can speed up again and then reaches a stable rate.

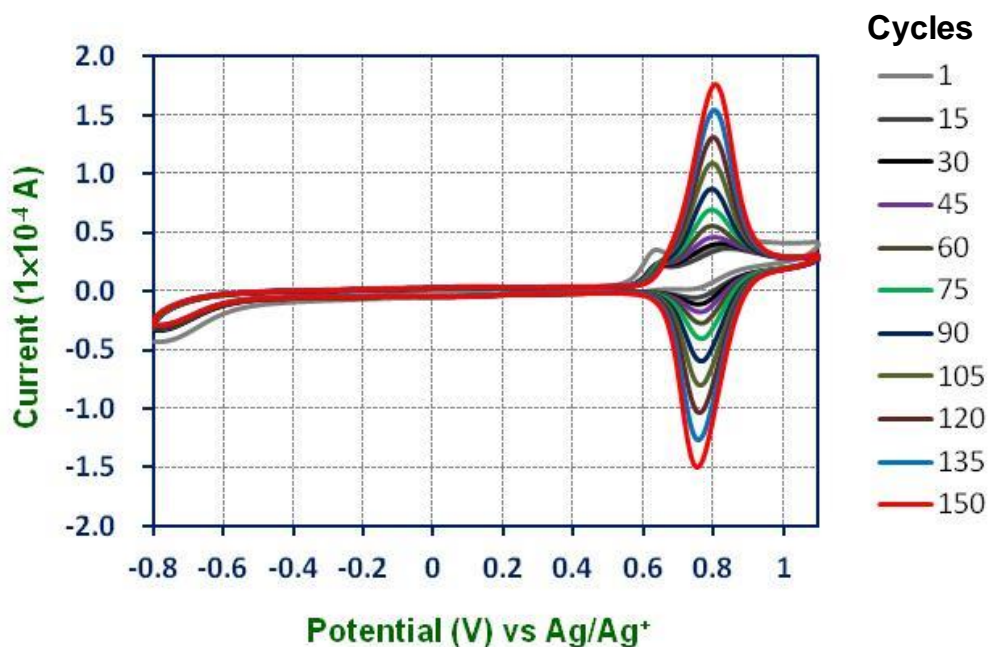


Figure 4-1 Cyclic voltammograms of the synthesis of the bis(terpyridine)iron molecular wire.

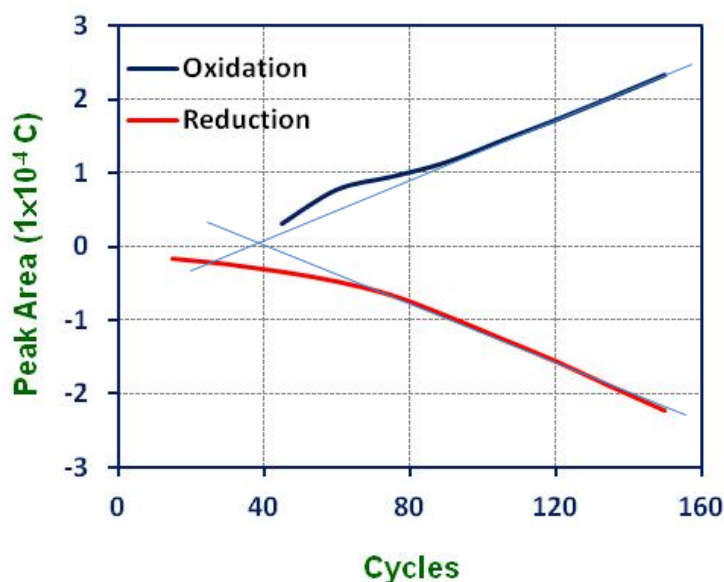


Figure 4-2 The peak areas of bis(terpyridine)iron complex versus scan cycles of cyclic voltammetry.

### 4.3.2 The anchor group of the electrochemically synthesized molecular wire

The chemical structure of the connection group between the molecular wires and the carbon electrode is very important for the electrochemical properties of this system. The reason is that this anchor group can decide orbital interactions between the wires and the electrode. However, the direct investigation of this anchor group structure is almost impossible because of their low ratio as compared to the whole system. Therefore, the junction structure is deduced from its formation condition and literatures.

According to literatures,<sup>8,9</sup> amine compounds can be immobilized on carbon surfaces via a free-radical addition reactions induced by an electrochemical oxidation. Most carbon electrode surfaces have a graphite structure, which consists of large number of conjugated double bonds and is a  $\pi$ -electron rich system. When an amino radical is generated near carbon electrode, the single electron of the radicals will add to a double bond of the surface to create a C-N covalent bond. At the same time, a new carbon free radical will be produced next to the C-N bond on the electrode. This surface radical probably reacts with the nitrogen of the adjacent C-N bond to form a three-membered ring through a radical coupling reaction accompanied by an oxidation reaction.

However, a three-membered ring is not an energy favorable structure. Therefore, this ring should be a labile structure in electrochemical processes. Under oxidation conditions, the nitrogen may convert to a cation to further stabilize the ring. In reduction conditions, the ring may be temporarily opened to form a mono-bonding linkage.

Although the direct observation of the three-membered ring formation on carbon electrode cannot be found in literature, important supporting evidences come from fullerene chemistry. Fullerene is one of the best molecules to mimic the carbon electrode because of their similar chemical structures. Moreover, as fullerene is a small molecule, the characterization of modified fullerene is much easier than that of graphite.

N-C-C three-membered rings can form easily on fullerene via reacting with nitrene compounds, which can be considered as a di-free-radical molecule.<sup>10</sup> The three-membered ring structure can also be generated from a reaction between fullerene and aniline with  $\text{CuCl}_2$  as an oxidation reagent.<sup>11</sup> This implies that three-membered rings on carbon surface can be generated via a free-radical reaction.

The N-C-C three-membered ring structure facilitates the electron transfer between the wires and the electrode. Due to the unusually small bond angle of the three-membered ring, its sigma bonding orbitals bend to form a hyper conjugation system from the electrode to the molecular wires. This extended conjugating system reduces the electron transportation energy barrier between the electrode and the wire.

### 4.3.3 The structure of the electrochemical synthesized molecular wire

Oxidation reactions of amines can generate a very wide spectrum of compounds, such as hydroxylamine, nitroso and nitro compounds. Moreover, if oxidation reactions occur on aromatic amines, polyaniline and azobenzene can be generated.

Azobenzene is one the most likely bridging groups resulting from this electrochemical synthesis. First, polyaniline is difficult to be generated from 4-substitutional anilines and no signal derived from polyaniline is found in the cyclic voltammogram of the resulting wires. Second, azobenzene group can stably connect and polymerize bis(4-aniline-terpyridine) metal complexes on the electrode. Third, the high electron transportability of the electrochemically synthesized molecular wire is similar with that of a molecular wire having azobenzene bridging.

To study the surface structure of a modified electrode, infrared spectroscopy is one of the most convenient methods. However, the -N=N- structure of *trans*-azobenzene is IR inactive due to its symmetric structure. Therefore, in this research, Raman spectroscopy was employed. In the measurements, *trans*-tpy-Ph-N=N-Ph-tpy free bridging ligand was used as a reference for azobenzene signals in a terpyridine system (**Figure 4-3**). The other reference was a random length bis(terpyridine)iron molecular wire prepared by mixing one equivalent of *trans*-tpy-Ph-N=N-Ph-tpy and one equivalent of Fe(BF<sub>4</sub>)<sub>2</sub>(H<sub>2</sub>O)<sub>6</sub> in acetonitrile.

In the Raman spectrum of the reference ligand (**Figure 4-4**), a strong signal at 1126 cm<sup>-1</sup> can be assigned to the aryl-nitrogen single bond stretching of the azobenzene. Another medium signal at 1436 cm<sup>-1</sup> comes from the nitrogen-nitrogen double bond stretching. These two peaks are the characteristic signals of the azobenzene structure in Raman spectroscopy.

In the spectrum of the iron-based molecular wire reference, the aryl-nitrogen signal at 1144 cm<sup>-1</sup> becomes much smaller than that of free ligand, because a long wire structure may restrict the stretching along the wire direction. Also, the change of vibration mode or a reduced mass of the wire may cause a signal shift. However, the nitrogen-nitrogen double bond stretching at 1454 cm<sup>-1</sup> is still strong, because this stretching is not along the wire direction. Although the azobenzene Raman signals of the reference wire are different from those of the reference ligand, the spectra can still be explained reasonably depending on their structures.

On the other hand, the Raman spectrum of the electrochemically synthesized molecular wire measured under the same conditions shows surprising similarity with the reference iron wire. Other than some small differences, these two spectra have almost identical signals. From these two spectra, it can be concluded that the chemical structure of the electrochemically synthesized molecular wire is the same as the coordination reaction synthesized molecular wire. Therefore, the chemical structure of electrochemical synthesized wire should be a linear rigid wire with the azobenzene bridging group.

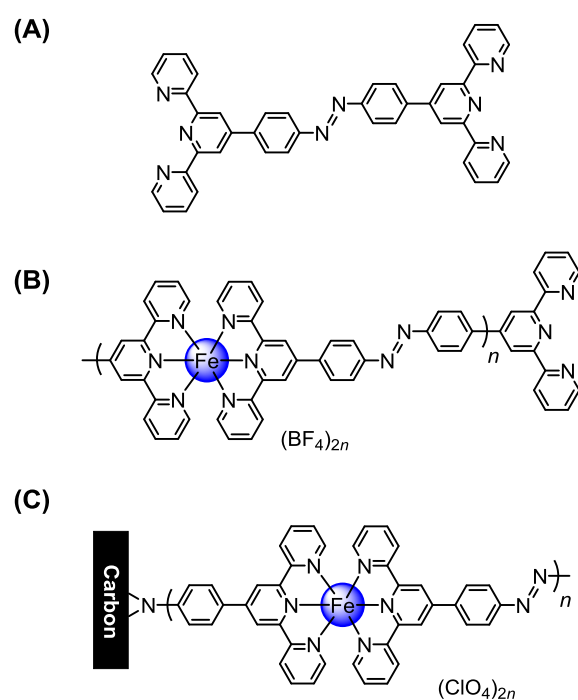


**Figure 4-3** The structures of references (A and B) for Raman spectroscopy and the electrochemical synthesized molecular wire (C).

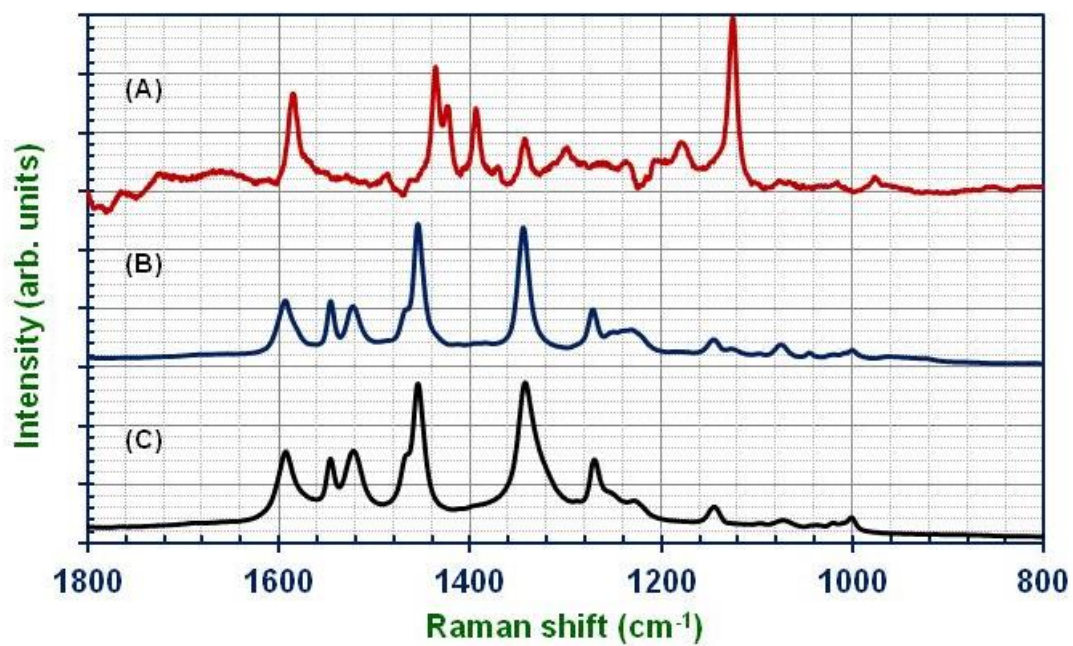


**Figure 4-4** Raman spectra of the reference bridging ligand (A), the reference molecular wire (B), and the electrochemical synthesized molecular wire (C).

#### 4.3.4 The surface structure of the molecular wire modified electrode

The surface structure of a modified electrode can directly affect its properties and is therefore important for its applications. In the case of the molecular wire modified electrodes, their surface structures are especially important, because wires distribution and uniformity can be known. In this research, atomic force microscopy (AFM) was used to measure the molecular wire modified glassy carbon electrode under ambient conditions (**Figure 4-5**).

From the phase image of the AFM measurement, a pattern of about  $60\text{ nm} \times 30\text{ nm}$  ovals totally covers the surface of the modified electrode. This image is totally different from that of pristine glassy carbon. From this result, it can be noted that the electrode surface is totally covered by molecular wire.

From the topography of the modified electrode, the height differences between the molecular wires are very small. On average, the difference between the longer wires and the shorter wires are about  $10\text{ nm}$ . This small difference indicates that this electrochemical synthesis can fabricate a rather uniform molecular wire array on an electrode surface.

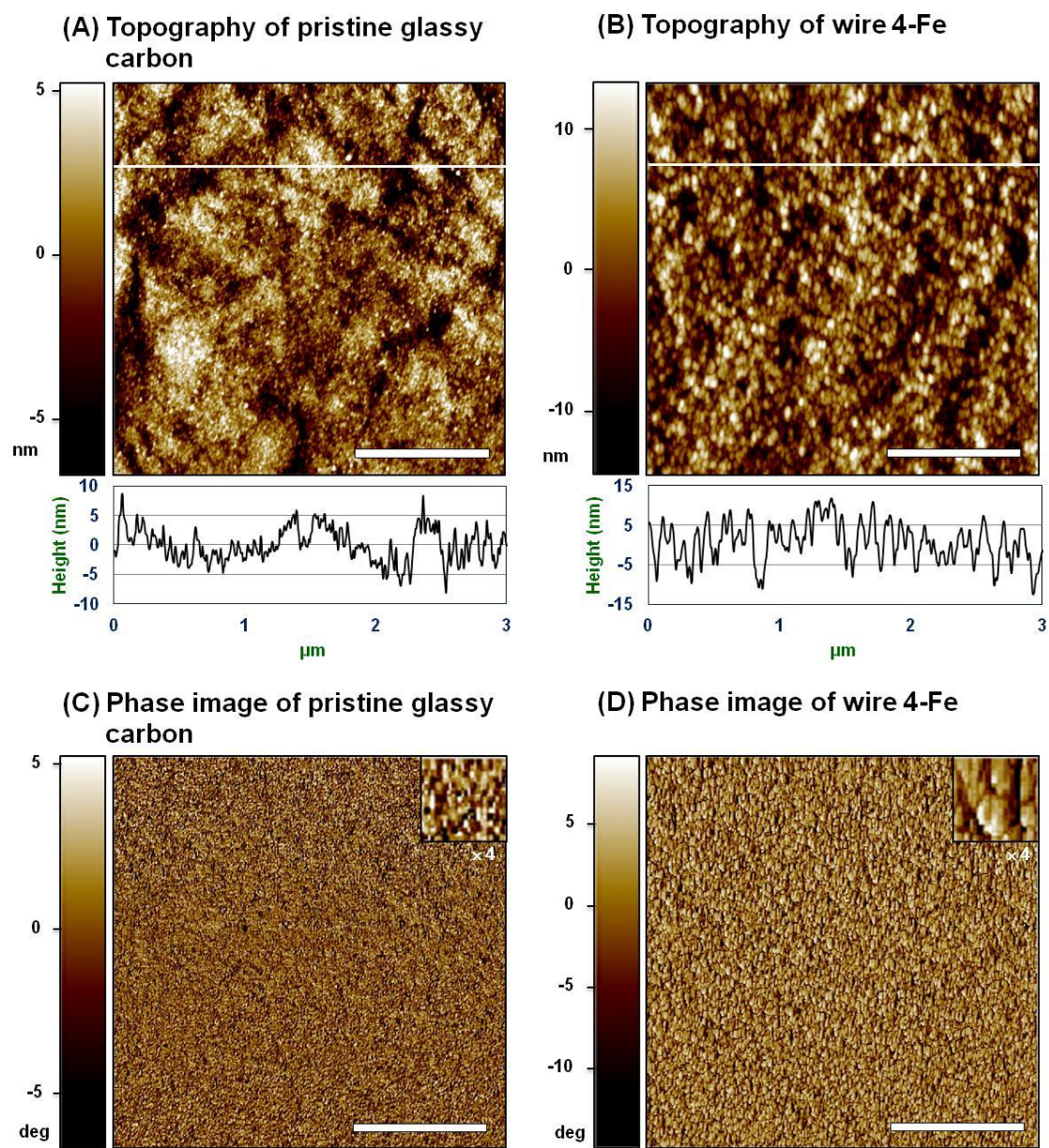


**Figure 4-5** The topographies and phase images of pristine glassy carbon and the molecular wire modified electrode. The scale bars are 1 μm.

### 4.3.5 The formation mechanism of the molecular wire

From the chemical structure and synthesis condition of the molecular wire, the formation mechanism can be deduced as the following (**Figure 4-6**): first, one aniline group of the monomer complex is electro-oxidized to generate an amino-free-radical. Next, the radical reacts with the carbon electrode to covalently immobilize itself with a N-C-C three-member ring linkage. The other aniline group of the immobilized complex is then electro-oxidized to form an immobilized free-radical. This surface free-radical will couple with another aniline free-radical in solution to form a hydrazine linkage. Finally, this hydrazine bridge is electro-oxidized to form the azobenzene linkage. Then the other aniline group of the terminal complex will go through the same process to elongate the molecular wire layer by layer.

In this reaction mechanism, the most important intermediate is the aniline free-radical. This radical can be generated easily by the electro-oxidation reaction at around 0.63 V. As the addition reaction of aniline free-radical to benzene is relatively slow,<sup>12</sup> almost no branching structure will be formed in this modification.

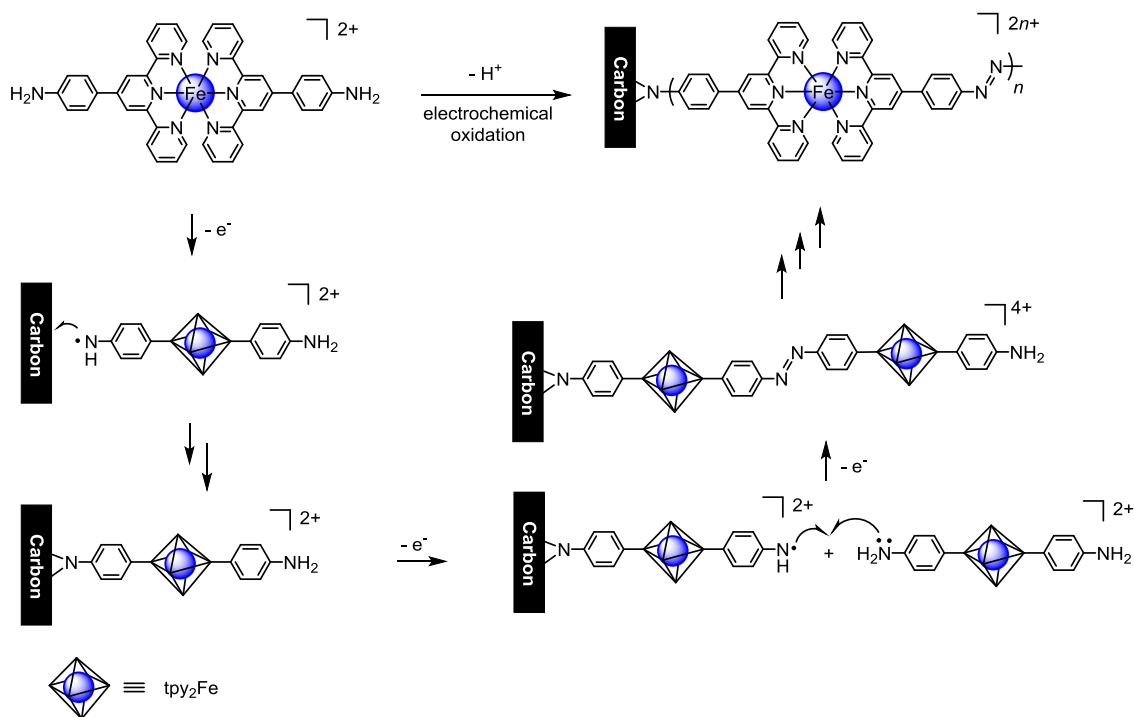


**Figure 4-6** The mechanism of the electrochemical synthesis of the molecular wire.

### 4.3.6 Surface coverage of the molecular wire on the electrode

Surface coverage of a molecule on a substrate has a strong influence on the surface properties of the surface affecting its catalytic reactivity, sensor responsibility and light harvesting efficiency of the substrate. Moreover, surface coverage can be the evaluation basis for the average length of immobilized molecular wires by electrochemical methods.

Theoretically, bis(terpyridine)metal complex wires can be assumed to be an array of cylinders with 1 nm diameter having a close packing structure on a surface (**Figure 4-7**). With this assumption, the theoretical maximum coverage of these wires is found to be  $1.6 \times 10^{-10}$  mol cm<sup>-2</sup>. However, this value is much higher than the known values.<sup>13</sup> In the literature, coverage values were measured from a self-assembly monolayer of (4'-(pyridin-4-yl)-2,2':6',2''-terpyridine)(terpyridine) ruthenium and osmium complex on gold electrodes. When measured from electrochemical methods, the ruthenium complex has a coverage of  $2.5 \times 10^{-11}$  mol cm<sup>-2</sup> and the osmium complex has a coverage of  $3.3 \times 10^{-11}$  mol cm<sup>-2</sup>. When calculated from the measurements of scanning tunneling microscope (STM), a slightly similar result,  $2.2 \times 10^{-11}$  mol cm<sup>-2</sup>, is obtained for the ruthenium complex.

In order to evaluate the coverage of the electrochemically synthesized molecular wires on glassy carbon surface, a construction-destruction process is used to offer a substrate with bare anchor ligands (**Figure 4-8**). First, 650 layer-long iron molecular wires were grown on the glassy carbon surface by the electrochemical method. Next, these molecular wires were decomposed by an aqueous solution of 1 M KOH under oxidation potentials. In alkaline solutions, bis(terpyridine)iron(III) complexes easily dissociate, because the hydroxide anion has very strong affinity for the iron(III) center. After this treatment, the molecular wires would be all dissociated, and only the bare anchor terpyridine would still stably remain on the electrode surface.

This electrode was then immersed in an ethanol solution of 0.1 M iron(II) tetrafluoroborate and a chloroform solution of 0.2 M terpyridine, successively. A monolayer bis(terpyridine)iron complex would have been immobilized by this stepwise coordination method.

This monolayer complex modified glassy carbon was used to evaluate the density of the anchor ligand. As the coverage of the anchor ligand is the same with the original wires, the coverage of the molecular wire can be known indirectly from this method.

From cyclic voltammetry, the coverage of the immobilized bis(terpyridine)iron complex is  $2.2 \times 10^{-11} \text{ mol cm}^{-2}$  which is almost similar with the literature values. However, this experimental value is much smaller than the theoretical prediction. This indicates that the molecular wires do not form a close packing structure on the electrode surface.

According to this discussion, some void space between the molecular wires is expected to exist on the modified electrode (**Figure 4-9**). On the other hand, the AFM image of the electrode shows the molecular wires uniformly covering the surface. Therefore, it can be deduced that the void space is evenly separated in this molecular wire array. A surface structure of close packing cylinders with 2.9 nm diameter on the electrode fits the coverage of  $2.2 \times 10^{-11} \text{ mol cm}^{-2}$  better than the 1 nm diameter close packing structure.

This view suggests that each molecular wire on a real sample occupies about 9 times of the smallest necessary area. Therefore, only the center of the cylinder contains the wire, and the remaining outer part is void space. This space is around 1.9 nm width and is enough for electrolyte migration.

The reason why void spaces exist between the molecular wires on the electrode surface is that first, electrostatic repulsion between the divalent precursors of the wires prevents the formation of close packing structure. In the modification process, bis(terpyridine)metal complexes immobilized on the electrode surface will build up positive electric fields around them. These fields will prevent other identical complexes from coming closer to them. As a result, the latter complexes cannot immobilize just next to the former complexes.

Second, solvent molecules and counter ions accompanying with the complex will also occupy a space around it. Because this modification is carried out in solution, the complexes are always solvated by acetonitrile or water. Moreover, counter ions attracted by its positive charge will also surround the complex with solvent molecules and form an electric double layer around the complex.

Finally, thermal vibrations and collision of molecules possibly also cause a void space around the molecular wires. At room temperature, all the molecules in solution move relatively faster and collide more frequently than in the solid state. These motions will cause an increase in the effective volume of a molecule; hence close packing structure cannot be formed.

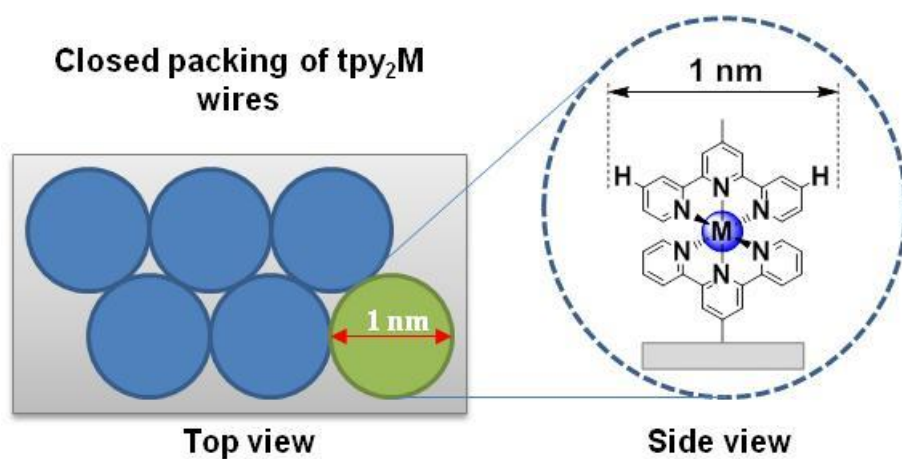


**Figure 4-7** Illustration of the close packing structure of a bis(terpyridine)metal complex on a electrode.

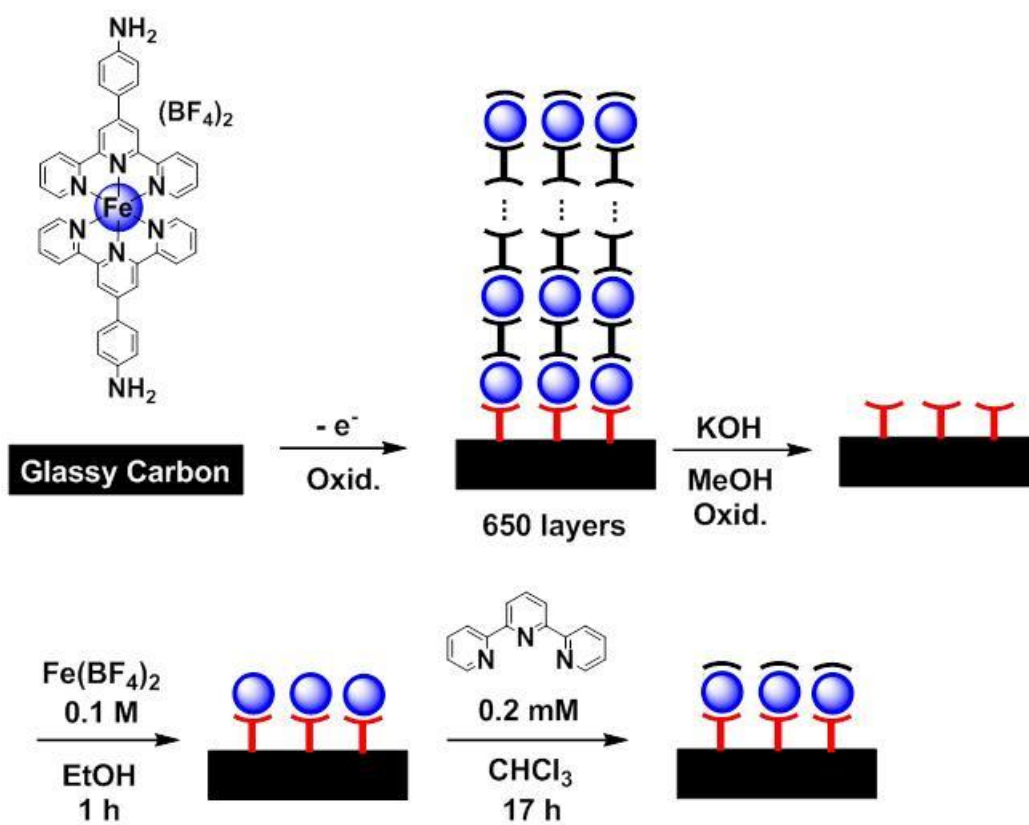


**Figure 4-8** The preparation process of the monolayer bis(terpyridine)iron complex on a glassy carbon electrode.

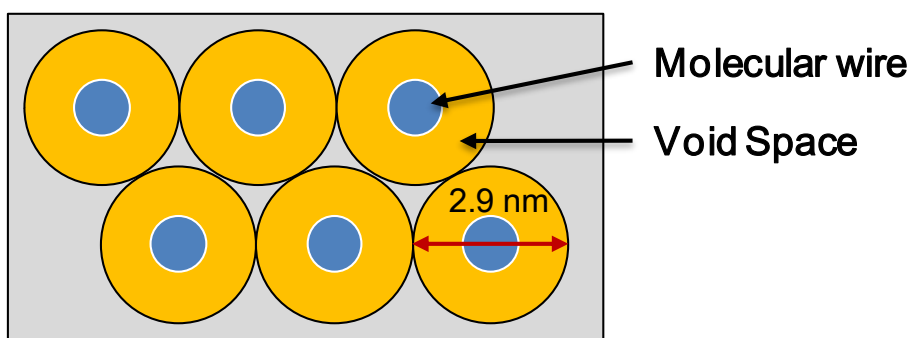


**Figure 4-9** Illustration of the real occupation of the molecular wires on a electrode surface.

### 4.3.7 Synthesis of the longest bis(terpyridine)iron molecular wire

The longest molecular wire can be synthesized using a continuous potential scan by cyclic voltammetry. In the modification, the peak currents of the bis(terpyridine)iron(III)/(II) couple show a parabolic tendency of increasing, slowing down and then stopping of wire growth with increasing scan cycles (**Figure 4-10**). After an initiation period, the peak currents of the oxidation and reduction reaction of bis(terpyridine)iron complex start to grow almost proportionally to the scan cycles. When the potential sweeps reached 220 cycles, the growth of the peak currents starts to slow down. After 400 cycles, the peak currents almost stop growing and, after 450 cycles, the wire length shows slight decay.

On the other hand, from the cyclic voltammograms as shown in **Figure 4-11**, the peak size of bis(terpyridine)iron(III)/(II) couple shows similar increasing tendency with the peak current. However, after 400 scan cycles, the peaks show slight difference from those of the previous scans: the peak heights stop changing, but become wider. This indicates that the wire reached the maximum length of efficient electron transportation distance. In other words, although the wires can still grow slowly after this length by electrochemical synthesis, the electron transportation from the terminal part will become more and more difficult. The molecular wire longer than this electron transportation length will have much inert electric properties.

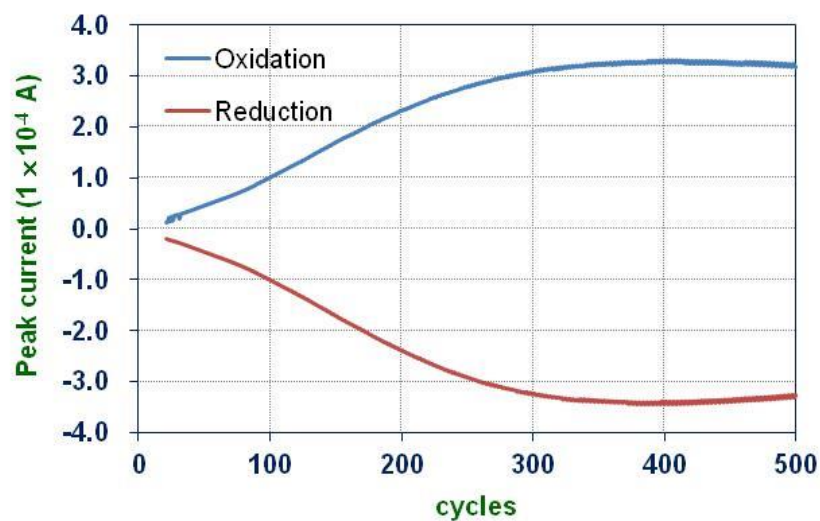


**Figure 4-10** The peak currents of the molecular wire electrochemical synthesis versus the scan cycles.

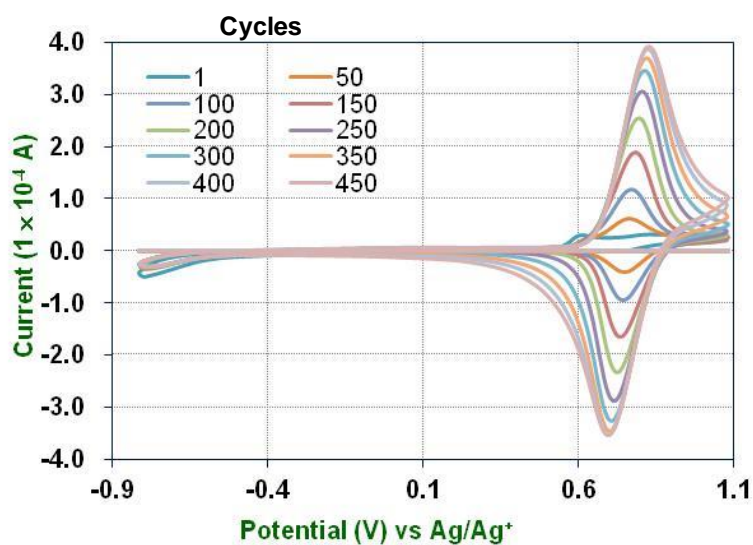


**Figure 4-11** The cyclic voltammograms of the molecular wire electrochemical synthesis.

### 4.3.8 Characterization of the longest molecular wire

The length of the longest bis(terpyridine)iron complex molecular wire is evaluated by cyclic voltammetry at a scan rate of  $1 \text{ mVs}^{-1}$  (**Figure 4-12**). The coverage of the bis(terpyridine)iron complex of the longest wire is  $(1.63 \pm 0.007) \times 10^{-7} \text{ mol cm}^{-1}$  on the electrode. This corresponds to  $7410 \pm 30$  layers of molecular wire and is about  $14.82 \pm 0.06 \text{ }\mu\text{m}$  long. Based on our best knowledge, this wire is the longest bis(terpyridine)metal complex wire ever synthesized.

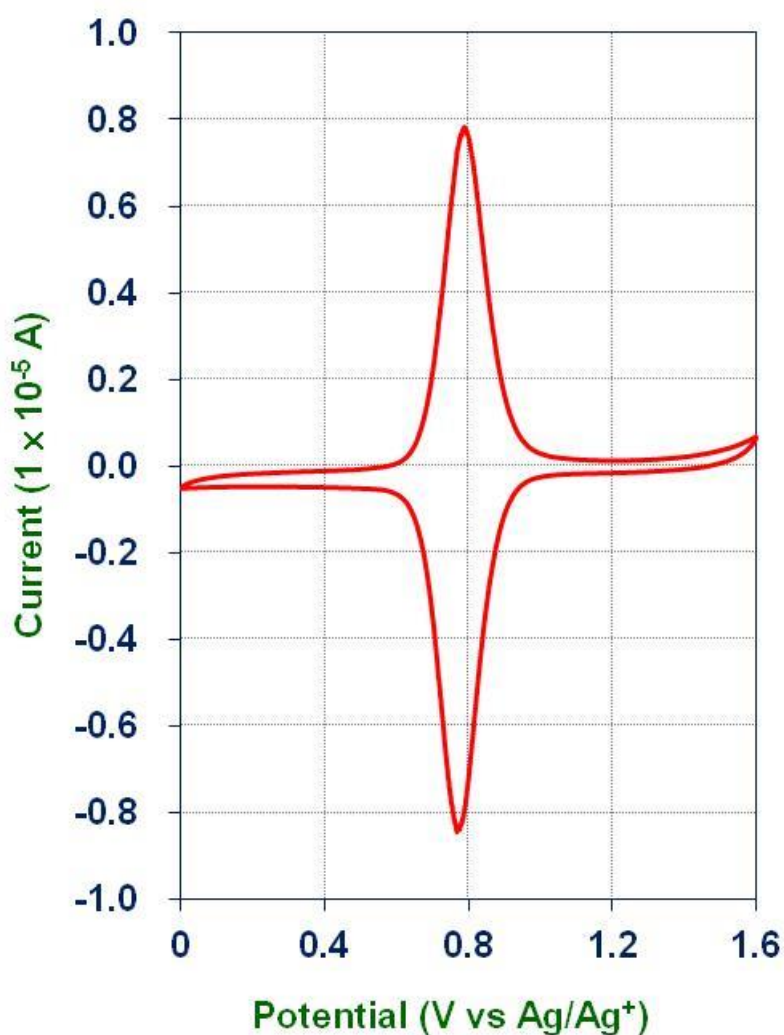


**Figure 4-12** The cyclic voltammogram of the longest bis(terpyridine)iron wire at a scan rate of  $1 \text{ mVs}^{-1}$ .

In a molecular wire with redox active complex units, electrons can be transported by a series of continuous redox reactions happening along the wire. This process looks like electrons jumping forward in the redox wire. This electron movement is known as hopping mechanism. The other well known mechanism is tunneling mechanism, where electrons tunnel through a molecular wire by quantum tunneling effect. Comparing these two mechanisms, electron hopping mechanism usually dominates long range electron transfers and has a lower attenuation value,  $\beta$ . This indicates that molecular wires with redox units can much efficiently transport electrons in long distance, because these redox centers are the energy local minimum and can act as temporary hosts for electrons. In other words, the energy barrier of the electron transportation is decreased by these redox centers.

The electron transporting behavior in the wire can be studied by electrochemical measurements. Although the attenuation value of the longest molecular wire cannot be evaluated by these electrochemical measurements, the relative electrochemical properties and electron transportability can still be examined.

From the voltammogram (**Figure 4-12**), high symmetrical peaks of the iron(III)/(II) couple suggest that the electron transportation in this wire is efficient and smooth. Moreover, from a chronoamperogram of the longest molecular wire (**Figure 4-13**), the current changes of oxidation and the reduction process of this molecular wire show that all the complex centers have quick responses to the applied potential within several seconds.

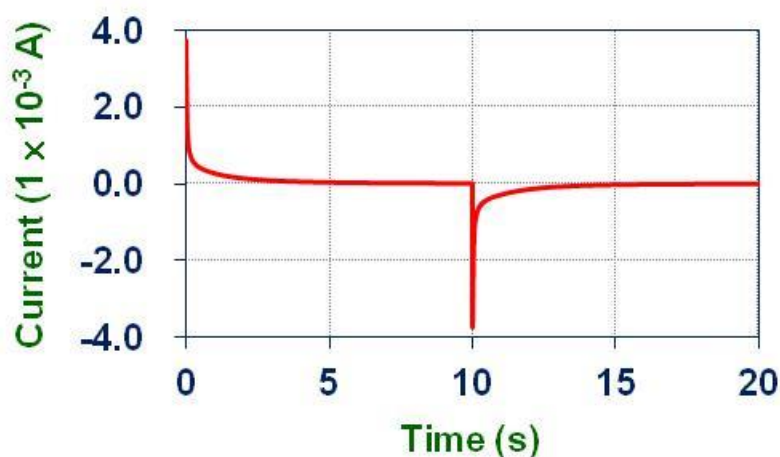


**Figure 4-13** The chronoamperogram of the longest molecular wire at a potential step of 0.6 V.

### 4.3.9 Hetero metal wires

The synthesis of hetero metal molecular wires can be studied as a model for producing complicated molecular devices. Metal complexes with different metal centers often show different chemical and physical properties, and therefore, can be used as different molecular device components. Apart from this, the entire hetero metal wire often also has unique physical properties.

To prepare these hetero metal wires, electrochemical methods are very efficient and suitable techniques. Although stepwise coordination methods can also be used to prepare short hetero metal wires with precise control, they usually require longer time and multi-steps to synthesize the longer structures. Furthermore, sometimes complexation reactions of certain metal species cannot be carried out smoothly by stepwise coordination method, such as bis(terpyridine)ruthenium and iridium complexes, or the complexes cannot be divided into two components, for example, porphyrins. However, in electrochemical processes, the syntheses of complex monomers can be carried out before wire polymerization. Moreover, electrochemical methods can afford long hetero molecular wire in a much shorter time.

The synthetic procedure of hetero metal wires is almost the same with the homo metal wires. The only difference is that electrochemical reaction must be carried out in two types of complex solution successively.

In the cyclic voltammogram of the resulting iron-ruthenium wire (**Figure 4-14 A**), signals of bis(terpyridine)iron(III)/(II) couple show almost no change from homo metal wires, but the oxidation and reduction rates of the bis(terpyridine)ruthenium(III)/(II) couple and their peak shapes are very different. Comparing with homo metal bis(terpyridine)ruthenium wire, the oxidation reaction of the ruthenium units in the hetero wire becomes slower and hence this signal is broadened very much at the scan rate of  $100 \text{ mVs}^{-1}$ .

In the wire with a reverse sequence (**Figure 4-14 B**), the ruthenium-iron wire, the electrochemical measurement also shows a reverse response. The bis(terpyridine)ruthenium complex section is closer to carbon electrode, so the redox signals behave as normal homo metal wires. However, the external bis(terpyridine)iron complex component shows fast oxidation rate but slow reduction response.

These behaviors of the hetero metal wires are similar to diode devices. In a diode, electrons can go easily from its n-type semiconductor layer to its p-type layer, but it is difficult for the reverse (p to n) to occur without extra energy. In the hetero metal wires, electric current can flow easily from the bis(terpyridine)iron complex section to the ruthenium complex section. However, from the ruthenium part to the iron part, electrons cannot flow smoothly.

This diode property can be explained by the HOMO energy level difference between bis(terpyridine)iron complex and bis(terpyridine)ruthenium complex (**Figure 4-15** & **Figure 4-16**). In these electrochemical measurements, electrons are mainly transported in the HOMO level of the wires, because this electron current flow is accompanied by the redox reactions happening at the HOMO energy level. The HOMO energy level of bis(terpyridine)iron complex is higher than the bis(terpyridine)ruthenium complex. When electrons move from the iron complex side to the ruthenium complex side, it is a spontaneous reaction. However, when electrons transfer from the ruthenium complex end to the iron complex end, an energy gap of 0.16 eV exists between the HOMO of these two complexes. Therefore, this electron transfer will be hindered by the barrier and the rate of this process will be much slower than that for the reverse sequence.

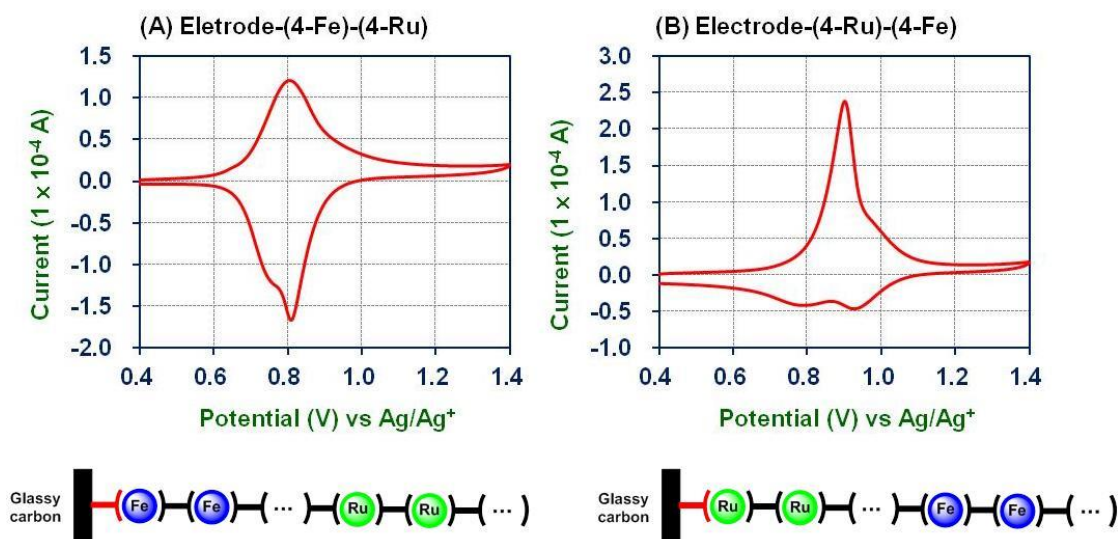


**Figure 4-14** The cyclic voltammogram of hetero metal wires.

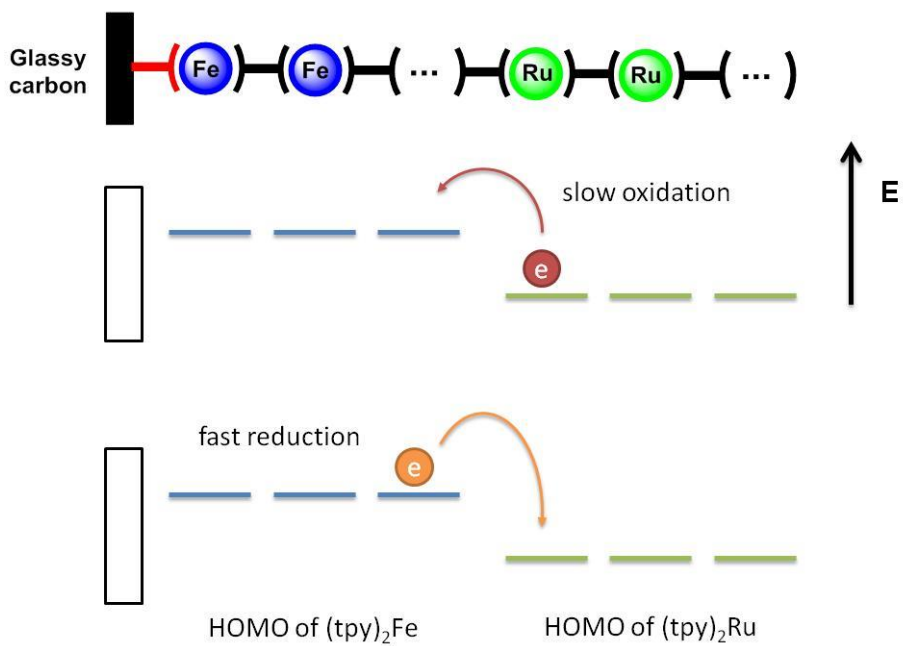


**Figure 4-15** The energy diagram of a iron-ruthenium wire.

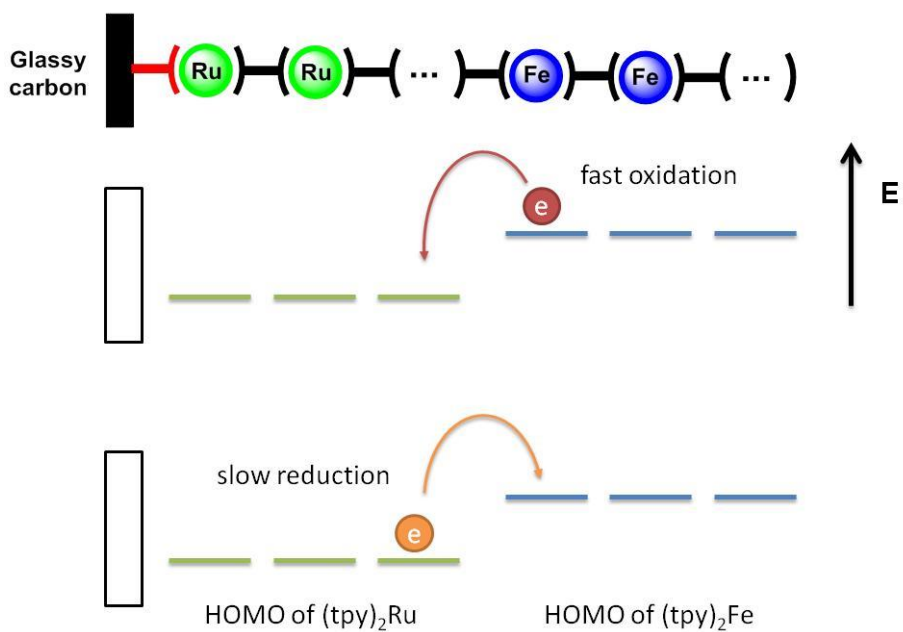


**Figure 4-16** The energy diagram of a ruthenium-iron wire.

## 4.4 Conclusion

Ultra-long bis(terpyridine)metal complex wires arrays on carbon surface were synthesized successfully by an electrochemical coupling reaction. The molecular wires have rigid linear chemical structures with azobenzene bridging. Moreover, it is confirmed by AFM measurements that this wire array forms an even length upright standing structure on carbon surface. The longest molecular wire evaluated by electrochemistry is 7410 layers corresponding to 14.82  $\mu\text{m}$ , which is the longest bis(terpyridine)metal complex wire ever synthesized. In chronoamperometry, all iron centers of the longest bis(terpyridine)iron complex wire can be oxidized and re-reduced within several seconds. This means that electrons can move freely in this long wire without much resistance. Moreover, this electrochemical synthesis can efficiently prepare hetero metal wires which show unique properties similar to that of a diode.

Based on these results, this electrochemical synthesis could be a possible efficient method to integrate molecular scale computing systems to achieve high calculation ability. It also offer a new way to construct functional electrodes with long molecule arrays for high efficient light harvesting devices, sensors and memories.

## 4.5 References

---

1. IBM 100 - Copper Interconnects: The Evolution of Microprocessors. 17th, Oct., 2012.
2. (a) Sakamoto, R.; Katagiri, S.; Maeda, H.; Nishihara, H. *Coord. Chem. Rev.* **2013**, 257, 1493. (b) Nishihara, H.; Kanaizuka, K.; Nishimori, Y.; Yamanoi, Y. *Coord. Chem. Rev.* **2007**, 251, 2674. (c) Tuccitto, N.; Ferri, V.; Cavazzini, M.; Quici, S.; Zhavnerko, G.; Licciardello, A.; Rampi, M. A. *Nat. Mater.* **2009**, 8, 41.
3. Creager, S.; Yu, C. J.; Bamdad, C.; O'Connor, S.; MacLean, T.; Lam, E.; Chong, Y.; Olsen, G. T.; Luo, J.; Gozin, M.; Kayyem, J. F. *J. Am. Chem. Soc.* **1999**, 121, 1059.
4. (a) Schumm, J. S.; Pearson, D. L.; Tour, J. M. *Angew. Chem. Int. Ed.* **1994**, 33, 1360. (b) Huang, S.; Tour, J. M. *J. Am. Chem. Soc.* **1999**, 121, 4908. (c) Pearson, D. L.; Schumm, J. S.; Tour, J. M. *Macromolecules* **1994**, 27, 2348. (d) Young, J. K.; Nelson, J. C.; Moore, J. S. *J. Am. Chem. Soc.* **1994**, 116, 10841.
5. (a) Ajayan, P. M. *Chem. Rev.* **1999**, 99, 1787. (b) Cassell, A. M.; Raymakers, J. A.; Kong, J.; Dai, H. *J. Phys. Chem. B* **1999**, 103, 6484. (c) Li, Y. L.; Kinloch, I. A.; Windle, A. H. *Science* **2004**, 304, 276.
6. (a) Efimov, O. N. *Russian Chem. Rev.* **1997**, 66, 443. (b) Roncali, J. *Chem. Rev.* **1992**, 92, 711. (c) Cheng, Y. J.; Yang, S. H.; Hsu, C. S. *Chem. Rev.* **2009**, 109, 5868.
7. Storrier, G. D.; Colbran, S. B.; Craig, D. C. *J. Chem. Soc. Dalton Trans.*, **1997**, 3011.
8. Deinhammer, R. S.; Ho, M.; Anderegg, J. W.; Porter, M. D. *Langmuir*, **1994**, 10, 1306.
9. Buttry, D. A.; Peng, J. C. M.; Donnet, J.-B.; Rebouillat, S. *Carbon*, **1999**, 37, 1929.
10. Smith, A. B., III; Tokuyama, H. *Tetrahedron*, **1996**, 52, 5257.
11. Yang, H.-T.; Liang, X.-C.; Wang, Y.-H.; Yang, Y.; Sun, X.-Q.; Miao, C.-B. *J. Org. Chem.*, **2013**, 78, 11992.

- 
12. Neta, P.; Maruthamuthu, P.; Carton, P. M.; Fessenden, R. W. *J. Phys. Chem.*, **1978**, 82, 1875.
  13. Figgemeier, E.; Merz, L.; Hermann, B. A.; Zimmermann, Y. C.; Housecroft, E.; GuIntherodt, H.-J.; Constable, E. C. *J. Phys. Chem. B* **2003**, 107, 1157.

# **Chapter 5**

## **Concluding remarks**

This thesis majorly focuses on the syntheses and the electrochemical properties of bis(terpyridine)metal complex polymers with network and linear structures. These polymer complexes are constructed by bis(terpyridine)metal complexes, which are one of the most investigated coordination compounds, due to their structure diversity, high stability, unique physical and chemical properties. In this thesis, bis(terpyridine)metal complex networks and wires were synthesized successfully by an electrochemical polymerization method, which is a highly efficient way to fabricate functional nano material on carbon surfaces.

In Chapter 2, a bis(terpyridine)iron network complex was synthesized via an electrochemical polymerization by cyclic voltammetry. This network complex is stably immobilized on glassy carbon. The complex film has a random surface structure with particles of 100 to 200 nm diameter. In electrochemical examinations of its charging and discharging properties, the network complex shows high capacity retention at high potential scan rates. The capacity at a scan rate of  $10 \text{ Vs}^{-1}$  is only 24% lower than that at  $0.025 \text{ Vs}^{-1}$ . Also, as the scan rate increase, the charging and discharging peak in cyclic voltammograms only separates slightly. On the other hand, the capacities of the network complex measured by chronocoulometry exhibit a parabola-like increasing tendency when the potential steps increase. The initial faster increase is from the faradaic reactions of bis(terpyridine)iron(III)/(II) couple, and the later slower increase is from the double layer capacitor effect of the surface of the electrode and the network complex. Moreover, from chronoamperometry, the network complex exhibits extremely fast charging and discharging speed. In a chronocoulomogram with a potential difference of 0.4 V, the network complex can be charged to 80% in 0.08 s, 90% in 0.16 s and 95% in 0.35 s. On the other hand, the charged material can be discharged to 80% in 0.08 s, 90% in 0.16 s and 95% in 0.62 s. Finally the network complex shows high stability for continuously charging and discharging process. After 3000 cycles, the capacity of this network decreases only 5%.

In Chapter 3, the network complex was successfully immobilized on a porous carbon nanotube electrode prepared by the drop and cast method. The employment of carbon nanotubes effectively increases the electrode surface area. In the electrochemical measurement, the hybridized material similar to the network complex exhibits high charging and discharging rate and good stability. Moreover, this hybridized material dramatically increases electrode areal capacitance. Therefore, the network complex shows good compatibility with carbon nanotubes and results in even greater capacity than just using the network alone.

In Chapter 4, an ultra-long molecular wire was synthesized by an electrochemical coupling reaction on carbon electrode surface. The chemical structure is characterized by Raman spectroscopy to be a rigid wire with azobenzene bridging groups. Also, the AFM measurements indicate that the wire array on electrode surface have an even length upright standing structure. From electrochemical measurements, the longest molecular wire synthesized by this method is found to be 7410 layers and corresponding to 14.82  $\mu\text{m}$ . Based on our best knowledge, this is the longest bis(terpyridin)metal complex wire. In its chronoamperogram, all iron centers of the longest wire can be oxidized and reduced within several seconds. This means electrons can move freely in any part of this long wire. Based on this electrochemical synthesis, hetero metal wires can be easily prepared. These hetero wires show unequal oxidation and reduction rate. This indicates that an energy gap exists in the wires and endows the wires with diode-like properties. Based on these data, it can be concluded that this electrochemical molecular wire synthesis method can not only efficiently generate long molecular wire but can also be used to link different metal complexes to form molecular devices.

In this thesis, it is demonstrated that electrochemical syntheses are efficient for the preparation of bis(terpyridine)metal complex polymers with network or linear structures. These polymers not only show unique structures but also have remarkable electrochemical properties.



## **Acknowledgement**

I would like to express my deepest and sincere gratitude to Professor Dr. Hiroshi Nishihara for supervising my research in The University of Tokyo, teaching me a lot of knowledge and giving me so much life support in Japan.

Moreover, I would like to express my great thanks to Professor Dr. Hiroyuki Kagi, Professor Dr. Mitsuhiko Shionoya, Professor Dr. Takeaki Ozawa and Professor Dr. Tetsuya Hasegawa for their important and enthusiastic suggestions to my thesis.

I also want to express my gratitude to Professor Dr. Yoshinori Yamanoi, Professor Dr. Ryota Sakamoto, Professor Dr. Tetsuro Kusamoto, Professor Dr. Mariko Miyachi and Professor Dr. Maw Lin Foo for their kind support in my research.

Furthermore, I would like to express my thanks to all our laboratory members for their help in my research and my life in Japan.

Finally, I would like to thank my parents, my sister and my friends to their supporting and accompanying.